High-Speed Faulting Measuring Device for Jointed Concrete Pavements

Jorge Prozzi
Ruohan Li
Robin Yaxiong Huang
Joaquin Hernandez

Technical Report Documentation Page

1. Report No. FHWA/TX-23/0-7060-1	2. Government Accession No.	3. Recipient's Catalog No.
4. Title and Subtitle High-Speed Faulting Measuring Device for Jointed Concrete Pavements		5. Report Date Submitted: July 2023
		6. Performing Organization Code
7. Author(s) Rouhan Li, Joaquin B Hernandez, Robin Yaxiong Huang and Jorge A Prozzi		8. Performing Organization Report No. 1-7060-R1
9. Performing Organization Name and Address Center for Transportation Research The University of Texas at Austin 3925 W. Braker Lane, 4th Floor Austin, TX 78759		10. Work Unit No. (TRAIS)
		11. Contract or Grant No. 0-7060
12. Sponsoring Agency Name and Address Texas Department of Transportation Research and Technology Implementation Division 125 E. 11th Street Austin, TX 78701		13. Type of Report and Period Covered Technical Report September 2021 – August 2023
		14. Sponsoring Agency Code

15. Supplementary Notes
Project performed in cooperation with the Texas Department of Transportation and the Federal Highway Administration.

16. Abstract

Current equipment to measure faulting of jointed concrete pavements at the network level is ineffective and inefficient. One the one hand, joint detection at high speeds is challenging. On the other hand, the actual measurement is not accurate and fails to capture the transverse variability of faulting. In this project, a high-definition, high-speed laser was developed, calibrated and validated in the field. In addition, a methodology for joint detection and a new faulting specification were developed. This research report summarizes the work performed and the main findings of this research project.

17. Key Words Faulting, Jointed Concrete Pavement, High Speed, 3D Laser, Profiler, Joints		18. Distribution Statement No restrictions. This document is available to the public through the National Technical Information Service, Alexandria, Virginia 22312; www.ntis.gov.	
19. Security Classif. (of report) Unclassified	20. Security Classif. (of this page) Unclassified	21. No. of pages TBD [Total count excl. cover]	22. Price

Form DOT F 1700.7 (8-72) Reproduction of completed page authorized

THE UNIVERSITY OF TEXAS AT AUSTIN
CENTER FOR TRANSPORTATION RESEARCH

High-Speed Faulting Measuring Device for Jointed Concrete Pavements

Rouhan Li
Joaquin B Hernandez
Robin Yaxiong Huang
Jorge A Prozzi

Center for Transportation Research
The University of Texas at Austin
3925 W. Braker Lane, 4th floor
Austin, TX 78759

http://ctr.utexas.edu/

Disclaimers

Author's Disclaimer: The contents of this report reflect the views of the authors, who are responsible for the facts and the accuracy of the data presented herein. The contents do not necessarily reflect the official view or policies of the Federal Highway Administration or the Texas Department of Transportation (TxDOT). This report does not constitute a standard, specification, or regulation.

Patent Disclaimer: There was no invention or discovery conceived or first actually reduced to practice in the course of or under this contract, including any art, method, process, machine manufacture, design or composition of matter, or any new useful improvement thereof, or any variety of plant, which is or may be patentable under the patent laws of the United States of America or any foreign country.

Engineering Disclaimer

NOT INTENDED FOR CONSTRUCTION, BIDDING, OR PERMIT PURPOSES.

Research Supervisor: Jorge A Prozzi

Acknowledgments

Table of Contents

List of Tables

List of Figures

Chapter 1. Background and Available Technologies

Faulting reduces riding quality and leads to cracking of the slabs as it continues to develop. Its effect on riding quality, however, depends not only on the level of displacement itself, but also on many other factors (Spellman et al, 1972). As joint faulting grows to be significant, it can also adversely impact pavement maintenance and rehabilitation costs and vehicle operating costs (Agurla and Lin, 2015). Typically, faulting is not noticeable until the average faulting of the pavement section is about 2.5 mm (0.10 in.). When the average faulting reaches 3.8 mm (0.15 in.), it is recommended that some type of rehabilitation measures be applied, such as diamond grinding. The Fixing America's Surface Transportation (FAST) Act classifies sections with less than 2.5 mm (0.1 in) faulting as "good," between 2.5 mm and 3.8 mm (0.1 and 0.15 in) as "fair," and over 3.8 mm (0.15 in) as "poor".

In July 2012, MAP-21, the Moving Ahead for Progress in the 21st Century Act (P.L. 112-141), a long-term highway authorization, was signed into law. It created a streamlined and performance-based surface transportation program built upon existing ones established since 1991 and transformed investment policy and framework to guide the development of the surface transportation system. The Act has been designed to fund surface transportation programs at over $105 billion for fiscal years (FY) 2013 and 2014, and to guide the development of the highway system. The FAST Act (Pub. L. No. 114-94) was signed into law on December 4, 2015. It authorized $305 billion over fiscal years 2016 through 2020 for highway, highway and motor vehicle safety, public transportation, motor carrier safety, hazardous materials safety, rail, and research, technology, and statistics programs, to continue and extend the efforts of MAP-21. Amongst its many requirements, it states that state DOTs measure faulting every 0.1 miles.

Federal Highway Administration (FHWA) Highway Performance Monitoring System (HPMS) Field Manual details, in Item 51, the requirements for faulting data collection. According to the manual, the practice for faulting data collection should be in accordance with AASHTO Standard R36-13 while reporting should follow the requirements in 23 CFR 490.309 and 490.311. Data should be "collected for the full extent of the mainline highway" along sections on both the Interstate System and the non-Interstate System National Highways Systems (NHS), measuring every joint in the right wheel-path and reporting the average absolute faulting. The manual recommends against the use of manual fault measurement.

Under this framework, State Departments of Transportation (DOTs) shall develop a reliable measurement system to identify, measure, and calculate faulting on all jointed concrete pavements (JCP). In particular, this project has the objective of developing a system to collect and verify faulting data of JCP in an accurate manner at highway speeds during daylight conditions.

The two currently available automated methods described in the AASHTO Standard use a two-dimensional (2D) approach to identify the location of the joints: the longitudinal direction and the vertical direction. Meanwhile, the Long-Term Pavement Performance (LTPP) Automated Fault Measurement (AFM) algorithm incorporates three profiles and analyzes them in parallel. One of the reasons that faulting measurement has not been widely automated as many other pavement characteristics is the need and challenge to locate the joints at high speeds.

Chang et al. identified several challenges to this task, from both profiler and pavements. The ones from profiler include not meeting the AASHTO R56 Standard for repeatability and accuracy requirements, sampling intervals too wide to identify joint locations, lack of repeated runs to allow techniques such as pattern searches, and Distance-Measurement-Instruments (DMIs) drifts, especially when profiles are relatively long. Those from the pavement are primarily associated with the joints, including joints being filled with sealants or incompressible materials, closed due to thermal expansion, skewed with inconsistent downward spike locations along left and right wheelpaths, and distributed in uneven spacing patterns, as well as factors not related to joints, for example, the presence of cracks along the pavement.

As documented in AASHTO Standard R 36-21, Standard Practice for Evaluating Faulting of Concrete Pavements, a sampling interval of no more than 0.75 in (19 mm) is required for project-level survey, and 1.5 in (38 mm) for network-level survey (AASHTO, 2021). In a study conducted using data collected with a high-speed inertial profiler along the southbound inside lane of State Road 24 in Waldo, Florida, Nazef et al. (2009) obtained a joint detection rate of 95% using longitudinal profiles collected at 0.68 in (17.3 mm) interval, 69% at 1.36 in (34.6 mm), and 36% at 6.13 in (15.6 cm). Given that the typical width of a widened joint is approximately between 0.39 in (10 mm) and 0.59 in (15 mm), even with a sampling rate strictly following the standard practices described by AASHTO R 36-17, a 100% joint detection rate might not be achieved. The question then becomes: what fraction of the joints need to be surveyed to ensure the average faulting reported for the 0.1-mi (161 m) section is sufficiently accurate? To determine this required sample size, variability in faulting along both the longitudinal and transverse directions need to be considered. Current equipment does not have such capabilities.

1.1. Available Technologies

The two currently available automated methods described in the AASHTO Standard use a two-dimensional (2D) approach to identify the location of the joints: the longitudinal direction and the vertical direction. While the LTPP Automated Fault Measurement algorithm incorporates three profiles and analyzes them in parallel, it still has the limitations of 2D methods, as the three profiles are not continuous. Some recent studies, however, explored the potential in using three-dimensional (3D) profile data in joint detection and faulting calculation. As part of the effort for completing the National Cooperative Highway Research Program (NCHRP) Synthesis 501 of Highway Practice, a web-based survey was distributed to pavement management engineers in 52

state transportation agencies (including Puerto Rico and the District of Columbia), inquiring about current practices and potential enhancements in pavement management, out of which 41 provided completed responses. As one of the questions asked was regarding migrating towards a 3D automated data collection system for pavement management, 18 of the respondents reported that their state DOT had such a system currently in practice, while 17 expected this enhancement to be made within two years. Since the survey was completed in February 2016, as of now, 3D profiling technology is likely to have been adopted by more agencies.

1.1.1. Faulting Measurement with High-Speed Inertial Profiler (HSIP)

1.1.1.1. Kansas DOT

Every spring, the Materials and Research employees at the Kansas DOT (KDOT) measure roughness, rutting, and faulting with automated equipment and enter the data into the Network Optimization System (NOS), a network-level pavement management system used by the department. In 2003, in response to AASHTO's Provisional Standards for condition surveys to harmonize data collection efforts across different states, KDOT conducted a study to compare roughness and faulting measurements using the state DOT standards to those using the AASHTO Provisional Standards. Though AASHTO Standards PP 37 and PP 39 have now been withdrawn, the report describes the automated fault detection and calculation algorithms used by KDOT for NOS data. Profile data along both wheel paths were collected using an International Cybernetics Corporation (ICC) South Dakota-type profiler at highway speeds, typically 50 mph (80 km/h). The sensors measured the vertical distance between the vehicle body and the pavement surface. Three Selcom 220 laser sensors were equipped on the profiler: two outer ones spaced at about 1.67 m (65.8 in.) apart, and a third sensor located in the middle. Accelerometers were used to compensate for the vertical motion of the vehicle body at each of the wheel path sensors. Profile elevations were aggregated at every 75 mm (3 in.). The algorithm used to identify faulting started by algebraically summing up the relative elevation difference values once the absolute relative elevation detected by the right sensor between two points 6 inch apart exceeded 0.09 in, until three consecutive differences were less than 0.09 in or until 3 feet have been traversed. The calculated fault value was determined as the algebraic sum of elevation differences divided by two. Once a point was identified as a faulting location, the next had to be at least 10 feet away. For analysis purposes, data were aggregated over 0.1-mi sections.

The study selected 20 sections of Kansas highways with different pavement types, totaling 215 mi (346 km), out of which 4 sections were jointed concrete pavements (JCP), where faulting was measured using both the KDOT method and AASHTO method and compared. It was found, however, that the faulting values measured were statistically different along all JCP sections tested.

As found in the preliminary data analysis, Kansas is one of the few states that, as Texas also does, observed more faulting mid-lane as compared to the two wheelpaths. This characteristic

might be one of the reasons that the DOTs includes the center of the lane for faulting measurement. If longitudinal profiling will be one of the approaches considered, including a laser to capture mid-lane faulting might be a good idea for application in Texas. However, as the method originated as early as 2003, digital filtering had to be applied for noise removal due to limitation in laser accuracy, failing to fulfill the AASHTO standard for faulting measurement using high-speed inertial profilers (HSIP).

1.1.1.2. Florida DOT

Nazef et al. (2009) conducted a study on the jointed plain concrete pavement (JPCP) roadway along the southbound inside lane of State Road 24 in Waldo, FL. The test section had a total of 2,000 ft (609.6 m) with a 500 ft (152.4 m) lead-in and lead-out, and 1,000 ft (304.8 m) effective test length spanning over 50 slab joints. The slabs were typically 20 ft (6.1 m) by 12 ft (3.7 m) with a relatively smooth surface finish. The study had two main objectives: (i) to use longitudinal profile data to detect and locate transverse joints, and (ii) to estimate the degree of faulting with two alternative methods: one in accordance with the AASHTO R36-04, which identifies n sets of points P1 and P2 located between 3 (76.2 mm) and 8.8 in (223.5 mm) away from a joint and separated by a constant distance of 11.8 in (299.7 mm), where:

$$n = \frac{5.8\ in}{Sampling\ Interval} + 1$$

$$faulting = \sum_{i=1}^{n} \frac{\left|Elev_{P_1} - Elev_{P_2}\right|}{n}$$

referred to as the AASHTO Method. The other method estimated faulting as measured by a faultmeter (2 points 4.5 in (114.3 mm) on either side of a detected joint, faulting = absolute difference in elevation), referred to as the In-House Method.

The used a multi-purpose survey vehicle (MPSV) profiler which performed five repeat passes at two different rates (spacing between consecutive measurements): Rate 1 = 0.6812 in (17.3 mm) and Rate 2 = 1.3624 in (34.6 mm) at a posted speed limit of 45 mph. An algorithm was developed to locate the longitudinal position of joints by identifying peaks and valleys in the elevation profile. At Rate 1, the joint detection rate ranges from 93% to 97% among the 5 runs, while at rate two, the range was 64% to 74%.

The study, however, compared results from two automated approaches, without measurement based on a manual approach to verify their accuracy. A later study by the same group of researchers found that under field conditions, the system had an accuracy level with bias between 0.01 in (0.2 mm) and 0.03 in (0.7 mm), repeatability of 0.025 in (0.6 mm), and reproducibility of 0.04 in (0.9 mm) (Mraz et al., 2012).

1.1.1.3. LTPP AFM

In 2015, FHWA conducted a study using LTPP Program profile data collected with the program's HSIP. The study evaluated both methods described in the AASHTO Standard, as well as a third method, developed based on LTPP profile data, using an automated algorithm to locate the joints, for each of which faulting calculation is achieved by simulating the manual faulting measurement approach using the Georgia Faultmeter (GFM).

The LTPP AFM algorithm performs five tasks: writing the profile into an Engineering Research Division (ERD) file output, importing the ERD file into MATLAB, filtering and normalizing data, detecting joints, and computing faulting. Profile data are collected at a sampling interval of 25 mm (0.98 in) along the left and right wheelpaths as well as the center of the lane over a minimum of five runs on each 152.4-m (500 ft) long test section. A 300-mm (12 data points) (11.8 in) moving average filter is then applied, so that each profile p is used to calculate the smoothed profile P_{fl} by the following equation:

$$P_{fl}(i) = \frac{1}{N} \sum_{j=i-\frac{B}{2\Delta X}}^{i+\frac{B}{2\Delta X}} p(j)$$

Where B is the base length of the moving average (300 mm (11.8 in) in this case), ΔX is the sampling interval (25 mm in (0.98 in) this case), N is the number of samples included in the summation (12 data points in this case). A high-pass filtering is then applied to eliminate the small deviations. A smaller base length is important for accurately detecting transverse joints along profile data. After applying both filters, the filtered profile is normalized with the root-mean-square. Peakdet, a peak detection function in MATLAB developed by Eli Billauer, is used, along with the moving window method, to locate the valleys. The algorithm cross-checks between both wheelpaths and the center of the lane to avoid false positive in joint detection, and the code for it can be found on https://www.mathworks.com/matlabcentral/mlc-downloads/downloads/submissions/48641/versions/1/previews/SCA/peakdet.m/index.html.

The algorithm defines the current elevation point (CEP) at V(i), current elevation position (CEPos) at X(i), and a moving window width of 4 m (13.1 ft). For initialization, the current maximum elevation (CMaE) is set at negative infinity (Inf), current maximum elevation position (CMaEP) at not a number (NaN), current minimum elevation (CMiE) at Inf, and current minimum elevation position (CMiEP) at NaN. The iterative process locating peaks and valleys can be visualized in the flowchart presented in Figure 1.1.

Initialize CMaE=-Inf,
CMaEP=NaN, CMiE=Inf,
CMiEP=NaN, and
A=1

For i =1 to end (i)
CEP=V(i)

If CEP > CMaE, set
CMaE=CEP & CMaEP=X(i)

If CEP < CMiE, set CMiE=CEP
& CMiEP=X(i)

If A=1

If CEP < CMaE-ΔY

No

Yes

Set Peak (i)=CMaE & Store
Peak_Loc(i)=
CMaEP, change CMiEP=X(i),
CMiE=CEP &
A=0

If A=0

If CEP > CMiE+ΔY

Yes

Set Valley (i)=CMiE & Store
Valley_Loc(i)=
CMiEP, change CMaEP=X(i),
CMaE=CEP
& A=1
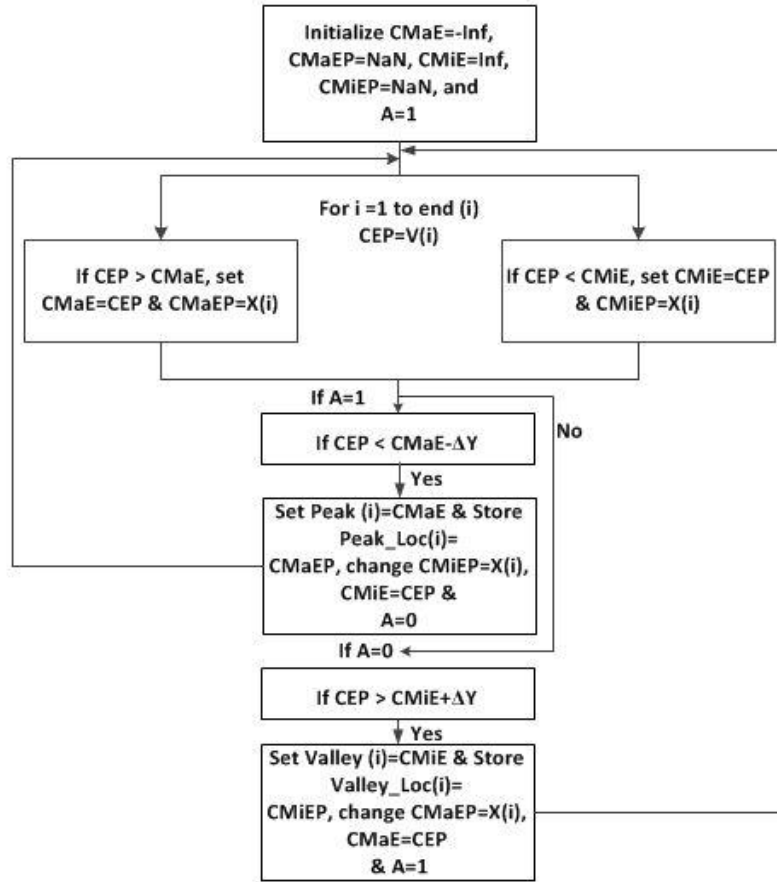
Figure 1.1 Figure 1.1 Peakdet Algorithm Flowchart (Agurla and Lin, 2015)

Two approaches were implemented to minimize the potential of a false positive in joint detection. One was that the difference between the lowest valley coordinates (longitudinal and vertical) between at least two profiles among the three (left wheelpath, right wheelpath, and center lane) should be less than 0.2 m (0.66 ft). The other was that once a true positive joint was established at a location, the next moving window would start at 2.5 m (8.2 ft) from the detected joint since, in this study, consecutive transverse joints in JPCP were spaced at least 3 m (9.8 ft) from each other.

For faulting calculation, apart from the average elevation change method in accordance with the AASHTO standard, a slope method was described, calculating faulting as the difference between the elevation of two points, P_1 and P_2, located on the approach slab and the departure slab, respectively. The two points were selected so that the absolute slope between the joint and both points, calculated as $|S| = \left|\frac{Y_P - Y_J}{X_P - X_J}\right|$ was less than 10, where X_P and Y_P were the position and elevation of either P_1 or P_2, and X_J and Y_J were the position and elevation of the detected joint. Faulting was then reported as the elevation difference between P_1 and P_2.

The findings from the study showed a 95 – 100% joint detection rate (JDR) using the LTPP AFM method, and 58 – 99% JDR using ProVAL, as described by AASHTO Standard Method A. The authors recommended that reducing the profiler sampling interval to less than 25.4 mm (1 in) may lead to better results in both transverse joint detection and faulting measurements.

This study, similarly to the one previously described, only recommended a range of sampling intervals at which joint detection rate improves, while neither of them provided an optimized sampling interval for joint detection. The effectiveness of inertial profiler for joint deterction and faulting calculating is very limited. Todate, available technologies can reduce sampling intervals to a fraction of a millimeter, the potential of using a much narrower sampling interval should be considered.

1.1.2. Three-Dimensional (3D) Profiling

1.1.2.1. 3D Continuous Pavement Data with Laser Crack Measurement System (LCMS)

Tsai et al. (2011) conducted a feasibility analysis on the usage of 3D continuous pavement data for faulting measurement. The study used laser technology integrated into a sensing system to collect 3D continuous pavement profile data at highway speed. The integrated sensing system is composed of a full-size van, a laser crack measurement system (LCMS) mounted on its back to collect continuous transverse profiles, and a high-resolution distance measurement instrument (DMI) on the rear wheel to monitor the interval between two consecutive profiles. The LCMS sensors are designed to have a tilt angle of 12 degree clockwise to the transversal direction to prevent the acquired profiles from aligning with the transverse joints, ensuring that they always intersect, as shown in Figure 1.2.
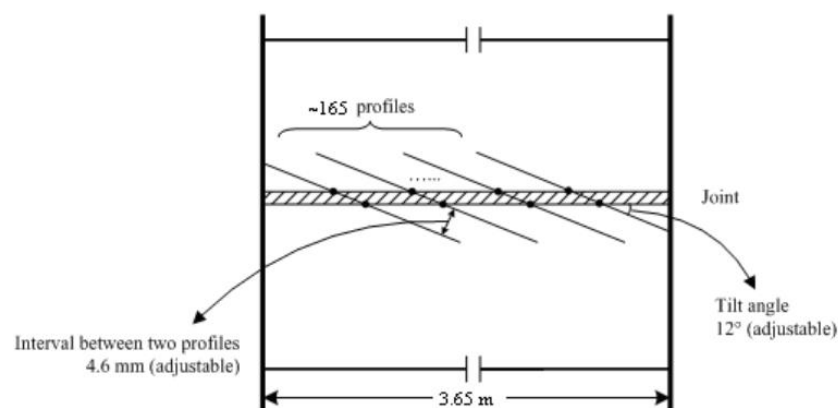
Figure 1.2 Alignment of the 3D Continuous Laser Profiles

With the tilt angle and a 0.18 in (4.6 mm) interval between consecutive profiles, approximately 165 profiles can be collected on a standard lane with a width of 12 ft (3.65 m). Both the tilt angle and the profile interval can be adjusted, and thus changing the number of profiles intersecting

with the joint. The elevation difference between two points, P_1 and P_2, located on two sides of the joint, separated by a distance of 2.0 in (50 mm) along the direction of the profile line, was calculated as the faulting value.

Before the field test was conducted, the researchers first did a set of controlled field tests to evaluate the accuracy and repeatability of the measurements obtained from the 3D continuous profiles under well-controlled environments, consisting of artificially constructed testing sites with known elevation differences ranging from 1/32 to 19/32 inches, which represent the range of the GFM. The average absolute differences were found to be within 0.04 in (1.0 mm) with standard deviations less than 0.02 in (0.5 mm). The only elevation difference the 3D laser failed to reliably detect was the 1/32 in (0.8 mm) one due to the limit of the 0.04 in (1.0 mm) resolution.

For the field test, a 450-ft test section consisting of 15 joints with 30 ft (9 m) × 12 ft (3.65 m) slabs on the eastbound I-16 between milepoints 154 and 155 was selected as the testing site. The integrated sensing system collected data for 3 runs each at 50 mph (80 km/h) and 62.5 mph (100 km/h). The standard deviations across 3 runs were less than 0.04 in (1.0 mm) for both speeds across all 15 joints.

The authors acknowledged the limitation of relatively small data set and pointed out that a more comprehensive validation using a wider variety of faulting depths, surface finishes, vertical grades, cross slopes, and other factors. They also identified the need to develop an algorithm to automate the procedures for joint detection and faulting measurement, and to detect and separate other distresses such as spalling or shoulder dropoff from faulting. The authors later, in a separate study, concluded that the proposed method was capable of taking multiple measurements along a standard lane 12 ft (3.65 m) in width, with approximately 0.87 in (22.1 mm) between two consecutive measurements, and suggested the potential of detecting different types of distresses using the 3D pavement profile data acquired in a single run (Tsai et al, 2012).

1.1.2.2. Laser-based Joint Faulting Meter (LJFM)

Hao et al. (2015) designed a Laser-based Joint Faulting Meter (LJFM) to obtain 3D information on joint faulting using laser triangulation method. The algorithm locates the joints with an automatic threshold determination method and computes faulting with the mean joint faulting value calculation method based on the double peak characteristic of the 3D height histogram. The LJFM is composed of a linear laser source, charge-coupled device (CCD) camera, encoder, industrial computer, and power supply, all assembled onto a vehicle. The laser is line-focused laser with fan angle of 60° and wavelength of 808 nm. It has resolution of 0.5 mm in both the vertical and the transverse directions. Collected data is stored as .dat files each made of 1,000 rows and 1,536 columns. A combination of biphasic standard deviation filtering method and the cascade morphological filtering algorithm was implemented to filter the data in order to ensure the removal of meaningless data while keeping useful details.

The threshold is determined based on the histogram of the profile elevation. Given a data matrix $O_{m \times n}$, the average can be calculated as:

$$avg = \frac{\sum_{i=1}^{m} \sum_{j=1}^{n} O_{ij}}{m \times n}$$

The calculated average was set as the origin of the x-axis. Along the histogram, a peak representing a local mode was to be identified both to the left and to the right of the origin, denoted as val_1 and val_2. If the two points are sufficiently apart, the threshold is calculated as:

$$th = \frac{val_1 + val_2}{2}$$

The elevation of all the data points was then compared to the threshold value *th*. If $M_{ij} > th$, then it was stored into the set O_1, otherwise it was stored into the set O_2. The difference between the averages of the two sets was then calculated as the faulting measurement.

Both indoor and field experiments were conducted to examine the accuracy and precision of the LJFM. With the indoor experiments, simulated joint faulting was constructed with two panels. Parallel, cross, and trapezoidal faulting were each measured with both the LJFM and a precision level. For each simulated faulting site, five points were marked on both panels, and every marked position was measured 10 times by each method. The absolute error between the two testing methods were within 0.5 mm (0.02 in), with an average of 0.27 mm (0.01 in). The standard deviation across the LJFM-measured results ranged from 0.0367 mm (0.0014 in) to 0.3612 mm (0.014 in), with a median value of 0.2017 mm (0.008 in), compared to those of the precision level (ranged from 0.2739 mm (0.01) to 0.8367 mm (0.84 in), with median value 0.5218 mm (0.02 in)).

For the field experiment, 30 sites were random selected for joint faulting measurement, with LJFM-measured results compared to those manually measured with a ruler. The correlation coefficient between the LJFM-measured and ruler-measured faulting values was found to be 0.979, indicating a promising result from the laser-based method.

However, as described in the methodology, the faulting detection system collected data while staying stationary over a joint and stored data for each joint into a single file. Future developments are anticipated to be carried out to open up the possibility of collecting data in motion and even at highway speed. In its current state, this system is not yet applicable to network-level faulting measurement and does not fulfill the requirements specific for this project.

1.1.2.3. PaveVision3D Ultra

Wang et al. (2014) developed a method for performing mask filtering and template matching to calculate faulting. Using Digital Highway Data Vehicle (DHDV) developed by the Way Link

Systems Corporation in collaborations with the University of Arkansas and the Oklahoma State University, incorporating the latest PaveVision3D Ultra (3D Ultra in short). The system can achieve a resolution around 0.3 mm (0.01 in) in vertical direction and 1.1 mm (0.04 in) in longitudinal direction through two separate left and right sensors, and perform full-lane data collection at highway speeds up to 96 km/h (60 mph). The DHDV-collected 3D profile data is first stored as raw image composed of samples each being 4,096 by 4,096 pixels in size. After the implementation of the neighborhood averaging method for data reparation and a high-pass moving average filter to remove unwanted noise while retaining important details, the template matched algorithm is applied to detect and identify the location of joints. The concept behind the algorithm is predefined filters that match the features of the joints and use these othe filters to match with features in the profile.

When defining the design filters, the cross section of the transverse joints is assumed to be a Gaussian-like shape, distributed as follows:

$$T(i) = -k \times \frac{1}{\sqrt{2\pi}\sigma} \exp\left(-\frac{i^2}{2\sigma^2}\right) \forall i \in (-N, N)$$

Where $T(i)$ = the discrete Gaussian distribution at location i;

k = the reciprocal of the standard deviation (σ); and

$N = 3\sigma$, representing the template window size.

To account for different joint widths, six templates with different σ are designed. There are two approaches for valley identification: (i) using the cross correlation (R) or the Minimum Square Errors (MSE) between the target profile section and the predefined template, or (ii) by convoluting the predefined kernel with the filtered profile and comparing the convolution coefficients with adaptive thresholds. The study selected the second approach. Based on the convolution outputs of the six defined templates, a standard deviation of two was selected.

Joints and cracks are distinguished and classified following the flowchart in Figure 1.3, starting from the first joint location. The location of the first joint may be manually designated using a supplementary function. Two variables: Nominal Joint Spacing (NJS) and Joint Window (JW) are used to estimate the potential location of the next joint, represented by the variable Next Joint Location (NeJL). If no spikes are identified within the range, the Nominal Joint Location (NoJL), calculated as the known joint location plus the NJS, is set as the NeJL. If more than one spikes are found within the range, the one closest to the NoJL is taken as the NeJL, while the rest are classified as cracks. Some pre-knolwedge of the pavement section characteristic (such as approximated joint spacing) is required to ensure accuracy.
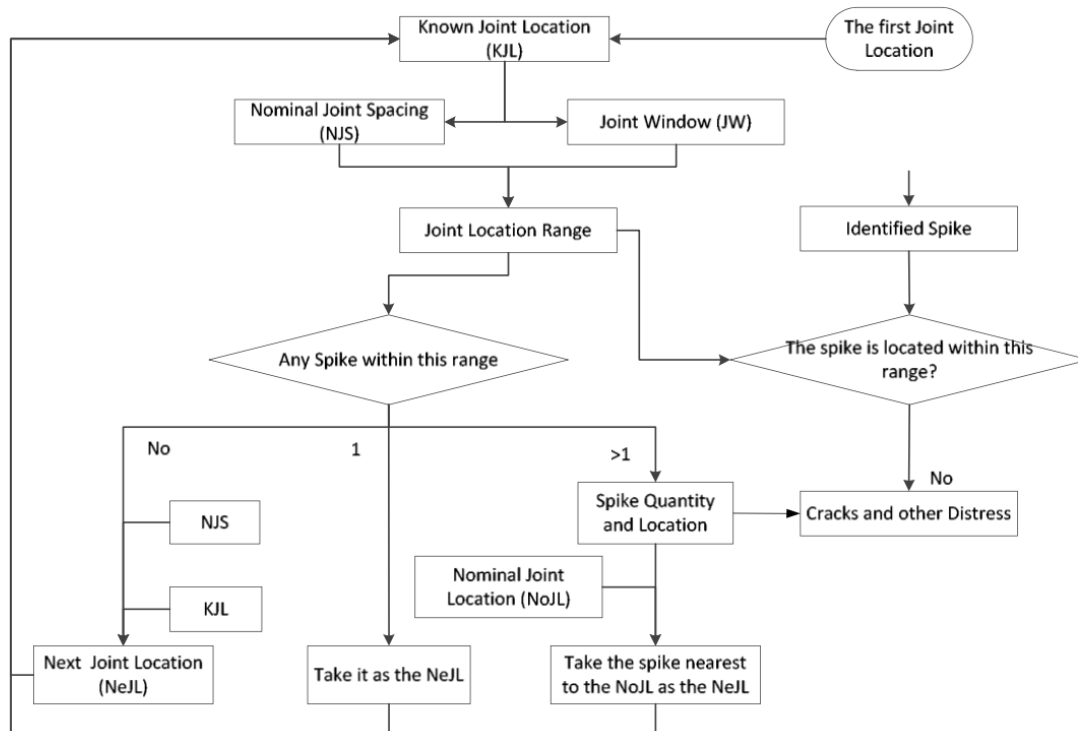
Figure 1.3 Flowchart for Distinguishing and Classifying Joints and Cracks (Wang et al., 2014)

The location and number of joints is calculated after all joints have been identified, as well as their dimensions in width and depth. Faulting is measured for all joints in accordance with the AASHTO method to the nearest 1.0 mm (0.04 in).

To validate the method, a test site was selected along a one-lane of JPCP located on N Husband St in Stillwater, OK. The test section was 1,200 ft (365.8 m) long with 300 ft (9.1 m) of lead-in and lead-out along with 600 ft (182.9 m) effective test sample. There were over 40 slabs, each approximately 15 ft × 12 ft (4.57 m x 3.65 m) in dimension. Measurements conducted with the 3D approach, as described above, were compared to those obtained using downward spike algorithm implemented in ProVAL. With a lack of actual field faulting data, the accuracy of the faulting calculation across the two methods could not be established. However, the proposed method obtained a 100% joint detection rate, which the ProVAL method failed to achieve.

Chapter 2. AASHTO Specifications

2.1. AASHTO R 36-04

Initially published in 2004 as AASHTO PP 38, this version was the earliest practice standardizing the procedures for faulting estimation and summarization on concrete pavement surfaces, with descriptions for both automated and manual measurement methods. It was later published as AASHTO R 36-04 in 2009. According to the standard, faulting should be calculated to the nearest 1.0 mm (0.04 in.) by the following formula:

$$F = P_1 - P_2$$

Where, F = faulting that is the absolute value for the measured difference, mm; and P_1, P_2 = heights measured on either side of a transverse joint or transverse crack in the outside wheelpath, in mm.

The standard sets the length of the data summary interval to be either 0.1 km or 0.1 mi and demands faulting measurements to be made across all transverse joints or cracks in the right wheelpath of the survey lane.

For automated surveys, measurements are taken at points 3.0 to 8.8 in (75 to 225 mm) from the joint or crack separated by a constant distance of 11.8 in (300 mm), as shown in Figure 2.1.
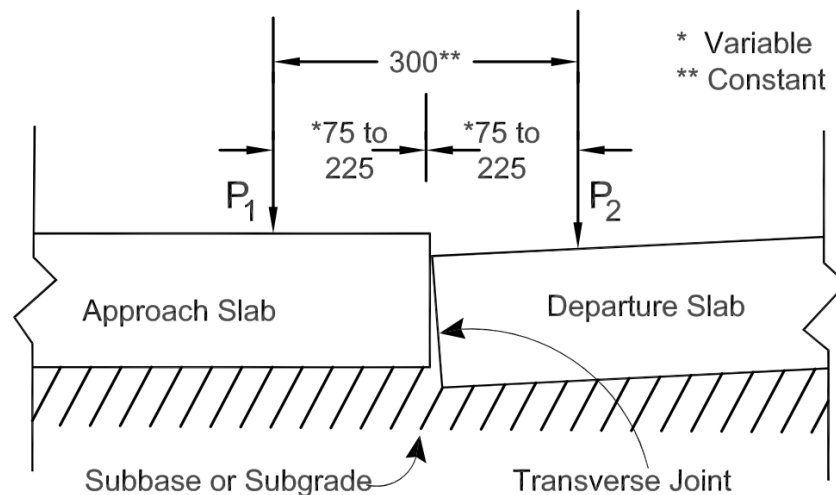
Note: All dimensions shown in millimeters unless otherwise noted.

Figure 2.1 Points to Measure for Faulting by Automated Measurements (AASHTO, 2009)

For manual measurements, a sampling rate of at least 10% of all transverse joints or transverse cracks is required, with the 10% being uniformly spaced throughout the project and locations

documented. It is obvious that this standard was developed accounting for the equipment that was available at that time.

2.2. AASHTO R 36-12

The AASHTO standard practice was revised in 2012 so that the effects from grade or slope are accounted for when measuring faulting. A more detailed description for using the Automated Fault Measurement (AFM) module in the FHWA Profile Viewing and Analysis (ProVAL) software is provided in this version of the standard. However, although it is required that all joint and crack locations be identified in the profile data for project level and joints with measurable faults to be identified for network level, no specification is provided in this version regarding the procedures for joint identification.

2.3. AASHTO R 36-13

The revised version, which was published in 2013, incorporated the automated joint detection methods of downward spike detection, step detection, and curled edge detection, as well as an alternative automated faulting measurement approach which combines the two steps of joint detection and faulting calculation.

2.4. AASHTO R 36-17

Consistent with its original version, the current standard includes the best practice for both manual and automated measurement approaches. And, in accordance with the update in 2012, both methods include means to remove the effects from grade or slope. For the manual approach, an illustration of the standard practice for measurement is shown in Figure 2.2.
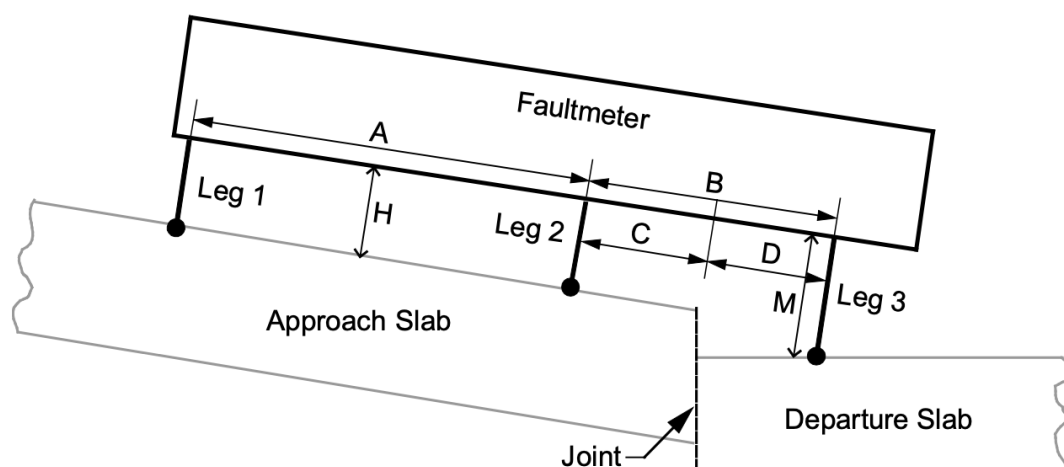
Figure 2.2 Manual Faulting Measurement Using a Faultmeter (AASHTO, 2017)

Faulting is calculated using the formula

$$F = M - H$$

Where:

F = faulting, mm (in);

M = height for measurement Leg 3, mm (in);

H = height for Leg 1 and Leg 2, mm (in);

A = distance between Leg 1 and Leg 2, mm (in);

$B = C + D$, recommended to be 300 mm (11.8 in);

C = distance between Leg 2 and the joint location with a value between 76 mm and 226 mm (3 in and 8.9 in); and

D = distance between the joint location and Leg 3 with a value between 76 mm and 226 mm (3 in and 8.9 in).

The AASHTO R 36-17 Standard describes two automated approaches for using high-speed inertial profilers (HSIP): (i) Method A, which is a two-step process utilizing the automated faulting measurement (AFM) module in the FHWA ProVAL software, and (ii) Method B, which combines the joint/crack location identification and fault calculation into a single process using Automated Fault Program (AFP), an Excel-based application developed by Florida Department of Transportation under the AASHTO Technology Implementation Group (TIG) program. For both methods, HSIP equipment in compliance with AASHTO Standard M 328-14 should be operated in accordance with AASHTO Standard R 57-14, with repeatability score no less than 92% and accuracy score no less than 90% based on cross correlation under AASHTO Standard R 56-14. A sampling interval of 0.75 in (19 mm) is required for a project-level survey, and 1.5 in (38 mm) required for a network-level survey, covering both left and right wheelpaths. Digital filtering is not allowed during postprocessing of data.

2.4.1. Method A

In Method A, joint and crack locations are first identified using an automated process, composed of three methods: downward spike detection, step detection, and curled edge detection.

2.4.1.1. Downward Spike Detection

The downward spike detection method derived from Chang et al. (2008)'s algorithm was originally developed to isolate individual slab profiles for analyzing curling and warping. This is accomplished by searching for narrow dips repeatedly appearing in multiple synchronized

measurements using a high-pass filter with cutoff at wavelength of 9.84 in (250 mm), normalizing the filtered profile with its root mean squares (RMS), can be calculated as follow:

$$RMS = \sqrt{\frac{1}{N} \sum_{n=1}^{N} |X_n|^2}$$

The following step is detecting from the obtained spike profile the locations exceeding the threshold value of –4.0. A clearance width of 0.5 m (1.64 ft) is set to ensure no two points located within such a distance between each other can both be identified as downward spikes.

2.4.1.2. Step Detection

The step detection method was derived from Mississippi DOT's BATCHCALCFAULT Software. In this method, an elevation difference is first calculated between each pair of consecutive data points. When a threshold level of 0.08 in (2.032 mm) is exceeded by an absolute value of elevation difference, a "step" is identified. A clearance width of 3.0 ft (0.91 m) is set to ensure no two points located within such a distance between each other can both be identified as steps.

2.4.1.3. Curled Edge Detection

In the curled edge detection method, a bandpass moving average filter with short cutoff at wavelength of 9.84 in (250 mm) and long cutoff at wavelength of 150 ft (50 m) is first applied to the profile. Then, conducting a 9.8 ft (3.0 m) rolling straightedge simulation, the locations are identified where the initial threshold level of 0.12 in (3.0 mm) is exceeded by the simulated rolling straightedge responses. A clearance width of 0.5 m (1.64 ft) is set to ensure no two points located within such a distance between each other can both be identified as downward spikes.

For all three methods, the identified locations are expected to include both joints and cracks, which should then be manually inspected to differentiate. For each joint identified, an 8 ft (2.44 m) profile segment is cropped centered around the joint, with 48 in (1,219 mm) of approach slab and equal length of departure slab. Within 3.0 in (76 mm) from the joint, the profile slice is marked on both sides. Least squares fitting is first performed from the approach side and extend to the departure side for an offset between 76 mm and 226 mm (3 in and 8.9 in). The elevations of all data points within the offset at the downstream end of the fitted line are recorded as $P_1{}^i$. Another least squares fitting is then performed from the downstream end toward the joint. The elevations of all data points matching the horizontal locations for $P_1{}^i$ measurements are recorded as $P_2{}^i$. This procedure is shown in Figure 2.3.
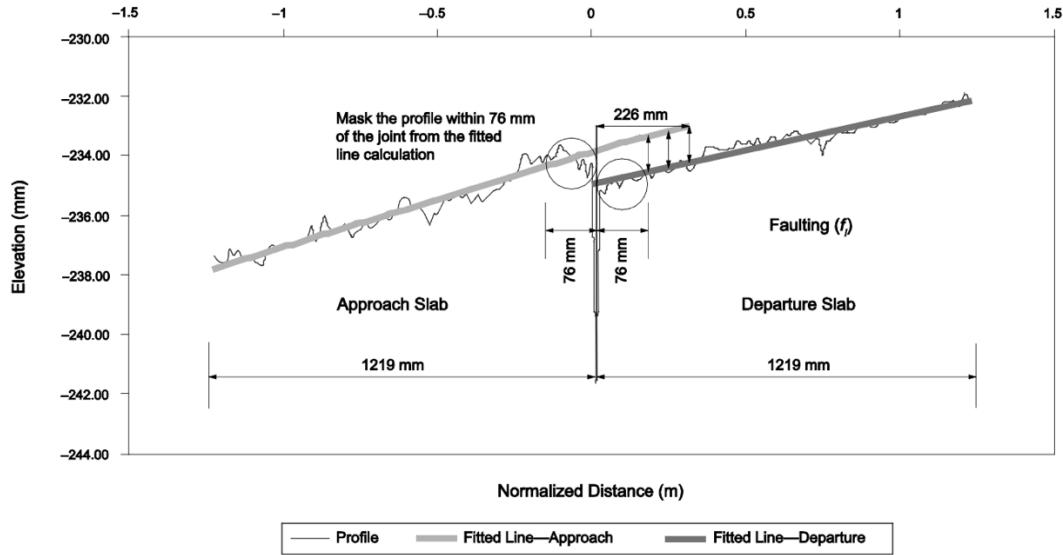
Figure 2.3 Curve-Fitting of Cropped Profile Slices and Computation of Faulting (AASHTO, 2017)

The difference in elevation between each pair of $P_1{}^i$ and $P_2{}^i$ is computed as individual elevation differences (f_i), which is then used in the following formula for calculating faulting:

$$F = \frac{\sum_{i=1}^{n} f_i}{n} = \frac{\sum_{i=1}^{n}(P_1^i - P_2^i)}{n}$$

F = calculated faulting, mm (in.);

f_i = elevation differences between P^i and P^i at locations of data points within the offset range, mm (in);

n = number of data points within the offset range;

P_1^i = elevation at the fitted line for the profile slice on the approach slab at locations of data points within the offset range, mm (in); and

P_2^i = elevation at the fitted line for the profile slice on the departure slab at locations of data points within the offset range, mm (in).

2.4.2. Method B

Method B is the procedure used by the Excel-based application Automated Fault Program (AFP) developed by the Florida Department of Transportation under the AASHTO Technology Implementation Group program. It combines the two steps of joint/crack identification and faulting calculation into a single process.

In this method, an initial sensitivity factor (*SF*) is first defined as follows:

16

$$SF = 0.01 \times SA$$

Where *SA* is the profile sampling interval in in or mm.

Between each pair of consecutive profile elevation points, a vertical grade in in/in or mm/mm is calculated and, when the predetermined SF is exceeded by the vertical grade, a joint or crack location is identified. For each identified joint, there should be n sets of points P_1 and P_2 located 3.0 in (76.2 mm) to 8.8 in (223.5 mm) away from it, and each set of points are separated by a constant distance of 11.8 in, with their individual elevation differences (f_i) used to calculate faulting, as shown in Figure 2.4.
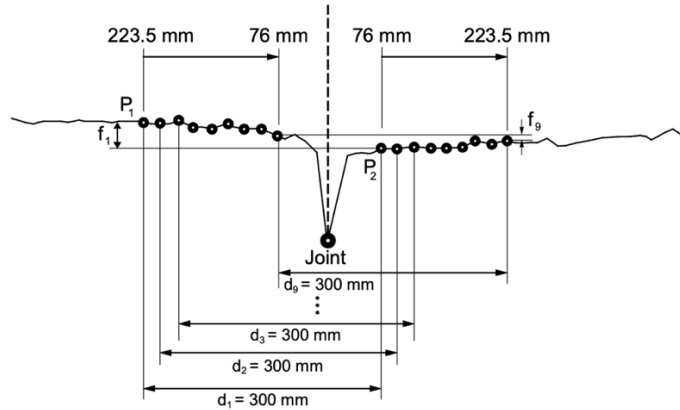
Figure 2.4 Profile Elevation Points P1 and P2 Used to Estimate Faulting (AASHTO, 2017)

Similar to Method A, the individual elevation change is averaged over the n pairs of P_1 and P_2 to compute faulting.

$$F = \frac{\sum_{i=1}^{n} f_i}{n} = \frac{\sum_{i=1}^{n}(P_1 - P_2)_i}{n}$$

F= calculated faulting, mm (in);

f_i= individual elevation change, mm (in); and

n= number of data sets, P_1 and P_2, within the 76.2 mm (3.0 in) to 223.5 mm (8.8 in) range from the center of a joint or crack.

The theoretical joint count JC_T can be obtained based on the total length of the tested pavement section (*TL*) and the slab length (*SL*), calculated by the formula

$$JC_T = \frac{TL}{SL}$$

TL and *SL* can be either in ft or m but must be consistent as JC_T is unitless.

Up to nine additional iteration attempts are recalculated and stored to optimize the sensitivity factor in order to match the detected number of joints to the theoretical number, and in each iteration, joint locations and faulting magnitudes.

2.5. AASHTO R 36-21

The AASHTO R 36-21 Standard introduces an additional automated calculation method utilizing 3D data. The standard consists of the following steps:

- Step 1: identify a point (A) 178 mm (7 in) away from the right edge of the lane marking, as shown in **Figure 2.5**.
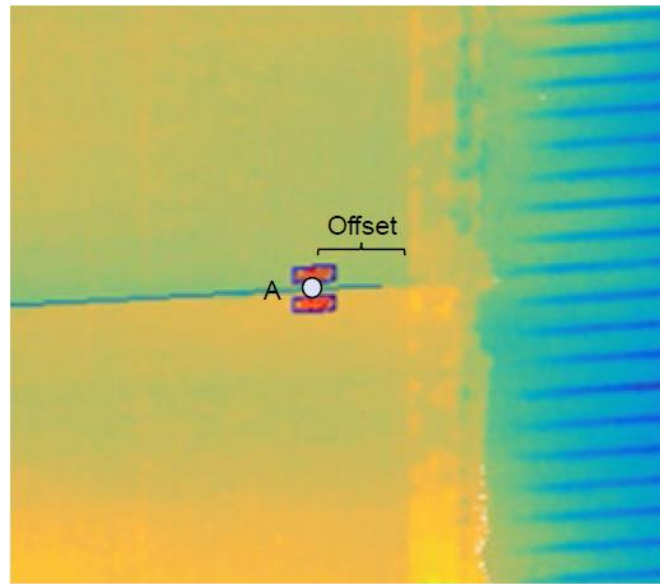
Figure 2.5 View of Joint Showing Offset to point A

$$o(mm) = 60 + \frac{w}{2}\tan\theta$$

Where: w = width of the box (100 mm (4 in)) and θ = angle made by the joint with the transverse direction. This is for skewed joints, and so o (mm) = 60 for perpendicular joints.

- Step 2: Locate the bottom center of box (P) at a point o distance away from A along the direction of travel and top center of box (Q) at a point o distance away from A along the opposite of the direction of travel. The width of the boxes is w = 100 mm (4 in) and height is h = 50 mm (2 in) as shown in **Figure 2.6**.
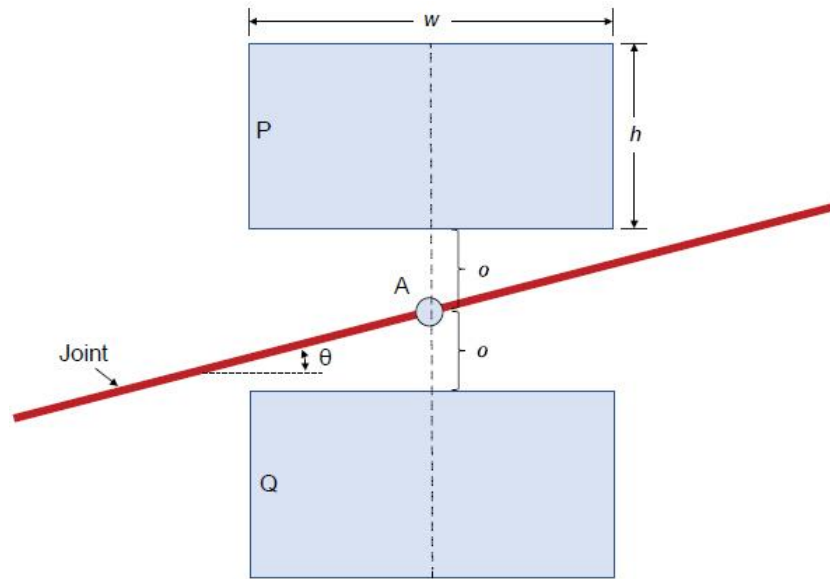
Figure 2.6 Offsetting Smoothing Boxes from Point A

Chapter 3. Preliminary Variability Analysis

The variability of faulting of jointed concrete pavements in the longitudinal and transverse directions were both assessed, as previous studies found that a single point faulting measurement does not represent the actual faulting across a joint.

To address this question, a variability study on field data was carried out. During the data collection process, three sections were chosen in the town of Rockdale, each containing 11 joints. All the joints were first numbered from 1 to 180 in ascending order consecutively. The first section contains joints with numbers 5 through 15, the second section from 97 to 107, while the third from 170 to 180. These numbers were uniquely used to define the joints. Along each joint, 13 locations in the transverse direction, with each adjacent pair separated by 1.0 ft distance were labeled with paint, as shown in Figure 3.1. These painted labels were used to identify locations for faulting measurement, so that along each joint, 13 measurements were taken, one at each of the labels. A manual faultmeter was used to manually measure the faulting value.

Figure 3.1 Paint Marking along Joint 107 as an Example

Figure 3.2 shows a manual faulting measurement tool called the HM-faultmeter. It consists of a reference surface, a measurement surface, and a digital dial. In the field, the tool was placed across the joint and the measurement surface would slide up or down. Then the digital dial shows the actual faulting reading with a resolution of 10 micrometer.

Figure 3.2 HM-Faultmeter

While taking measurements, the base of the faultmeter was set on the edge of the approach slab, while the movable foot was adjusted so that it touched the departure slab. The reading was given automatically by the faultmeter was then recorded. When the approach slab was higher, the reading is positive, and when the departure slab was higher, the reading is negative, consistent with the standard practice. The operation of the faultmeter is as shown in Figure 3.3.

Figure 3.3 Operating the Faultmeter in Field Data Collection

3.1. Transverse Variability

Transverse variability refers to the variability in faulting measured at different locations within the same joint. With the collected field data, for example, measurements were taken at 13 equally-spaced locations along each joint. A standard deviation was calculated among the 13 values and reported for each joint. In order to have an idea on how variability compares to the magnitude of faulting, the average faulting was also calculated, and a coefficient of variation (COV) was obtained by taking the ratio of the standard deviation over the average. A majority of the standard deviations were greater than the averages in terms of magnitude. The transverse variability along all joints was as shown in Table 3.1.

Table 3.1 Transverse Variability Across All Three Sections

Joint	1'	2'	3'	4'	5'	6'	7'	8'	9'	10'	11'	12'	13'	Average	Std. Dev.	COV
5	0.03	1.04	0.89	0.8	1.37	0.38	0.75	1.78	0.44	0.95	0.43	0.6	0.76	0.786	0.452	57.5%
6	-0.71	0.3	0.04	-0.41	0.11	-0.02	-0.03	0.36	0.29	0.9	0.47	0.59	0.09	0.152	0.416	273.1%
7	0.33	0.24	0.52	1.04	0.9	0.45	-0.36	1.06	0.11	0.38	0.41	-0.72	-0.64	0.286	0.575	201.1%
8	-0.62	0	0	-0.9	-0.26	0	0.09	0.25	-0.5	0.7	-0.34	0.78	-0.25	-0.081	0.481	-595.3%
9	1.46	1.52	0.32	-0.12	0.67	0.44	0.68	0.57	0.46	0.45	0.27	0.33	0.69	0.595	0.452	75.9%
10	1.76	0.39	-0.12	0.79	1.43	0.45	-0.01	-0.03	0.41	0.72	0.34	0.15	-0.25	0.464	0.593	127.9%
11	1.06	-0.11	0.47	0	-0.05	0.21	0.1	-0.13	-0.32	0.07	-0.04	0.76	0.53	0.196	0.398	202.7%
12	0.51	0.9	-0.28	1.2	0.48	3.37	0.03	0.05	0.23	0.28	0.32	0.73	-0.04	0.598	0.926	154.7%
13	0.04	0.36	-0.5	-0.3	0.16	0.08	-0.38	0.22	0.54	0.46	-0.36	0.44	0.39	0.088	0.362	409.2%
14	0.31	0.15	0	0.24	-0.09	0.32	-0.16	-0.37	-0.75	-0.38	0.03	-0.44	-0.73	-0.144	0.367	-255.0%
15	-0.28	-0.37	-0.13	-0.9	0.24	-0.58	0.44	-0.06	-0.72	-0.17	-0.34	-0.78	0.06	-0.276	0.400	-144.7%
97	0.07	0.18	1.07	0.73	0.13	0.31	0.64	0.48	-0.19	1.05	0.23	-0.1	0.29	0.376	0.399	106.2%
98	0.95	0.08	0.12	0.58	0.72	1.33	0.64	0.95	0.84	0.47	0.86	0.41	0.44	0.645	0.350	54.3%
99	1.11	0.13	0.76	0.54	0.54	0.96	0.92	1.36	0.87	-0.33	0.4	1.1	0.86	0.709	0.453	63.9%
100	3.02	3.52	4.23	-0.59	0.91	-2.22	-1.92	-2.94	-0.39	-1.36	-3.66	-0.99	-3.32	-0.439	2.626	-597.8%
101	-0.88	0.1	0.63	0	0.77	0.65	0.25	0.81	0.08	0.54	0.26	0.18	-0.06	0.256	0.453	176.9%
102	-0.42	-0.46	-0.63	-0.14	-0.25	0	-0.36	-0.09	-0.2	-0.07	-0.57	-0.82	-0.21	-0.325	0.245	-75.5%
103	1.27	0.76	-0.33	-0.52	-0.62	-0.25	-0.32	0.95	-0.3	-0.38	-0.42	-0.23	-0.59	-0.075	0.630	-835.4%
104	0.02	0.39	-0.15	0.08	0.71	0.26	0.36	-0.13	0.38	0.06	-0.27	-0.38	-0.04	0.099	0.308	310.4%
105	-0.39	-0.33	-0.48	-0.04	-0.26	-0.22	0.39	-0.03	-0.84	0.2	0.16	-0.19	-0.07	-0.162	0.321	-198.6%
106	0.64	0.67	0.11	0.43	0.26	0.74	0	-0.22	0.27	0.16	-0.64	-0.11	-1.18	0.087	0.543	624.3%

107	-0.35	-0.01	-0.24	-0.42	-0.16	-0.61	0.79	-0.49	-0.33	0.07	0.14	-0.34	-0.9	-0.219	0.414	-188.7%
170	1.35	-0.82	0.87	0.5	1.49	0.87	0.56	1.09	2.4	1.72	0.5	2.08	2.25	1.143	0.883	77.2%
171	3.07	1.25	1.67	0.09	-0.12	0.07	0.01	0.32	0.04	2.77	0.74	0.69	0.28	0.837	1.064	127.1%
172	1.11	-0.68	-0.16	1.2	0.65	0.55	0.34	0.32	0.76	1.36	0.26	0.61	0.2	0.502	0.558	111.3%
173	0.7	0.33	0.86	1.09	0.92	0.28	0.17	0.32	0.33	0.81	0.21	-0.04	0.3	0.483	0.348	71.9%
174	0.5	0.67	0.62	1.37	0.72	-0.13	-0.55	0.14	1.07	0.19	1.24	-0.48	1.07	0.495	0.628	126.9%
175	0.71	0.29	1.57	1.16	0.85	0.21	1.14	0.7	3.95	5.23	5.18	5.28	-0.18	2.007	2.088	104.0%
176	-0.09	1.57	0.7	0.68	0.98	0.67	0.63	1.26	0.19	1.15	0.8	0.48	0.49	0.732	0.441	60.3%
177	0.03	0.21	0.73	0.4	0.42	0.28	0.24	0.62	0.05	0.72	-0.13	0	0.09	0.282	0.281	99.9%
178	0.2	-0.39	-0.09	0.29	-0.05	0.12	0	0.17	0.25	0.76	0.44	0.73	0.07	0.192	0.319	165.9%
179	0.71	0.67	0.16	-0.8	-0.54	0	0	0.6	0.39	0.43	-0.11	0.03	-0.3	0.095	0.465	487.2%
180	0.33	-0.52	-0.25	-0.59	0.41	-0.34	-0.72	-0.52	0.13	-0.46	0.65	0.84	-0.14	-0.091	0.511	-562.8%

3.2. Longitudinal Variability

Longitudinal variability refers to the faulting variability measured at different joints along a section. For each section, average and standard deviation of faulting across all 11 joints were calculated at each of the 13 measurement locations, and the coefficient of variation was calculated. Longitudinal variability was slightly higher than transverse variability in magnitude, as all the standard deviations were greater than the mean along the longitudinal direction. This was partly due to the fact that the transverse variability was within the same joint distributed along a lane approximately 13 ft (3.96 m) wide, while the longitudinal variability was measured along 11 different joints spread over an entire section. The longitudinal variability across three sections is shown in Table 3.2 through Table 3.4.

Table 3.2 Longitudinal Variability Across Section 1

Joint	1'	2'	3'	4'	5'	6'	7'	8'	9'	10'	11'	12'	13'
5	0.03	1.04	0.89	0.8	1.37	0.38	0.75	1.78	0.44	0.95	0.43	0.6	0.76
6	-0.71	0.3	0.04	-0.41	0.11	-0.02	-0.03	0.36	0.29	0.9	0.47	0.59	0.09
7	0.33	0.24	0.52	1.04	0.9	0.45	-0.36	1.06	0.11	0.38	0.41	-0.72	-0.64
8	-0.62	0	0	-0.9	-0.26	0	0.09	0.25	-0.5	0.7	-0.34	0.78	-0.25
9	1.46	1.52	0.32	-0.12	0.67	0.44	0.68	0.57	0.46	0.45	0.27	0.33	0.69
10	1.76	0.39	-0.12	0.79	1.43	0.45	-0.01	-0.03	0.41	0.72	0.34	0.15	-0.25
11	1.06	-0.11	0.47	0	-0.05	0.21	0.1	-0.13	-0.32	0.07	-0.04	0.76	0.53
12	0.51	0.9	-0.28	1.2	0.48	3.37	0.03	0.05	0.23	0.28	0.32	0.73	-0.04
13	0.04	0.36	-0.5	-0.3	0.16	0.08	-0.38	0.22	0.54	0.46	-0.36	0.44	0.39
14	0.31	0.15	0	0.24	-0.09	0.32	-0.16	-0.37	-0.75	-0.38	0.03	-0.44	-0.73
15	-0.28	-0.37	-0.13	-0.9	0.24	-0.58	0.44	-0.06	-0.72	-0.17	-0.34	-0.78	0.06
Avg.	0.354	0.402	0.110	0.131	0.451	0.464	0.105	0.336	0.017	0.396	0.108	0.222	0.055
SD.	0.801	0.550	0.402	0.745	0.579	1.011	0.377	0.614	0.494	0.425	0.332	0.594	0.503
CoV	226.4%	136.9%	365.2%	568.9%	128.3%	218.1%	360.2%	182.6%	2862.1%	107.3%	306.5%	267.9%	907.7%

Table 3.3 Longitudinal Variability Across Section 2

Joint	1'	2'	3'	4'	5'	6'	7'	8'	9'	10'	11'	12'	13'
97	0.07	0.18	1.07	0.73	0.13	0.31	0.64	0.48	-0.19	1.05	0.23	-0.1	0.29
98	0.95	0.08	0.12	0.58	0.72	1.33	0.64	0.95	0.84	0.47	0.86	0.41	0.44
99	1.11	0.13	0.76	0.54	0.54	0.96	0.92	1.36	0.87	-0.33	0.4	1.1	0.86
100	3.02	3.52	4.23	-0.59	0.91	-2.22	-1.92	-2.94	-0.39	-1.36	-3.66	-0.99	-3.32
101	-0.88	0.1	0.63	0	0.77	0.65	0.25	0.81	0.08	0.54	0.26	0.18	-0.06
102	-0.42	-0.46	-0.63	-0.14	-0.25	0	-0.36	-0.09	-0.2	-0.07	-0.57	-0.82	-0.21
103	1.27	0.76	-0.33	-0.52	-0.62	-0.25	-0.32	0.95	-0.3	-0.38	-0.42	-0.23	-0.59
104	0.02	0.39	-0.15	0.08	0.71	0.26	0.36	-0.13	0.38	0.06	-0.27	-0.38	-0.04

105	-0.39	-0.33	-0.48	-0.04	-0.26	-0.22	0.39	-0.03	-0.84	0.2	0.16	-0.19	-0.07
106	0.64	0.67	0.11	0.43	0.26	0.74	0	-0.22	0.27	0.16	-0.64	-0.11	-1.18
107	-0.35	-0.01	-0.24	-0.42	-0.16	-0.61	0.79	-0.49	-0.33	0.07	0.14	-0.34	-0.9
Avg.	0.458	0.457	0.463	0.059	0.250	0.086	0.126	0.059	0.017	0.037	-0.319	-0.134	-0.435
SD.	1.104	1.080	1.360	0.462	0.517	0.957	0.799	1.160	0.531	0.615	1.197	0.569	1.121
CoV	241.1%	236.1%	293.9%	781.0%	206.8%	1107.8%	631.9%	1963.4%	3072.0%	1649.9%	-375.1%	-425.8%	-258.0%

Table 3.4 Longitudinal Variability Across Section 3

Joint	1'	2'	3'	4'	5'	6'	7'	8'	9'	10'	11'	12'	13'
170	1.35	-0.82	0.87	0.5	1.49	0.87	0.56	1.09	2.4	1.72	0.5	2.08	2.25
171	3.07	1.25	1.67	0.09	-0.12	0.07	0.01	0.32	0.04	2.77	0.74	0.69	0.28
172	1.11	-0.68	-0.16	1.2	0.65	0.55	0.34	0.32	0.76	1.36	0.26	0.61	0.2
173	0.7	0.33	0.86	1.09	0.92	0.28	0.17	0.32	0.33	0.81	0.21	-0.04	0.3
174	0.5	0.67	0.62	1.37	0.72	-0.13	-0.55	0.14	1.07	0.19	1.24	-0.48	1.07
175	0.71	0.29	1.57	1.16	0.85	0.21	1.14	0.7	3.95	5.23	5.18	5.28	-0.18
176	-0.09	1.57	0.7	0.68	0.98	0.67	0.63	1.26	0.19	1.15	0.8	0.48	0.49
177	0.03	0.21	0.73	0.4	0.42	0.28	0.24	0.62	0.05	0.72	-0.13	0	0.09
178	0.2	-0.39	-0.09	0.29	-0.05	0.12	0	0.17	0.25	0.76	0.44	0.73	0.07
179	0.71	0.67	0.16	-0.8	-0.54	0	0	0.6	0.39	0.43	-0.11	0.03	-0.3
180	0.33	-0.52	-0.25	-0.59	0.41	-0.34	-0.72	-0.52	0.13	-0.46	0.65	0.84	-0.14
Avg.	0.784	0.235	0.607	0.490	0.521	0.235	0.165	0.456	0.869	1.335	0.889	0.929	0.375
SD.	0.874	0.782	0.650	0.718	0.580	0.354	0.523	0.484	1.231	1.541	1.479	1.589	0.725
CoV	111.5%	333.4%	107.0%	146.6%	111.3%	151.1%	315.9%	106.1%	141.7%	115.5%	166.3%	171.1%	193.2%

3.3. Variability Analysis

Due to the large number of measurements, the central limit theorem applies, and the assumption of normality is valid. For a normal distribution, a 95% confidence interval (CI) for a random variable is given by:

$$95\% \; CI = \left(\bar{x} - 1.96 \frac{\sigma_{overall}}{\sqrt{n}}, \; \bar{x} + 1.96 \frac{\sigma_{overall}}{\sqrt{n}} \right)$$

Thus, the width of the 95% CI is given by:

$$w = 3.92 \frac{\sigma_{overall}}{\sqrt{n}}$$

25

Since the width of the confidence interval is a measure of the desire precision then, for example, to ensure a 1.0 mm (0.04 in) wide 95% CI, the minimum number of faulting measurements should be:

$$n = \left(3.92 \cdot \frac{\sigma_{overall}}{1\ mm}\right)^2$$

If along a 0.1 mi (160 m) long section, the true distribution of individual joint faulting values has a mean of μ and standard deviation of σ, when n joints are sampled, with n being sufficiently large, by central limit theorem, the reported average faulting $\bar{X}$ across the n joints follows approximately a normal distribution with mean of μ and standard deviation of $\frac{\sigma}{\sqrt{n}}$. Then, the measured average faulting across this section can be reported as $\bar{X} \pm Z_{1-\frac{\alpha}{2}} \frac{\sigma}{\sqrt{n}}$ to a confidence level of α. The goal of the variability analysis is to approximate the value of σ.

Overall variability across all 143 measurements was calculated for each section, with standard deviations of 0.595 mm (0.02 in), 0.931 mm (0.037 in) and 0.991 mm (0.039 in) across the three sections, respectively. The third section had the highest standard deviation among the three.

Obviously, for different levels of confidence and different required precision, the sample size needed to meet the demanded precision will vary. When different confidence levels are required with a 1.0-mm measurement precision, the number of measurement points needed (sample size) is accordingly calculated, as listed in Table 3.5.

Table 3.5 Number of Measurement Points Needed to Achieve 1 mm Width Confidence Intervals Based on Overall Variability

Confidence Interval	Number of Measurement Points Needed based on Section 1	Number of Measurement Points Needed based on Section 2	Number of Measurement Points Needed based on Section 3
80%	3	6	7
85%	3	8	9
90%	4	10	11
95%	6	14	16

However, according to Rao et al. (1999), faulting is typically not noticeable until the pavement section faulting averages about 2.5 mm (0.1 in). If precision level is set as 2.0 mm (0.08 in) rather than 1.0 mm (0.04 in), the number of measurement points reduces by a factors of four from the values presented in Table 3.5.

On the other hand, assuming a known standard deviation and achievable sample size, the width of the (1- α) confidence interval can be calculated by the following equation:

$$w = 2 \cdot z_{\alpha/2} \frac{\sigma}{\sqrt{n}}$$

The number of points needed to be sampled to achieve confidence levels at different widths are as shown in Table 3.6 through Table 3.8 for Sections 1, 2, and 3, respectively.

Table 3.6 Determination of Sample Size for Given Precision and Confidence Level for Section 1

	1.0 mm	1.5 mm	2 mm	2.5 mm
50%	1	1	1	1
60%	2	1	1	1
70%	2	1	1	1
80%	3	2	1	1
85%	3	2	1	1
90%	4	2	1	1
95%	6	3	2	1

Table 3.7 Determination of Sample Size for Given Precision and Confidence Level for Section 2

	1.0 mm	1.5 mm	2 mm	2.5 mm
50%	2	1	1	1
60%	3	2	1	1
70%	4	2	1	1
80%	6	3	2	1
85%	8	4	2	2
90%	10	5	3	2
95%	14	6	4	3

Table 3.8 Determination of Sample Size for Given Precision and Confidence Level for Section 3

	1.0 mm	1.5 mm	2 mm	2.5 mm
50%	2	1	1	1
60%	3	2	1	1
70%	5	2	2	1
80%	7	3	2	2
85%	9	4	3	2
90%	11	5	3	2
95%	16	7	4	3

From the data collected, it was determined that standard deviation tends to exceed average faulting in magnitude along both transverse and longitudinal directions, especially the latter. The overall standard deviation is as large as somewhere around 1.0 mm. With such a level of variability, even to achieve a 95% of 1.0 mm width, only approximately 16 measurements are required to be taken for every tenth of a mile. However, as the coefficient of variation indicates,

the overall magnitude of faulting along all three sections is not very significant. The variability that has been identified might not be truly representative of what happens along a section where severe faulting is observed, which would be of primary concern for the ultimate goal of the project.

Chapter 4. Product Description

The 3-Line laser faulting sensor developed and tested in this project features a 1-Watt red laser (640 nm wavelength) with a custom lens and a 3-D camera. Through the lens, the laser projects three parallel lines onto the pavement, with each line spaced 1.5 inches apart when mounted in a vehicle at 17.5 inches from the sensor bottom surface to the pavement.

The 3D camera within the sensor captures all three laser line images in a single picture and splits the images into three separate Areas of Interest (AOI). The sensor is connected to a computer inside the test vehicle via an ethernet cable. A built-in processor in the camera processes images in real-time and transfers depth profiles for each laser line to the computer. Users can observe line plots, or profiles, that represent the variations in height. Each line contains 2,352 points of height values. The depth profiles cover 13 inches long on the pavement surface in the travel direction.

The sensor was calibrated to give true elevation (height) in millimeter when mounted at a high of 17.5 inches with a measurement range of ± 2 inches. If the test vehicle suspension system is very soft, the sensor mounting high should be checked before running a test to ensure measurements do go out of range. This will make sure that the sensor has enough vertical measurement range to tolerant vehicle vibration while travel.

The sensor is designed to work at either time-mode or trigger-mode. In the time-mode, the sensor captures surface profiles at an even, user-set time interval. This mode is mainly used for check sensor operation when the vehicle is not moving. In the trigger-mode, the sensor captures surface profiles at a given travel distance. This distance is controlled by a vehicle wheel encoder. It can be adjusted by the operator through a software user interface. The profile data is also synchronized with GPS location coordinates. The GPS location information is used for mapping collected raw profile data and processed faulting data. It is particular useful when reviewing saved data offline.

 The prototype functioned in a trigger-mode for all of the data collection to have measurements based on the distance traveled by the vehicle. In the initial stage, the team incorporated a GPS-based encoder for the prototype to collect profiles every 1.57 inches (40 mm) of vehicle travel. This device uses GPS information as well as the vehicle's OBD-II port to gather data from the vehicle's engine control unit (ECU) to trigger at the specified distance. For initial testing, the research team employed a light-duty pickup truck with a hitch receiver in the rear, outfitted with a custom bracket for the positioning the system. The three laser lines were oriented parallel to the direction of travel, as depicted in Figure 4.1.
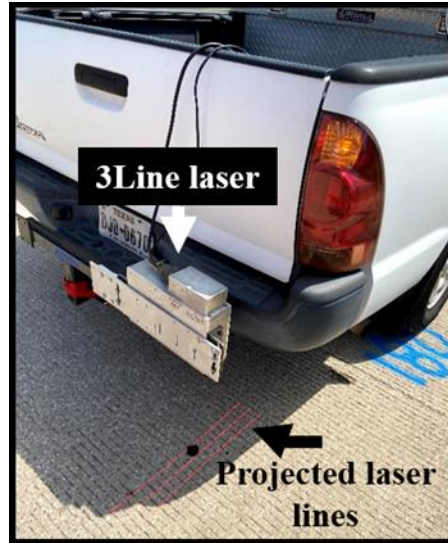
Figure 4.1 3-Line Laser and Projected Laser Lines on Pavement

In September 2021, the research team surveyed a series of sites in Austin, TX, that had jointed concrete pavement (JCP). The streets selected included Martin Luther King (MLK), just south of the University of Texas at Austin, and William Cannon Drive in the south side of Austin. MLK contained a small section of concrete (1,789 feet in length) for each of the four lanes (two in each direction). The research team tested the four lanes with the prototype installed on the light-duty pickup truck. The tests were repeated two times for each of the four lanes. The team also surveyed and tested William Cannon Drive which was longer (1.85 miles). The site had six lanes (three lanes in each direction) and both directions had longitudinal and transverse cracks, indentations, joints with fillers, asphalt patches and severe faulting making the site ideal for developing the software and testing the hardware. Three of the mentioned issues can be seen in Figure 4.2. Only the middle lane and the outer lane were measured, with two repetitions for each of the four tested lanes.

Figure 4.2 Distresses in William Cannon

From the tests performed at the sites in MLK and William Cannon, the research team discovered several issues with the prototype. The first main issue was that the camera was an older model that contained a software bug that the manufacturer acknowledged but could not fix. As a solution, the team, working with TxDOT personnel, found a different camera in TxDOT's inventory that was a newer model with no known software bugs. The second issue was that city

streets have significant unevenness. Therefore, the lightweight vehicle was sensitive to the road's unevenness when traveling at the speed limit, causing the camera to go out of range in the height axis when the suspension was low or high. The camera's viewing range at the time of testing was 3.0 inches. The research team still managed to collect over 45,000 profiles for each of the three laser lines in each of the four lanes (two in each direction). A portion of the data contained erroneous measurements from the aforementioned issues. Once the valid data were processed offline, the researchers noticed that certain distresses mimicked the pattern of joints in the data in terms of width, location, and depth in the three profiles.

In December 2021, the research went out again to William Cannon Drive. Having processed previously collected data, the team identified which sections had severe faulting along William Cannon. The prototype contained a newer model camera that allowed for a larger viewing size on the height axis. Previously the range was ±1.5 inches and was now increased to ±2.5 with the newer model camera. The camera was an upgrade in terms of performance, allowing the trade-off between data collection speed (Hertz) and viewing range to be maximized. The performance increase allowed for the prototype to collect at the same collection speed but with a larger camera's viewing range, solving the issues that were previously seen. The number of points in each line decreased from 2,352 to 2,048 but the spacing between points increased to approximately 0.242 mm, equaling 19.5 inches in length.

Additionally, a linescan camera was incorporated adjacent to the prototype to capture line images of the pavement for ground truth verification, as shown in Figure 4.3. The purpose of the linescan was to capture line images that are stitched together to result in high-resolution images of the pavement measured, serving as a ground truth for the location of the joints. The linescan captured line images every 4.0 mm at the time of testing and provided a visual verification of the joints. While this camera proved useful in three data sets, it was vulnerable to unstable lighting conditions, such as shadows and direct sunlight. The test with the prototype covered 1.43 miles of William Cannon Drive traveling in both directions and covering the outer and middle lane on both directions, with two repetitions for each. Three of the datasets collected contained acceptable images from the linescan camera before the environmental lighting was an issue. Figure 4.4 demonstrates the influence of the environmental lighting changes affecting the contrast of the linescan images in a single dataset.

Figure 4.3 Side View and Top View of the Linescan Camera Attached to the Vehicle
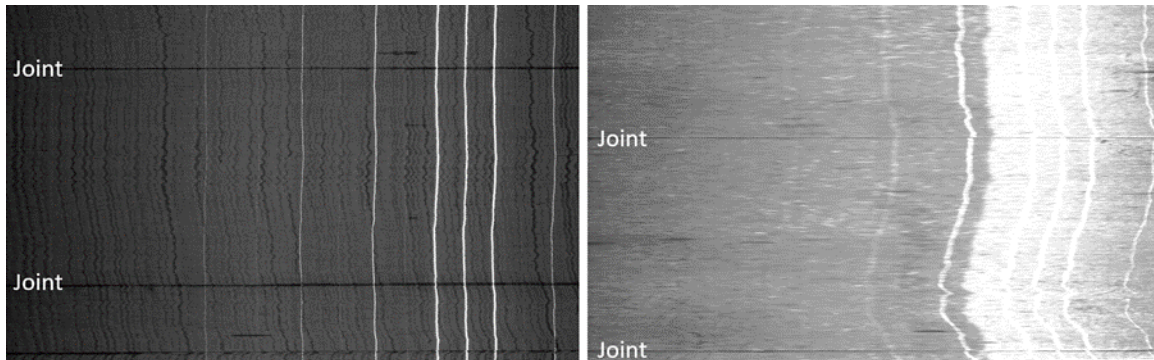
Figure 4.4 Exposure Image from a Region with Shadows (left) and Direct Sunlight (right)

The data were processed offline and issues that were previously seen were solved with the new camera. The increased working range of the camera had resolved the camera going out of range when measuring on a pavement of poor riding quality, however, when crossing intersections for this particular street, the camera would go out of bound temporarily. The linescan camera, while potentially useful, brought its own issues due to its sensitivity to environmental lighting. The images collected were useful for three of the datasets to identify the locations of joints and compare them to the prototype.

To validate the findings of the prototype's measurement, the team conducted a visual survey of William Cannon Drive in January, 2022, where each joint and distresses were annotated for each slab by visual inspection. Findings from the survey indicated that certain slabs had features that mimicked joints in both the prototype data and the linescan's images. The survey gave the team valuable information of each unique joints, their distance, spacing, features, distresses and other abnormalities. As a result, the survey demonstrated the limitation of the GPS-encoder distance which were not as accurate as the manufacturer's specifications indicated. Since each joint was physically measured, the spacing between joint was known and did not match the GPS-encoder.

To resolve the encoder issue, the team implemented an optical sensing encoder on the vehicle's wheel to measure the rotation of the vehicle's wheel. The wheel-encoder was mounted to the rear wheel's hub using three special lug nuts that serve to bolt the wheel to the hub and extend outwards and provide an internal threaded hole to fix the encoder's measuring shaft. The wheel-encoder housing, Figure 4.5, was fastened to the vehicle's body to keep it upright and fixed from rotation so only the encoder's measuring shaft rotates with the wheel.

Figure 4.5 Wheel-encoder Installed on rear wheel of test vehicle

The modifications implemented led to another field test in February 2022. The test was done in a section of Anderson Lane that has JCP and is a city street in Austin, TX. From the above-stated findings, three crucial changes were implemented before the next field test. The main change in the prototype was the wheel-encoder now served as the sensor that triggered the prototype every 1.57 inches (40 mm) of travel distance, measured by the wheel's rotation. The GPS-encoder was still installed and served to add latitude and longitude coordinates into the data approximately every 33.6 feet of travel. Secondly, the linescan camera was removed and replaced by a 4K laser-based camera, Figure 4.6, which only served as a ground truth for algorithm development. The 4K system attached to the rear hitch receiver of the vehicle and was positioned to cover the full lane's transverse width, perpendicular to the direction of travel. The 4K system provided both range images and intensity images that are not susceptible to environmental lighting, such as shadows or direct sunlight. The 4K system provided the researchers a tool for locating the joints and relating it to the prototype's collected data.

Figure 4.6 4K System Installed on the Test Vehicle

A third modification was the camera's range was increased from ±2.5 inches to ±2.75 inches. Similar to William Cannon Drive, the street had significant unevenness but very rarely would the camera go out of range with the latest increase in the camera's range. The Anderson Lane section had four lanes total (two in each direction) but only the outer lanes were tested and were repeated three times for each. The distance tested was 0.9 miles of JCP for each lane with some intersections having patches of asphalt pavement. From this test section, the prototype worked without any issues.

Until February 2022, all of the field tests were performed in challenging city streets that had distresses, joints with fillers, unevenness, asphalt patches, and features that mimicked joints. Once the team was comfortable with the prototype, the team worked with TxDOT personnel to identify JCP section on the TxDOT managed network. On April 2022, the team visited and tested US 84 in Waco, the city's main street, between Reference Marker 430.23 + 0.33 mi and 432.15 – 0.36 mi, 1.23 miles per lane were tested across the four lanes (two in each direction). Each of the four lanes were tested three times.

After February 2022, the majority of hardware-related problem were addressed, enabling the research team to confidently carry out testing in remote highways. A number of highways in Texas with JCP were surveyed to pinpoint test sites exhibiting severe faulting. The locations explored included Thorndale, Waco, Dallas, Houston, Hillsboro, and Corsicana, among which Hillsboro's SH 81 demonstrated the highest level of faulting.

Between April 2022 and May 2023, multiple tests were executed at the test site in Hillsboro, leading to various modifications to finalize the product. The initial modification involved utilizing a test vehicle with a stiffer suspension system, more representative of TxDOT's survey vehicles. This change resulted in reduced vertical vehicle movement, and subsequently, the camara never went out of range. The product's mounting mechanism was also revamped with

user-friendly T-Slot aluminum extrusions, allowing the system to easily slide into position. This mounting system permits both lateral and vertical adjustments at the vehicle's rear and is versatile enough to fit a variety of vehicles, ranging from smaller trucks like the Toyota Tacoma to full-sized ones like TxDOT's F-250. Figure 4.7 illustrates the mounting system on different vehicles. The horizontal profile enables lateral product placement, while the vertical beam separately adjusts the product's distance from the ground. Initial tests with a 3-foot vertical profile led to the final design featuring a 1-foot adjustable range, found to be optimal for most vehicles.

Figure 4.7 (left) UT's test vehicle with mounting system; (right) TxDOT's profiler vehicle with mounting system and product

The product's housing was constructed from aluminum due to its light weight, durability, and heat dissipation properties, crucial for drawing heat away from the camera. Cable connections within the enclosure were upgraded for ease of use and one-directional connectivity, ensuring connectors could only be plugged into their corresponding counterpart. Figure 4.8 shows the enclosure and connectors. The system has one connection for data communication via an ethernet port to the computer, and another for 12V power and triggering. An external button was incorporated into the enclosure design to indicate power receipt through a solid blue light and to allow for easy powering on/off.
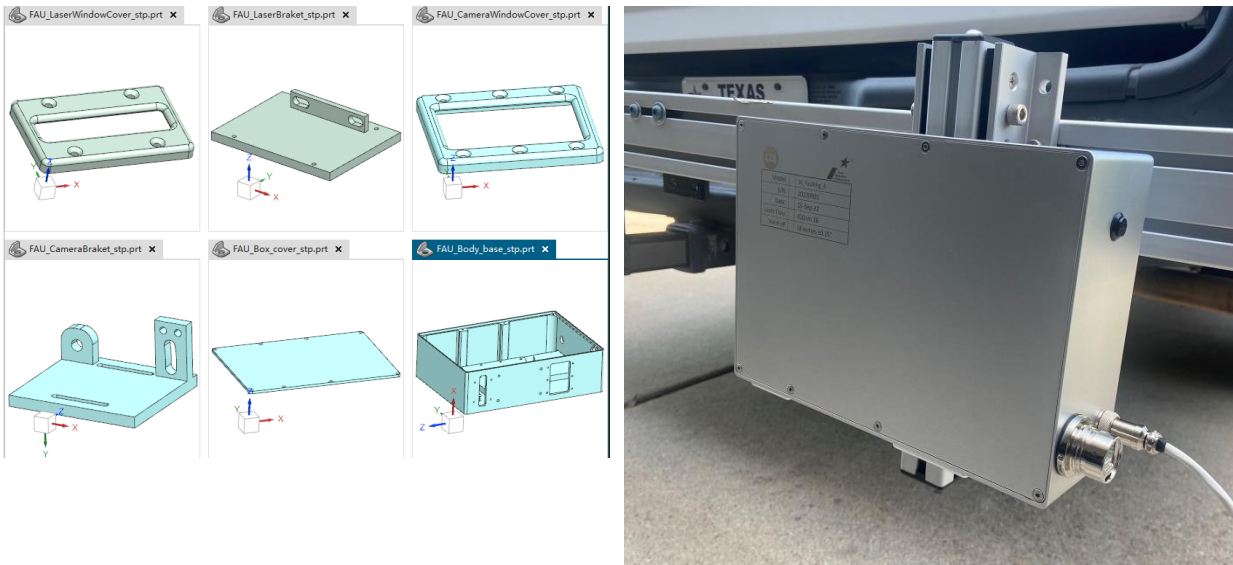
Figure 4.8 (left) CAD drawings of the designed enclosure; (right) final enclosure for the 3-Line

The power cable, emerging from the enclosure, is connected to a black metal box, Figure 4.9, designed to simplify cable connections. This box houses wire connections for the wheel encoder and a counter to interface with the encoder. The other three ports on the box include an input from the trigger, a 12V power input (such as a cigarette lighter plug), and a USB port connected to the computer to interface with the wheel encoder. A button is also present on the box for product power control. Figure 4.9 displays these four connections on the box. The ethernet cable from the product and the USB cable from the box connect to the corresponding ports on the computer.

Figure 4.9 Encoder interfacing box, housing encoder counter

In December 2022, the research team, in conjunction with TxDOT, evaluated the product in Corsicana, Texas. Five JCP sites featuring various surface finishes were surveyed using one of TxDOT's profiler vehicles, an F-250 truck, as shown in Figure 4.10. The 3-Line laser was mounted on the rear hitch receiver with the mounting system, and the wheel encoder was adapted to stabilize the encoder on the rear wheel. Each of the five sites was measured over a mile,

36

specifically on the outer lanes. While the tests successfully gathered data, issues arose from the wheel encoder not being calibrated for the larger wheel size, resulting in unexpected spacing between measurements. Another issue involved the transverse tining on SH 31, which mimicked joints, leading to false positives in joint detection. This latter problem was mitigated by adjusting the detection thresholds in the joint detection algorithm. Among the five sites, only one had severe faulting but was in a high-traffic commercial area.

Figure 4.10 3-Line laser installed on TxDOT's profiler vehicle

The rest of the evaluation continued on highway SH 81 in Hillsboro throughout the rest of 2023. The team conducted further testing of the product and performed a verification test as presented in the next two chapters.

Chapter 5. Preliminary Algorithm and Repeatability Testing

Based on the field test on US 81 in Hillsboro, TX, one particular test consisted of five repetitions along the same set of joints for analysis of repeatability and are discussed in this section. According to AASHTO Designation M 328-14 (2018), repeatability refers to consistency in successive measurements of the same quantity. It is a quantifier of the variability in measurement error using the same equipment and operator. In the context of faulting measurement, for each run, the pavement profile data were processed for joint detection, faultmeter measurement simulation, and averaging across measurements to obtain a single faulting value. The values for each run are then compared with each other for repeatability analysis.

5.1. Preliminary Algorithm

To simulate faulting measurement as defined in AASHTO R36-21 using a faultmeter, a line is fitted through a 5.0 in (127 mm) segment along the approach slab of the profile in which a joint is detected, and extended for a length of 11.8 in (300 mm). The difference is taken vertically between the projected elevation at the end of the 11.8 in (300 mm) long extended line, and the actual elevation on the departure slab at the point corresponding to the end point in terms of longitudinal position. The line-fitting is applied to reflect an imaginary faultmeter with a 5.0 in (127 mm) long base placed on the approach slab, while taking the difference in elevation 11.8 in (300 mm) downstream of the end of the 5.0 in segment reflects the foot of the faultmeter extruding towards the departure slab which is specified to be 11.8 in (300 mm) long measuring from the end of the base. For the analysis, a subset of the data pertaining to the middle of the entire dataset was used, starting with profile number 18,235 which contained a joint, labeled as Joint 1. Figure 5.1 shows the simulation conducted along profile 18,235 in Run 1, which captures Joint 1 for the first time. The yellow lines indicate the first position where the simulated faultmeter can potentially be placed, bounded by the 3-in minimum margin required between the center of the joint and Leg 3 (the third yellow vertical line). The red lines indicate the last feasible position, bounded by the end of the profile.
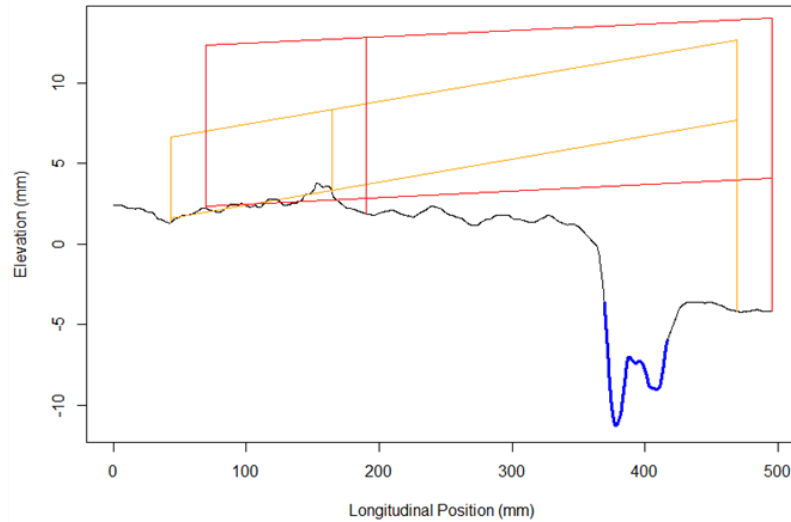
Figure 5.1 Faultmeter Simulation Capturing Joint 1 for the First Time

Figure 5.2 shows the simulation conducted along profile 18,239 in Run 1, which captures Joint 1 for the last time. The yellow lines indicate the first position where the simulated faultmeter can potentially be placed, bounded by the beginning of the profile. The red lines indicate the last feasible position, bounded by the 3 in (76.2 mm) minimum margin required between Leg 2 (the second red vertical line) and the center of the joint.
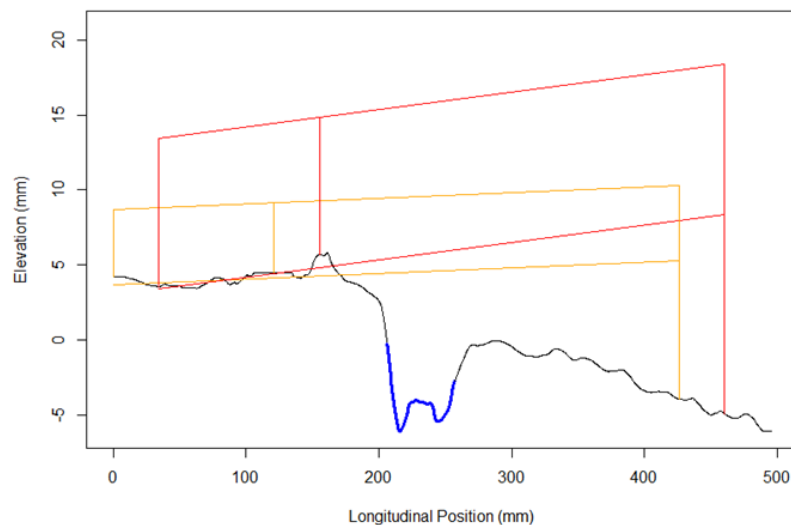
Figure 5.2 Faultmeter Simulation Capturing Joint 1 for the Last Time

A total of eight consecutive joints with adjacent ones separated by a spacing of approximately 60 ft (18.3 m) were selected among the joints surveyed in the Hillsboro sections, referred to as Joint 1 to Joint 8 for the purpose of this report. With each joint surveyed for five runs, and each run contains from four to six profiles that captures a unique joint in several positions that were adequate for faultmeter measurement simulation, and faulting calculation. A summary of the results is reported on a joint to joint basis in the next sections.

5.1.1. Joint 1

Table 5.1 shows the summary statistics from the 24 profiles from which faulting could be measured at Joint 1, with the first four runs each capturing five profiles, and the last run, four. For each run, average faulting and standard deviation were first calculated along each laser line. Then, a weighted average was obtained among the three average faulting for each laser lines with the inverse of their corresponding standard deviation as the weight. This ensured the laser lines with more stable measurements to contribute more to the overall average. Across the faulting values obtained from the five runs, the run-to-run standard deviation was 0.70 mm.

Table 5.1 Summary Table for Faulting Measurement along Joint 1

Run	Profile	Mean Faulting (mm)			Standard Deviation (mm)			Count		
		AOI1	AOI2	AOI3	AOI1	AOI2	AOI3	AOI1	AOI2	AOI3
1	18235	10.22	7.61	4.08	1.13	0.65	0.26	109	113	92
	18236	10.02	7.94	4.83	1.78	0.62	0.98	276	280	264
	18237	7.65	8.06	7.11	1.48	0.60	1.21	288	288	288
	18238	8.63	7.79	7.52	1.45	0.50	0.88	288	288	288
	18239	11.31	8.86	6.58	1.12	0.34	0.56	143	124	128
	Avg.	9.23	8.00	6.33	1.83	0.65	1.56			
2	18316	9.58	10.91	6.92	0.90	0.87	1.20	140	126	188
	18317	7.78	8.58	5.66	1.19	2.08	0.90	288	288	288
	18318	8.46	9.65	6.36	1.74	2.73	0.94	288	288	288
	18319	10.08	11.85	8.16	0.76	1.09	1.76	288	271	288
	18320	9.96	10.49	9.69	0.33	0.91	0.57	124	114	113
	Avg.	9.00	10.15	7.05	1.53	2.26	1.79			
3	18088	10.10	9.77	7.27	1.22	0.97	0.46	164	146	181
	18089	7.48	7.54	5.54	1.54	1.42	1.18	279	260	255
	18090	8.31	8.22	4.98	2.09	1.64	0.43	288	288	288
	18091	10.85	10.76	5.88	1.07	0.85	0.33	288	288	288
	18092	10.69	10.97	6.23	0.54	0.42	0.19	139	153	143
	Avg.	9.28	9.28	5.84	2.04	1.84	0.98			
4	18087	12.91	27.62	7.59	0.17	3.11	0.48	116	96	136
	18088	11.47	15.81	7.02	0.76	9.77	0.54	271	257	288
	18089	9.88	1.44	5.87	0.85	5.90	0.80	288	288	288
	18090	7.67	-16.11	5.49	0.59	12.05	0.52	288	288	256
	18091	7.52	-29.15	5.42	0.72	5.18	0.66	140	119	162
	Avg.	9.71	-0.94	6.22	2.02	19.38	0.98		7.08	
5	18362	7.88	7.14	10.16	0.97	1.10	1.42	282	204	175
	18363	7.14	6.84	9.01	0.92	0.80	2.31	288	288	288
	18364	4.65	8.17	4.46	0.68	1.30	2.12	288	288	288
	18365	3.83	8.90	1.69	0.43	0.59	0.78	214	216	224
	Avg.	6.01	7.73	6.19	1.83	1.28	3.76			

5.1.2. Joint 2

Table 5.2 shows the summary statistics from the 24 profiles from which faulting can be measured along Joint 2, with the first run capturing four profiles, and the rest each capturing five. Across the faulting values obtained from the five runs, the standard deviation was 0.51 mm.

Table 5.2 Summary Table for Faulting Measurement along Joint 2

Run	Profile	Mean Faulting (mm)			Standard Deviation (mm)			Count		
		AOI1	AOI2	AOI3	AOI1	AOI2	AOI3	AOI1	AOI2	AOI3
	18704	3.18	7.49	6.82	0.41	0.56	1.22	176	154	153
	18705	3.97	8.48	7.12	0.88	1.16	1.64	288	288	288
1	18706	3.52	4.10	2.29	1.63	3.68	3.68	288	288	288
	18707	-0.77	-2.70	-2.28	2.74	2.84	1.25	251	258	244
	Avg.	2.52	4.13	3.29	2.56	5.09	4.45			
	18784	6.41	7.85	4.77	0.23	0.27	0.77	107	101	75
	18785	5.20	7.46	7.36	0.28	0.31	1.48	262	241	240
2	18786	3.96	5.58	6.47	1.35	2.46	2.77	288	288	288
	18787	-0.03	-0.55	0.53	2.79	3.19	2.74	288	288	288
	18788	-2.70	-3.71	-2.32	0.39	0.59	0.55	162	166	157
	Avg.	2.48	3.16	3.60	3.46	4.80	4.27			
	18557	6.38	6.90	6.46	0.26	0.99	0.90	168	173	159
	18558	6.67	8.70	8.34	0.62	1.27	0.90	288	288	288
3	18559	3.68	5.43	5.60	2.83	3.67	3.68	288	288	288
	18560	-1.81	0.17	1.17	2.32	1.77	1.43	248	229	236
	18561	-5.15	-2.04	0.55	0.44	0.65	0.13	94	118	64
	Avg.	2.87	4.62	5.17	4.47	4.37	3.56			
	18556	2.65	-1.00	-1.05	0.64	0.11	1.19	154	146	115
	18557	2.23	0.37	1.61	0.63	1.85	1.97	288	288	285
4	18558	2.97	4.97	3.44	1.22	3.26	1.46	288	288	288
	18559	4.94	8.90	4.25	1.68	1.12	0.33	273	266	284
	18560	5.42	9.64	4.87	0.96	0.30	0.29	106	97	107
	Avg.	3.45	4.33	2.83	1.68	4.44	2.20			
	18830	-0.66	-2.56	-2.05	1.29	0.92	0.87	153	134	120
	18831	-0.94	-2.06	-0.55	1.51	2.26	2.06	288	288	288
5	18832	2.93	3.95	4.85	3.14	4.03	3.06	288	288	288
	18833	7.77	8.72	8.39	2.33	1.49	0.78	273	278	286
	18834	10.18	10.15	9.06	0.69	0.14	0.15	107	106	110
	Avg.	3.32	3.38	4.02	4.61	5.50	4.60			

5.1.3. Joint 3

Table 5.3 shows the summary statistics from the 23 profiles from which faulting can be measured along Joint 3, with the first, third and fifth runs capturing five profiles, and the second and fourth each capturing four. Across the faulting values obtained from the five runs, the run-to-run standard deviation was 0.16 mm.

Table 5.3 Summary Table for Faulting Measurement along Joint 3

Run	Profile	Mean Faulting (mm)			Standard Deviation (mm)			Count		
		AOI1	AOI2	AOI3	AOI1	AOI2	AOI3	AOI1	AOI2	AOI3
1	19172	2.64	2.84	2.96	0.92	0.69	0.06	86	84	68
	19173	6.85	3.62	3.24	0.88	0.50	0.14	242	245	229
	19174	6.12	4.78	3.18	1.41	0.36	1.11	288	288	288
	19175	6.79	3.98	4.05	3.12	1.87	1.13	288	288	288
	19176	1.47	1.07	2.87	1.66	1.77	1.48	192	174	173
	Avg.	5.37	3.55	3.37	3.03	1.75	1.12			
2	19253	3.49	4.77	4.27	0.98	0.47	1.10	207	209	213
	19254	4.84	3.92	4.53	1.12	0.57	0.66	288	288	288
	19255	4.93	4.72	3.39	0.80	1.36	0.80	288	288	288
	19256	2.69	4.81	1.41	1.53	0.53	0.71	223	209	194
	Avg.	4.11	4.52	3.52	1.46	0.94	1.41			
3	19025	4.86	4.45	4.02	0.48	0.44	0.49	112	111	87
	19026	4.03	4.74	4.10	0.41	1.15	0.31	270	273	245
	19027	3.92	5.64	4.40	1.04	0.59	1.15	288	288	288
	19028	4.96	4.23	1.72	0.54	1.29	2.62	288	288	288
	19029	4.44	2.68	-1.07	0.43	0.52	0.89	165	146	149
	Avg.	4.38	4.54	2.80	0.80	1.31	2.48			
4	19025	5.28	3.22	3.62	3.86	2.55	0.49	234	205	184
	19026	8.38	6.85	4.70	0.69	2.26	0.56	288	288	288
	19027	5.75	6.34	2.06	2.27	3.41	1.77	288	288	288
	19028	1.61	0.51	-1.55	2.45	3.05	1.84	202	215	221
	Avg.	5.56	4.59	2.31	3.40	3.81	2.68			
5	19298	4.76	6.67	-3.59	1.47	1.52	1.04	101	83	71
	19299	5.97	6.01	2.92	1.46	1.84	4.07	258	246	221
	19300	5.42	6.60	7.63	1.10	1.52	2.01	288	288	288
	19301	2.31	5.46	2.94	2.38	2.45	5.26	288	288	288
	19302	-1.20	1.67	-3.54	1.83	2.39	1.93	171	170	186
	Avg.	3.65	5.39	2.63	3.05	2.62	5.39			

5.1.4. Joint 4

Table 5.4 shows the summary statistics from the 24 profiles from which faulting can be measured along Joint 4, with the third run capturing four profiles, and the rest each capturing five. Across the faulting values obtained from the five runs, the standard deviation was 0.46 mm.

Table 5.4 Summary Table for Faulting Measurement along Joint 4

Run	Profile	Mean Faulting (mm)			Standard Deviation (mm)			Count		
		AOI1	AOI2	AOI3	AOI1	AOI2	AOI3	AOI1	AOI2	AOI3
1	19639	4.36	5.49	5.74	0.44	0.91	0.42	198	179	161
	19640	3.93	7.15	6.18	0.57	0.96	0.21	288	288	288
	19641	5.16	7.40	6.44	1.10	0.55	0.41	288	288	288
	19642	5.64	6.75	7.08	0.84	0.39	0.18	221	223	228
	19643	4.48	6.52	7.31	0.13	0.13	0.13	55	57	64
	Avg.	4.74	6.81	6.45	1.02	0.97	0.57			
2	19719	5.90	6.35	6.10	0.31	0.39	0.22	165	175	141
	19720	5.97	6.73	5.19	0.26	0.38	0.48	288	288	288
	19721	6.64	6.89	5.04	0.49	0.59	0.48	288	288	288
	19722	7.69	8.10	5.38	0.43	1.04	0.36	260	234	254
	19723	8.06	9.05	4.42	0.19	0.27	0.34	92	78	78
	Avg.	6.72	7.18	5.26	0.88	1.02	0.58			
3	19492	6.58	6.75	2.57	0.28	0.33	0.27	229	209	176
	19493	6.36	6.42	3.40	0.51	0.46	1.35	288	288	288
	19494	5.93	7.05	4.92	0.56	0.58	1.05	288	288	288
	19495	6.74	7.15	3.43	0.97	0.18	1.08	190	195	217
	Avg.	6.36	6.82	3.71	0.68	0.52	1.36			
4	19491	1.11	6.63	3.47	0.17	0.61	0.83	147	135	112
	19492	2.63	5.48	4.75	1.63	0.76	1.54	288	288	285
	19493	6.14	5.87	7.30	2.19	1.24	0.66	288	288	288
	19494	6.96	7.03	7.67	0.83	0.34	0.49	277	272	281
	19495	6.08	6.95	7.56	0.51	0.19	0.22	108	98	102
	Avg.	4.76	6.25	6.34	2.64	1.02	1.81			
5	19765	3.58	4.08	4.09	0.77	0.13	0.17	155	148	146
	19766	5.62	4.13	4.24	1.56	0.70	0.57	288	288	288
	19767	8.30	8.12	4.71	1.37	3.20	0.38	288	288	288
	19768	8.90	11.29	4.12	0.78	0.89	0.45	263	259	248
	19769	7.83	10.90	3.92	0.41	0.46	0.09	93	86	69
	Avg.	7.02	7.48	4.30	2.22	3.51	0.50			

5.1.5. Joint 5

Table 5.5 shows the summary statistics from the 25 profiles from which faulting can be measured along Joint 5, with each run capturing five profiles. Across the faulting values obtained from the five runs, the run-to-run standard deviation was 0.53 mm.

Table 5.5 Summary Table for Faulting Measurement along Joint 5

Run	Profile	Mean Faulting (mm)			Standard Deviation (mm)			Count		
		AOI1	AOI2	AOI3	AOI1	AOI2	AOI3	AOI1	AOI2	AOI3
1	20110	7.25	7.98	4.71	2.17	2.50	1.07	194	165	163
	20111	4.21	3.93	3.70	2.18	2.73	0.51	288	288	288
	20112	3.49	1.41	3.63	1.14	0.77	1.02	288	288	288
	20113	2.71	1.80	1.12	1.08	0.74	1.67	238	251	240
	20114	1.29	1.62	-1.12	0.19	0.43	0.57	72	79	70
	Avg.	4.04	3.20	2.93	2.35	2.90	1.96			
2	20190	8.14	9.64	4.92	1.47	1.57	1.30	132	116	97
	20191	5.07	5.62	3.54	3.23	3.44	1.48	288	277	265
	20192	2.93	1.49	2.68	1.12	0.78	0.26	288	288	288
	20193	3.44	1.03	1.24	0.24	0.58	1.43	288	288	288
	20194	3.23	1.05	-0.14	0.11	0.89	0.59	128	130	131
	Avg.	4.26	3.22	2.36	2.44	3.53	1.84			
3	19963	6.94	6.10	5.37	2.80	1.10	0.65	179	179	168
	19964	3.54	5.73	4.35	1.92	0.76	1.02	288	288	288
	19965	1.69	5.83	2.52	0.67	0.86	0.78	288	288	288
	19966	-0.39	4.95	1.59	1.65	0.89	0.50	251	237	235
	19967	-2.01	3.98	0.66	0.18	0.11	0.41	85	67	67
	Avg.	2.27	5.54	3.15	3.19	1.03	1.68			
4	19962	8.94	9.33	5.97	0.43	0.13	0.71	100	87	75
	19963	8.01	8.36	3.79	0.49	0.74	1.79	259	251	246
	19964	6.32	5.70	3.32	1.70	1.96	0.90	288	288	288
	19965	2.37	1.36	2.96	2.49	1.90	1.15	288	288	288
	19966	-0.61	-0.86	1.78	1.29	0.61	0.88	167	159	155
	Avg.	4.87	4.48	3.29	3.64	3.86	1.53			
5	20236	4.09	4.75	5.36	1.66	0.72	0.94	165	158	133
	20237	3.24	5.01	4.49	1.14	1.06	0.88	288	288	288
	20238	1.17	5.19	2.78	1.79	1.03	1.52	288	288	288
	20239	-0.70	2.78	0.42	0.69	1.30	0.75	262	255	267
	20240	-0.11	1.35	-0.33	0.66	0.22	0.29	94	89	92
	Avg.	1.60	4.19	2.71	2.22	1.64	2.22			

5.1.6. Joint 6

Table 5.6 shows the summary statistics from the 25 profiles from which faulting can be measured along Joint 6, with each run capturing five profiles. Across the faulting values obtained from the five runs, the standard deviation was 1.04 mm.

Table 5.6 Summary Table for Faulting Measurement along Joint 6

Run	Profile	Mean Faulting (mm)			Standard Deviation (mm)			Count		
		AOI1	AOI2	AOI3	AOI1	AOI2	AOI3	AOI1	AOI2	AOI3
1	20577	3.97	6.17	7.07	0.62	0.69	0.26	137	140	130
	20578	3.93	8.68	7.05	1.32	2.29	0.75	288	288	288
	20579	6.35	13.07	10.15	2.42	1.97	2.08	288	288	288
	20580	12.86	13.69	12.44	3.34	2.10	0.78	288	266	261
	20581	16.88	11.10	12.03	0.34	1.27	0.48	119	98	83
	Avg.	8.23	10.98	9.64	5.12	3.34	2.58			
2	20658	4.27	3.77	-0.02	0.52	0.10	0.74	206	193	185
	20659	6.42	5.04	4.43	2.87	2.06	2.97	288	288	288
	20660	11.16	9.87	10.06	2.30	2.49	2.36	288	288	288
	20661	12.23	10.81	11.07	1.40	1.08	1.17	223	203	213
	20662	10.09	8.69	9.32	1.20	0.31	0.41	57	57	67
	Avg.	8.70	7.49	6.87	3.73	3.36	4.60			
3	20430	4.44	6.26	3.86	0.73	0.23	0.59	145	138	108
	20431	5.18	7.51	5.66	1.49	1.40	1.56	288	288	279
	20432	8.97	11.38	10.37	3.24	2.42	2.69	288	288	288
	20433	13.16	14.31	13.72	1.54	0.53	0.85	278	275	288
	20434	14.51	14.47	13.28	0.15	0.51	0.84	111	101	111
	Avg.	9.00	10.73	9.69	4.22	3.47	4.04			
4	20430	6.06	7.56	4.92	0.53	0.48	0.41	188	163	152
	20431	7.04	7.89	5.76	1.91	1.25	0.81	288	288	288
	20432	10.67	11.34	8.99	2.20	1.77	1.91	288	288	288
	20433	12.42	11.93	10.28	0.86	1.40	0.98	234	248	212
	20434	11.58	10.38	7.91	0.71	0.73	0.49	71	76	56
	Avg.	9.33	9.89	7.65	2.95	2.30	2.39			
5	20703	2.19	3.67	4.05	0.56	1.02	0.84	105	90	102
	20704	3.50	6.66	6.35	1.86	2.25	1.61	264	255	274
	20705	6.41	10.86	9.34	1.89	2.19	1.39	288	288	288
	20706	7.22	12.62	11.51	1.12	0.79	1.00	288	288	288
	20707	6.04	11.85	10.42	0.92	1.22	1.38	159	153	140
	Avg.	5.47	9.88	8.81	2.29	3.38	2.80			

5.1.7. Joint 7

Table 5.7 shows the summary statistics from the 22 profiles from which faulting can be measured along Joint 7, with the first, third and fifth runs capturing four profiles, and the second and fourth each capturing five. Across the faulting values obtained from the five runs, the run-to-run standard deviation was 2.08 mm.

Table 5.7 Summary Table for Faulting Measurement along Joint 7

Run	Profile	Mean Faulting (mm)			Standard Deviation (mm)			Count		
		AOI1	AOI2	AOI3	AOI1	AOI2	AOI3	AOI1	AOI2	AOI3
1	21046	1.62	4.39	7.35	3.16	0.48	2.77	246	209	215
	21047	6.93	5.35	8.62	3.08	0.52	3.12	288	288	288
	21048	7.63	5.67	3.86	1.54	0.19	2.51	288	288	288
	21049	6.26	5.53	1.49	1.43	0.16	0.61	172	194	176
	Avg.	5.70	5.27	5.62	3.52	0.61	3.72			
2	21126	5.49	7.60	0.72	0.19	0.19	0.06	96	71	69
	21127	3.40	4.99	1.85	0.69	0.72	1.13	256	233	228
	21128	1.01	2.22	3.10	1.27	1.64	0.79	288	288	288
	21129	-0.67	0.55	3.02	0.95	1.21	0.33	288	288	288
	21130	0.26	2.11	3.10	1.81	1.42	0.41	174	168	166
	Avg.	1.40	2.73	2.65	2.27	2.40	1.01			
3	20899	7.76	3.92	3.03	0.48	0.61	0.94	196	185	179
	20900	5.57	4.72	4.12	1.66	1.12	0.45	288	288	288
	20901	3.97	6.84	5.31	0.25	1.46	1.11	288	288	288
	20902	4.21	7.47	7.39	0.40	1.21	1.02	223	222	212
	Avg.	5.23	5.81	4.99	1.70	1.83	1.74			
4	20899	2.62	2.65	1.05	0.23	0.37	0.39	176	177	196
	20900	2.15	1.14	0.55	0.36	0.67	0.38	288	288	288
	20901	2.98	0.91	-0.40	1.05	0.50	0.39	288	288	288
	20902	3.45	1.90	-0.11	0.34	0.58	1.10	250	239	225
	20903	3.32	2.54	1.30	0.54	0.16	0.64	92	81	69
	Avg.	2.84	1.60	0.29	0.79	0.86	0.86			
5	21172	7.14	27.46	2.75	0.50	10.69	1.84	119	142	158
	21173	6.61	26.47	8.04	0.55	8.06	4.65	278	288	288
	21174	3.75	6.58	13.48	2.03	12.70	2.21	288	288	288
	21175	0.63	-3.61	7.29	0.99	6.33	5.42	288	269	252
	Avg.	4.06	12.61	8.59	2.87	16.23	5.36			

5.1.8. Joint 8

Table 5.8 shows the summary statistics from the 26 profiles from which faulting can be measured along Joint 8, with the fourth run capturing six profiles and the rest each capturing five. Across the faulting values obtained from the five runs, the run-to-run standard deviation equals 1.82.

Table 5.8 Summary Table for Faulting Measurement along Joint 8

Run	Profile	Mean Faulting (mm)			Standard Deviation (mm)			Count		
		AOI1	AOI2	AOI3	AOI1	AOI2	AOI3	AOI1	AOI2	AOI3
1	21515	1.97	6.68	7.01	0.19	0.17	0.39	117	108	92
	21516	1.73	6.84	7.20	0.85	0.27	0.52	281	231	211
	21517	4.25	7.48	7.26	2.70	0.72	0.45	288	288	288
	21518	9.01	7.96	8.84	2.17	0.48	1.06	288	288	288
	21519	10.35	7.37	9.62	0.33	0.18	0.83	183	177	178
	Avg.	5.56	7.38	8.05	3.87	0.64	1.24			
2	21596	11.24	3.38	2.56	1.10	0.97	0.20	110	80	64
	21597	11.11	7.44	3.18	1.07	2.51	0.48	274	245	231
	21598	10.21	9.16	3.39	0.76	0.85	0.16	288	288	288
	21599	8.62	8.09	3.28	0.77	1.19	0.19	288	288	288
	21600	6.94	7.06	3.35	1.34	1.43	0.18	151	158	163
	Avg.	9.68	7.72	3.25	1.77	2.13	0.34		4.70	
3	21369	7.30	7.06	5.51	0.68	0.91	0.27	214	189	167
	21370	7.02	8.37	7.03	0.69	2.10	1.56	288	288	288
	21371	8.22	12.20	11.62	1.64	2.35	2.38	288	288	288
	21372	9.36	14.00	13.06	0.29	0.33	0.41	200	206	218
	21373	7.94	13.29	13.20	0.52	0.91	0.45	98	84	67
	Avg.	7.91	10.67	9.75	1.30	3.18	3.36			
4	21368	4.66	5.44	11.26	0.06	0.23	0.12	77	58	39
	21369	3.18	5.45	10.26	0.30	0.58	1.62	228	224	205
	21370	2.81	7.23	8.25	0.92	1.49	0.88	288	288	288
	21371	3.50	7.76	6.89	0.90	2.01	1.35	288	288	288
	21372	2.10	4.90	4.83	1.89	2.36	1.87	194	153	188
	21373	-1.92	-0.22	1.05	0.66	0.32	0.64	42	33	37
	Avg.	2.89	6.32	7.51	1.17	2.19	2.36			
5	21641	11.74	8.63	12.76	0.72	0.66	0.44	142	127	86
	21642	10.10	9.05	10.62	0.79	0.52	2.07	276	288	257
	21643	7.46	6.11	5.12	1.70	3.01	3.20	288	288	288
	21644	2.84	0.85	0.06	2.97	1.71	1.19	288	285	288
	21645	-0.97	-0.63	-0.25	1.70	0.15	0.85	147	112	123
	Avg.	6.38	5.12	5.08	4.57	4.13	5.21			

Based on the table, it can be observed that variability is considerably higher along Joints 7 and 8 especially in Run 5. As a result, the profiles of these joints in Run 5 were individually analyzed to explore the anomalies present in the profile that are causing the extremely high variability.

5.2. Faulting Calculation

Based on the analysis of the data collected on SH 81 in Hillsboro, several different methods for calculating faulting were developed and applied in search of the method that produced the most consistent and robust approach. The value of faulting cannot be capture by just one number because it has a distribution. It means that faulting varies a lot depending on the transverse location where it is measured, the conditions of the joint, time of the year and the day when it is measured because of warping and curling, the relative angle between the approach and leave slab, and the distance from the joint where it is measured. For this reason, faulting needs to be considered a characteristic of the joint that is not fixed, but rather, has a distribution or a range of values. It has a transverse distribution and for every 0.1 mile, it also has a longitudinal distribution.

With the system developed as part of this project, when travelling at 50 mph, each joint is captured within the range of the laser lines from 4 to 6 times. Every time a joint is captured, the system provides three profiles (AOI1, AOI2 and AOI3) for faulting calculation because of the three-line characteristic of the equipment.

The first method for calculating faulting consisted of selecting only the center reading out of the 4 to 6 times the joint is captured. That is when the joint is located in the center of the laser line so as 288 faulting measures are available. These 288 values are then averaged. This is referred to as "Average of Center Line" in Table 5.9. The next approach was to determine the median of all the readings and this value is referred to as "Median of Center Line". Because of the number of outliers, it was assumed that the median was going to produce a less variable measurement but that was not the case. While the average had a standard deviation of 1.52 mm and a coefficient of variability of 25 percent; the median values were 1.95 mm and 31 percent, respectively (**Error! Reference source not found.**).

Table 5.9 Summary Results of the Data Analysis

Approach Used	Standard Deviation (mm)	Coefficient of Variability (%)
Average of Center Line	1.52	25
Median of Center Line	1.95	31
Average of All Data	1.35	22
Median of All Data	1.36	22

The next two approaches consisted of utilizing all the data collected by all three laser lines every time that the joint was captured. The first calculation was performed utilizing all data and is

referred to as "Average All Data" in Table 5.9. The second faulting calculation was done utilizing the median of all measurements and is referred to as "Median All Data". It can be observed that both calculations of faulting have similar characteristics and they are both less variable than when the center line was used. Therefore, based on this analysis, it is recommended that the average of all data is reported as well as the standard deviation and the coefficient of variability.

5.3. Repeatability

The data presented in Section 5.1 were also utilized to assess and establish the repeatability of the equipment developed as part of this research project. This analysis also allowed the estimation of the longitudinal faulting variability.

Eight consecutive joints on SH 81 in Hillsboro (Texas) were selected for this analysis. The summary results are presented in Table 5.10. Each of the eight joints along a 0.1 miles (0.16 km) section was surveyed five times and the average and standard deviation of these measurements are reported in the table. It should be noted that the standard deviation at six of the eight joints is closer to one or significantly smaller. It should also be noted that surface features present before Joints 7 and 8 are responsible for the high standard deviation of the values calculated at these joints. It should also be noted that the standard deviation shown in Table 5.10 represents the combined transverse variability of the joint plus the equipment variability. It is therefore established that an acceptable level of variability should be 1.0 mm (0.04 in) or smaller.

Table 5.10 Equipment Variability and Joint Variability

Joint	Average Faulting	Standard Deviation
1	7.61	0.70
2	3.49	0.51
3	4.05	0.16
4	5.89	0.46
5	3.54	0.53
6	8.82	1.04
7	4.21	2.08
8	6.30	1.82

The data in Table 5.10 can also be used to determine the longitudinal variability of faulting. In this case, the longitudinal variability was associated with a standard deviation of 2.0 mm (0.079 in) and a coefficient of variability of 36%. While these two statistics are based on the analysis of this particular section, it is important to note that the longitudinal faulting variability cannot be ignored. For this reason, it is recommended that at least 50 percent of the joints should be measured for each 0.1 miles (0.16 km) section and that the average faulting is reported together with the associated standard deviation and the equipment and method that was used for the calculations.

Chapter 6. Final Specification and Verification

6.1. Final specification

6.1.1. 3-Line Laser Data Processing

For demonstration purposes, a specific profile from high-speed Run 1 is shown in this section as an example, with all three AOIs, each corresponding to one single laser line. Figure 6.1 shows the raw profile data collected by each of the three laser lines. Comprising 2,048 points, with each pair of consecutive points being approximately 0.24 mm (0.01 in) apart, each profile covers a longitudinal length of approximately 495.3 mm (19.5 in). Two adjacent laser lines are separated by a transverse distance of 44.5 mm (1.75 in), with the three profiles capturing a transverse width of 88.9 mm (3.5 in) over the same longitudinal position.
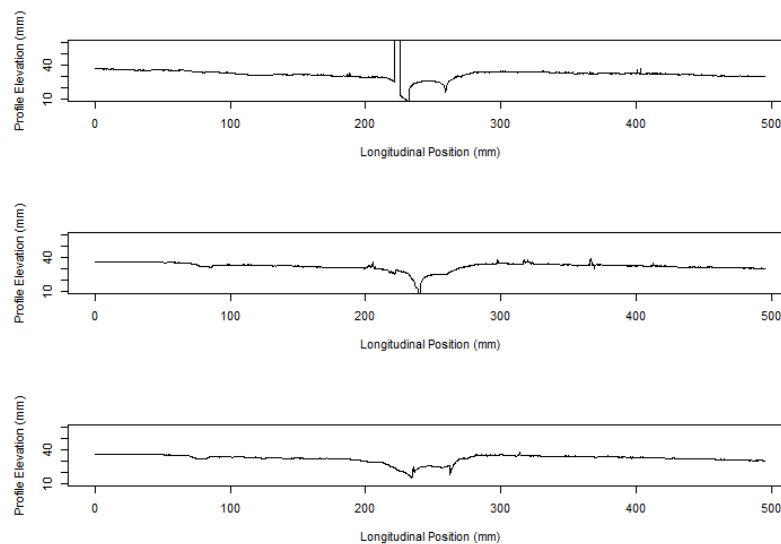
Figure 6.1 Profile 514 from High-Speed Run 1 Original Profile

During data processing, each profile is first detrended by the 5.0 m (16.4 ft) rolling average. This step accounts for the potential slanting of the laser line relative to the pavement due to the position and motion of the vehicle on which the equipment is mounted. With a sampling interval between consecutive profiles of 40 mm (1.5 in) along the longitudinal direction, 125 profiles are averaged to form the baseline for detrending. Including the current profile itself, 62 profiles before and 62 after are used for averaging. A line is fitted through the averaged profile, as shown in Figure 6.2. Using profile 514 as the example, the averaged line takes data from profile 452 to 576 to calculate their mean. Detrending is performed by subtracting the profile by the line fitted from the 5.0 m (16.4 ft) rolling average profile.
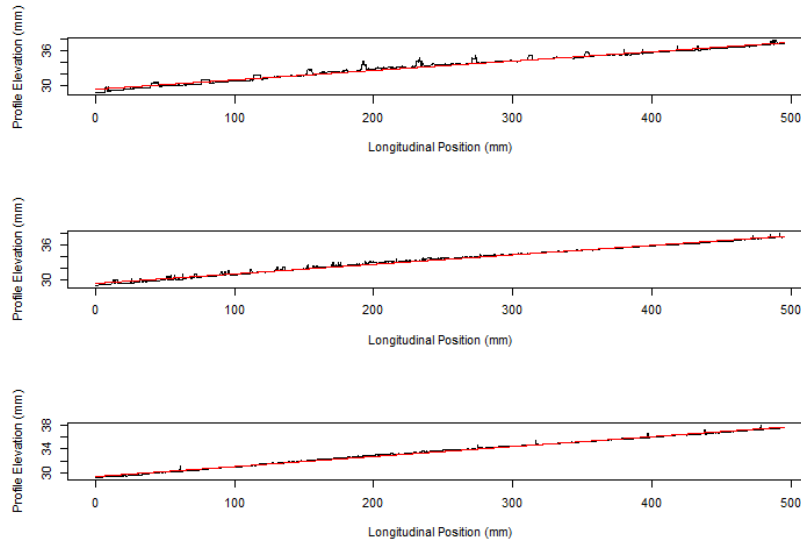
Figure 6.2 Averaged Profile and Fitted Line for Detrending Profile 514

After removing the linear trend, extreme values and unwanted noise are removed by identifying
and eliminating points with elevation differences exceeding 2.0 mm from the median across the
adjacent 3.0 mm of profile. Figure 6.3 shows the profile with filtered and unfiltered data plotted,
overlapping with each other, where the red line indicates the unfiltered profile and the black line
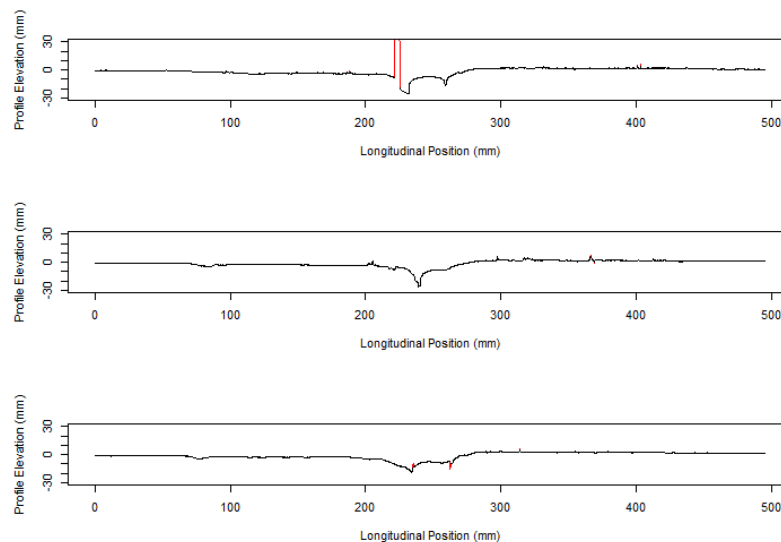is filtered.

Figure 6.3 Profile #514 from High-Speed Run 1 before and after Extreme Value Removal

For faulting calculation using the 3-Line laser equipment, the longitudinal position of the
measurement is chosen based on the specification detailed in the AASHTO R36-21. An offset of
60 mm (2.3 in) adjacent to the joint on either side is marked, while a 50 mm (2.0 in) long
segment starting from the offset is used on each slab to calculate the elevation difference.

Figure 6.4 shows the faulting calculation with the adjusted margins along the example profile for all three laser lines. The red section labels the identified joint, the green vertical line indicates the center of the joint, while the two blue boxes mark the segments on the approach and departure slabs used for faulting calculation. Consistent with the convention, the departure slab elevation is subtracted from the approach slab elevation, with a higher approach slab indicating positive faulting, and higher departure slab resulting in negative faulting.
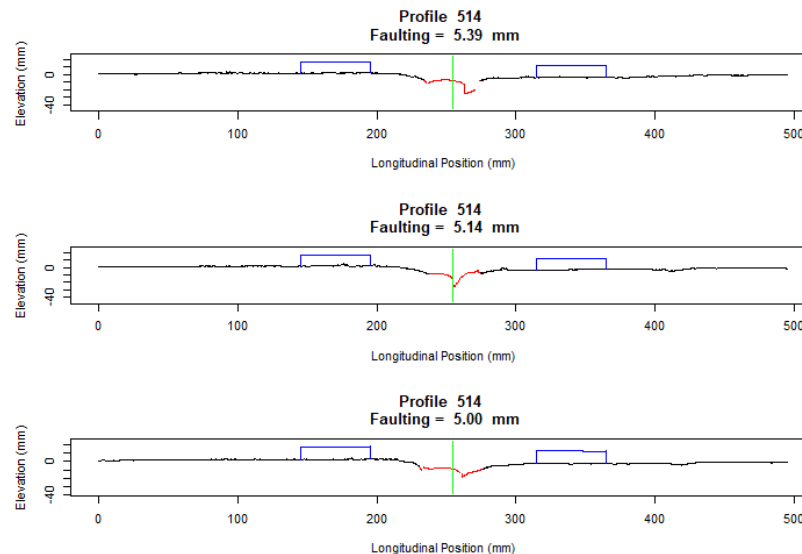
Figure 6.4 Faulting Calculation for 3-Line Laser Data Using Profile #514 with Longitudinal Position Based on AASHTO R36-21

6.2. Verification

6.2.1. Considered Options for Verification

In this section, the establishment of a benchmark methodology to verify and validate the faulting data collected by a service provider is presented. This methodology is intended for TxDOT to be able to verify the faulting measurement data and equipment of different vendors or service providers. Two different options were considered, and the option of evaluating benchmark sections at various districts is recommended. The two considered options included:

6.2.1.1. Option 1: Permanent Facility

This option considered the feasibility and effectiveness of establishing a permanent facility in a fixed location in Texas where the equipment of the service provider could be sent for verification on an annual basis, before data collection. This option has a very high initial cost of constructing JCP with variable faulting but, once constructed, the maintenance and operation costs are relatively low. At least 0.5 miles of JCP would have to be built with a combination of joint spacings ranging from 15 to 30 feet and including a section with 60-feet joint spacing. The main

disadvantage of this option is that once it is constructed, faulting will remain almost constant year-after-year and the service provider could "learn" what the faulting is. Modifying the faulting at the joints on an annual basis would significantly increase the operating cost of the facility. The high initial cost of this option made it less desirable, as does the limitation in terms of changing the faulting.

6.2.1.2. Option 2: Benchmark Field Sections at Various Districts.

This option evaluated the feasibility and effectiveness of establishing field test sections in three different districts where the vendors shall have to run their equipment and the faulting they measure shall be compared with reference faulting values. As part of this option, quality control charts could be developed that would be used to evaluate the equipment of the service providers. The well-established concept of Percentage Within Limits (PWL), which quantifies the fraction of measurements within given tolerable limits based the sampled sections, could be utilized for these purposes. Another option considered was the use of the concept of confidence intervals, where the agency could select and specify the level of confidence and the desired precision based on the field distribution of faulting values. At this point, this second option is preferred.

The verification/control sections will be relocated on an annual basis so the service providers cannot "learn" the faulting values. The initial cost of this option is very low, and it will also have a slightly lower annual operating cost than the first option because there will be no need to maintain any facility and to simulate new levels of faulting on an annual basis. The main disadvantage of this option is the establishment and benchmarking of the verification and control sections every year, which will require traffic control. However, including the traffic control costs, this option is still more effective and efficient than option one. The main advantage of this option is that the equipment will be evaluated during actual operation conditions and on actual highway joints. Based on its lower cost and other significant advantages, this option was preferred.

6.2.2. Beam Description

The research team used a highly accurate piece of equipment, the Joint Laser Scanner (JLS), to establish the ground-truth faulting measurement along a joint. The JLS consists of a line laser scanner attached to a 4.0 m (13 ft) long stage driven by a belt that is moved at any speed between 1.0 to 300 mm/s (0.04 to 11.8 in/s). The particular benefit of the equipment in comparison to other joint measurement devices is that it measures 4.0 m in a straight line atop a joint with a very high precision. Figure 6.5 shows the Joint Laser Scanner standing alone as well as in operation. When measuring faulting, the JLS is positioned on the joint transversely, measuring an area of 240 mm (9.5 in) (longitudinal, or along the direction of travel) by 4,000 mm (157.5 in) (transverse, or along the direction of the joint). The vertical resolution is 5.0 microns.

Figure 6.5 (a) JLS at Joint 10 Standing Alone   (b) JLS at Joint 3 in Operation

Figure 6.6 shows the data collected with the JLS along Joint 0 as an example. Data processing is conducted on a profile-by-profile basis. Analogous to the noise removal approach for the 3-line laser data, extreme values and unwanted noise are removed by identifying and eliminating points with elevation difference exceeding 2.0 mm (0.079 in) from the median across the adjacent 3.0 mm (0.12 in) of profile.
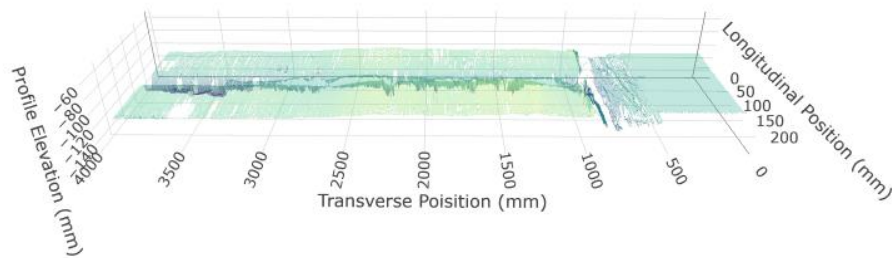

Figure 6.6 3D Data Collected along Joint 0 with the JLS (bigger)

To calculate faulting with the 3D data collected with the JLS, offset distance and measuring area are based upon the specification for 3D data defined in the AASHTO R36-21. As shown in Figure 6.7, a box is located on either side of the joint, marking 60 mm (2.4 in) from the center of the joint, each covering an area of 200 mm (7.9 in) (transverse) by 50 mm (2 in) (longitudinal). Both the width and length of the boxes are adjustable, and the choice of a larger width compared to both 100 mm (4 in) specified by the standard and 76.2 mm (3 in) as the spread across the three laser lines is to account for the drifting of the vehicle's transverse position across runs when traveling at highway speed.
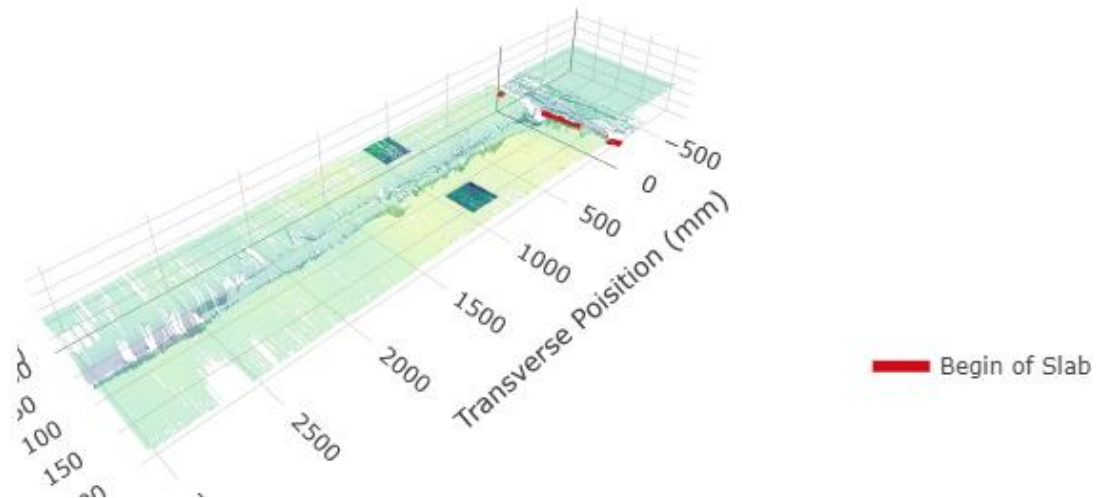
Figure 6.7 Faulting Calculation for JLS Data Using Joint 0 with Longitudinal Position Based on AASHTO R36-21 and Adjusted Transverse Position

6.3. Hillsboro results

To validate and verify the measurements, faulting data was collected with both pieces of equipment along the same set of joints to compare their results. The slabs along the section were 60 ft (18.3 m) long. Eleven joints were labeled from 0 to 10 for identification. Over each joint along the section, three passes were made with the 3-Line laser and a single scan over each joint with the JLS were conducted. The first round was the 3-Line laser mounted on a TxDOT vehicle collecting data for the first high-speed run. Then, the JLS was used to scan each joint. Finally, two additional high-speed runs were then carried out with the 3-Line laser.

Results from the three high-speed runs using the 3-Line laser and the calculation of repeatability are shown in Table 6.1. For each run, faulting values calculated with all three laser lines for the two profiles where the joint is located closest to the center are averaged to obtain the run-average. Then, the run-averages are compared across the three high-speed runs. The standard deviation was lower than 0.5 mm (0.02 in) for every joint, indicating a high repeatability across runs. An overall standard deviation of 0.24 mm (0.01 in) was achieved.

55

Table 6.1 Run Average Faulting Values and Equipment Repeatability

Joint	Run 1	Run 2	Run 3	Mean	Std. Dev.	CoV
0	2.55	3.04	2.88	2.82	0.20	7%
1	8.65	7.58	7.69	7.97	0.48	6%
2	1.46	1.62	1.14	1.41	0.20	14%*
3	-0.29	-0.58	-0.78	-0.55	0.20	-37%*
4	3.74	3.08	3.14	3.32	0.30	9%
5	4.13	5.15	4.48	4.59	0.42	9%
6	4.51	4.26	4.13	4.30	0.16	4%
7	1.50	1.68	1.79	1.66	0.12	7%
8	2.08	2.17	2.15	2.13	0.04	2%
9	8.63	8.18	8.65	8.49	0.22	3%
10	3.51	3.57	4.16	3.75	0.29	8%

*Notice that these high coefficient of variations (i.e., standard deviation over the mean) are due to the low mean faulting value: for a given numerator, a reduction in the denominator increases the ratio.

Comparison across results from the two pieces of equipment are shown in Table 6.2. The absolute difference between the two does not exceed 1.0 mm (0.04 in) for any joint.

Table 6.2 Comparison of Faulting Calculated with 3-Line Laser Data and JLS Data

Joint	3-Line	4-m Beam	Difference	Error
0	2.82	3.38	0.56	18%
1	7.98	8.11	0.13	2%
2	1.36	1.39	0.03	2%
3	-0.56	-0.17	0.39	-107%**
4	3.31	4.07	0.76	21%
5	4.63	5.04	0.41	8%
6	4.27	3.93	-0.34	-8%
7	1.54	0.94	-0.60	-48%**
8	2.11	2.15	0.04	2%
9	8.42	8.71	0.29	3%
10	3.71	3.91	0.20	5%

**Notice that the relatively high percent error (i.e., difference over the expected value) is due to the low expected faulting value calculated with the JLS.

As discussed in previous chapters, faulting varies significantly depending on the transverse location along a joint. To account for its potential contribution to the difference, transverse variability was calculated with the JLS data. For each joint, one faulting value was calculated for each 240 mm (9.45 in) long longitudinal profile across the entire span measurable along the slab. The number of profiles used and their transverse variability for each joint is shown in Table 6.3. Across the entire measurable width along each joint, mostly around 3,000 mm (118 in), though varying from joint to joint due to JLS position, a transverse variability ranging from 0.97 to 2.74 mm (0.04 to 0.12 in) in standard deviation was obtained. This indicates that the transverse location where measurement takes place does impact the faulting value calculated. It would be helpful to keep track of and match the exact transverse location of measurement to improve consistency.

Table 6.3 Transverse Variability Calculation with JLS Data

Joint	Mean	Std. Dev.	Length	Profiles
0	2.70	1.85	3,069	8,692
1	5.71	2.74	2,874	8,895
2	1.87	2.11	2,931	7,357
3	1.24	1.94	3,165	6,677
4	3.54	1.45	2,860	6,446
5	6.21	1.34	3,101	7,748
6	3.37	0.97	3,064	9,455
7	-0.67	1.01	3,045	6,899
8	1.96	1.18	3,201	5,156
9	6.48	2.65	3,032	6,261
10	4.94	1.60	3,083	6,440

Overall, the 3-line laser demonstrated excellent equipment repeatability across runs at highway speed. The results compare very well with the JLS data collected statically. If, however, the exact measuring location along the transverse joint could be determined, both repeatability and consistency across different pieces of equipment have potential to further improve. Finally, the JLS also proved its applicability to be used as a verification tool in daylight conditions.

Chapter 7. Conclusion

On an annual basis, TxDOT gathers most of its required distress information through a contracted vendor. However, faulting, one of the essential distresses, is estimated from longitudinal profile data, which is neither reliable nor accurate enough for establishing performance measures. As a result, this research project was launched to develop a system to collect and verify faulting data of jointed concrete pavements (JCPs) in an accurate manner at highway speeds during daylight conditions.

During the project, researchers from the University of Texas at Austin investigated available technologies that could be used to measure highway faulting and reported their advantages and disadvantages. All the available technologies at this time were identified but showed significant limitations in terms of accuracy, effectivess or efficiency. Accurate equipment exists for project level investigations but cannot be utilized at the network level. The researchers concluded that to date, no equipment exists that meets the needs of the Texas Department of Transportation. Based on the findings, a system that can be used to collect faulting data at highway speeds during daylight conditions was developed. As early field tests were carried out, modifications and improvements on hardware from the camera to the triggering system were made as issues were encountered during field data collection. By February 2022, the hardware was sufficiently developed to meet the technical objectives of this research project. Afterward, through multiple tests of the equipment in the field to ensure accuracy and precision, it was found that the equipment produced repeatable results with standard deviation across runs less than 0.5 mm and high accuracy with error compared to static measurements less than 0.5 mm, accurate enough to meet the requirements of the FAST Act. These characteristics even surpassed the expectation of the researchers.

In terms of products to deliver, a faulting measuring system (Product 1) that the TxDOT can implement directly for network-level faulting measurement and for vendor data verification will be delivered at the end of the project. Specifications for measuring and reporting faulting (Product 2) and methodology for verification of faulting measuring equipment (Product 3) that the TxDOT can use to verify in the field the accuracy and precision of the vendor's equipment are attached in Appendices A and B. Appendix C contains the algorithms to determine the location of the joints and Appendix D contains the algorithms to calculate the faulting value.

Chapter 8. Value of Research

8.1. Introduction

In a Policy Paper by the Research, Innovation, and Science Policy Experts (RISE) of the European Commission, Georghiou (2015) cited Salter and Martin (2001) in acknowledging the "multiple ways in which research achieves impact and creates value". In accordance with the scope of TxDOT Project 0-7060, the Research Team determined the project's Value of Research (VoR) based on the development of the qualitative and economic benefit areas designated by TxDOT. The relevant sources of benefit are divided into 17 functional areas, each requiring qualitative or economic values for TxDOT or the State of Texas, as summarized in Table 8.1.

Table 8.1 Designated Benefit Areas for Project 0-7060

Benefit Area	Qualitative	Economic	Both	TxDOT	State	Both
Level of Knowledge	X			X		
Management and	X			X		
Quality of Life	X			X		
Customer Satisfaction	X			X		
System Reliability		X		X		
Increased Service Life		X		X		
Improved Productivity and Work Efficiency		X		X		
Expedited Project Delivery		X		X		
Reduced Administrative Costs		X		X		
Traffic and Congestion Reduction		X			X	
Reduced User Cost		X			X	
Reduced Construction, Operations, and Maintenance Cost		X			X	
Materials and Pavements		X			X	
Infrastructure Condition		X				X
Freight Movement and Economic Vitality		X				X
Engineering Design Improvement			X			X
Safety			X			X

8.2. Qualitative Benefit

8.2.1. Level of Knowledge

The project enhances the level of knowledge in three aspects. First, with the thorough literature review and information gathering early in the project, available technologies out there with the potential to measure faulting automatically were examined. However, none of the available technologies meet the requirements of either accuracy or speed as specified by the project objectives. To overcome those limitations, the 3-Line Laser equipment was developed, addressing those shortages, and capable of measuring faulting at highway speed automatically in daylight conditions, with both standard deviation across runs and the error from statically measured faulting values less than 0.5 mm (0.02 in). Second, by utilizing the equipment, TxDOT will be able to monitor all the joints within the state network, measuring each with multiple faulting values. In this way, a much better understanding of the JCP performance across the network will be obtained as compared to inferring from other distresses or only measuring faulting for a portion of the joints with manual equipment. Finally, with the verification method provided, TxDOT will be able to compare results provided by external vendors to an accurate benchmark for data quality control and assurance and ensure the accuracy of future data collected with new pieces of equipment.

8.2.2. Policy and Management

In July 2012, MAP-21, the Moving Ahead for Progress in the 21st Century Act (P.L. 112-141), a long-term highway authorization, was signed into law. It creates a streamlined and performance-based surface transportation program built upon existing ones established since 1991 and transforms investment policy and framework to guide the development of the surface transportation system. The Act has been designed to fund surface transportation programs at over $105 billion for fiscal years (FY) 2013 and 2014, and to guide the development of the highway system. The notice of proposed rulemaking (NPRM) published at 80 FR 326 on January 5, 2015, was among the several NPRMs issued by FHWA to implement Section 1203 of MAP-21 to establish performance management to transform the highway program by concentrating its focus on national transportation goals and increasing its accountability and transparency. To better achieve the national goal of *"maintaining the condition of highway infrastructure assets in a state of good repair"* which MAP-21 aims for, the NPRM proposed a set of measures designed to reflect a pavement's predominant condition for State DOTs to use to assess and quantify the infrastructure condition on the National Highway System (NHS).

Defined as *"the average vertical displacement (difference in elevation) between adjacent jointed concrete panels in the direction of travel,"* faulting is one of the metrics proposed in the NPRM and required to be collected and reported in accordance with practices outlined in the Highway Performance Monitoring System (HPMS) Field Manual for all jointed concrete pavement (JCP) sections with surface type codes corresponding to jointed plain concrete pavements (JPCP),

jointed reinforced concrete pavements (JRCP), unbonded jointed concrete overlay on al Portrland Cement Concrete (PCC) pavements, bonded PCC overlay on PCC pavement, and others. A pavement section's overall condition is rated by these metrics collectively. For example, a JCP section for which the three relevant metrics are roughness, cracking, and faulting, is rated in Good condition only if all three exceed the thresholds specified in the NPRM. On the contrary, it would be rated in Poor condition if any two out of three are below the designated thresholds.

FHWA's Highway Performance Monitoring System (HPMS) Field Manual details in Item 51 the requirements for faulting data collection. According to the manual, the practice for faulting data collection should be in accordance with AASHTO Standard R36-13 while reporting should follow the requirements in 23 CFR 490.309 and 490.311. Data should be *"collected for the full extent of the mainline highway"* along sections on both the Interstate System and the non-Interstate System NHS, measuring every joint in the right wheel-path and reporting the average absolute faulting. The equipment allows this requirement to be met.

8.2.3. Quality of Life and User Satisfaction

Pavement roughness, defined as *"the deviation of a surface from a true planar surface with characteristic dimensions that affect vehicle dynamics and ride quality"* in ASTM E867-06, is widely acknowledged to associate with travelers' level of comfort. Hveem (1960) noted people's awareness of *"the relative degrees of comfort or discomfort experienced in traveling"* since early times roads and highways were first constructed, and the human perception *"of road smoothness or roughness as being synonymous with pleasant or unpleasant."* In the case of jointed concrete pavements, much of the roughness of the pavement is dependent on the level of joint faulting. Selezneva et al. (2000) investigated the effect of faulting on ride quality for jointed plain concrete pavement (JPCP) sections and found a strong correlation between the rate of change in faulting values versus that in IRI values, concluding faulting was a major contributor to increase in roughness for JPCP. Wang et al. (2022) conducted a study on roughness prediction models for JPCP sections. The authors found total faulting to be one of the two important parameters, together with initial IRI, for the smoothness of JPCP, which was identified as an important index for pavement condition evaluation *"affecting driving quality, driving safety, and road service quality."* Because initial IRI is an objective parameter of the road surface, the authors recommended road engineers to pay more attention to total faulting when maintaining road surface smoothness for JPCP sections. With the 3-Line Laser Equipment, TxDOT will now be able to monitor rigid pavements more efficiently, correcting sections with higher roughness due to faulting in a timely manner. Reducing travelers being exposed to rough, unpleasant rides will increasing both their quality of life and satisfaction with the roadway system.

8.3. Economic Benefit

Based on research results, Swanlund (2000) claimed that smooth roads reduce both the expenditure for the agency and the operating costs for the highway users. The author further pointed out the importance of state highway agencies performing maintenance activities timely and effectively to improve the smoothness on the network. The development of this project enables TxDOT to achieve this objective.

As part of TxDOT Research Project 0-1739 performed by CTR in 1999, a comprehensive life cycle cost analysis (LCCA) methodology was developed for Portland cement concrete pavements, accounting for *"all aspects of pavement design, construction, maintenance, and user impacts throughout the analysis period"* (Wilde et al., 1999). Costs analyzed were categorized as follows:

- Direct and External Societal Costs

    o Travel time delay

    o Vehicle operating costs

    o Emissions

    o Accidents

    o Evaluation factors

    o Discount rate

    o Reliability

- Agency Costs

    o Pavement performance and distress

    o Construction, maintenance, and rehabilitation

In another study evaluating the effect of pavement roughness on user costs, Islam and Buttlar (2012) predicted roughness with the Mechanistic-Empirical Pavement Design Guide (MEPDG) and analyzed user costs based on fuel consumption, vehicle repair and maintenance, vehicle depreciation, and tire wear with the Highway Development and Management Model Four (HDM-4). The comparison between agency investment and user costs due to pavement roughness showed that the former is much smaller (less than 4% of total cost) as compared to the latter. Based on the initial condition considered smooth with an IRI equal to 63 in/mi, the increase in user cost per vehicle-mile traveled (VMT) is shown in Table 8.2.

Table 8.2 Increase of User Cost with IRI (Islam and Buttlar, 2012)

IRI (in/mi)	Total Increase in User Cost ($/mi)	User Cost Increase ($/mi) per IRI Increase(in/mi)
63	0	
76.3	0.00039	0.00003
80.1	0.00063	0.00006
83	0.00082	0.00007
86.6	0.00179	0.00027
89.6	0.00297	0.00039
93.5	0.00449	0.00039
98.5	0.00641	0.00038
101.4	0.00751	0.00038
104.3	0.00861	0.00038
108.3	0.01011	0.00038

Since the aforementioned study used flexible pavements instead of rigid, in our case, the MEPDG IRI model for rigid pavement was used as follow (AASHTO, 2008):

$$IRI = IRI_I + 0.8203 * CRK + 0.4417 * SPALL + 0.4929 * TFAULT + 25.24 * SF$$

where:

$IRI =$ Predicted IRI, in./mi,

$IRI_I =$ Initial smoothness measured as IRI, in./mi,

$CRK =$ Percent slabs with transverse cracks (all severities),

$SPALL =$ Percentage of joints with spalling (medium and high severities),

$TFAULT =$ Total joint faulting cumulated per mi, in.

$SF =$ Site factor

When other variables are held constant, the equation indicates a linear relationship between IRI and total faulting. Therefore, in this study, only the effect of faulting was examined when considering roughness costs. Because TFAULT is the total joint faulting cumulated per mile, assuming a slab length of 15 feet, somewhere around 352 joints are likely to be observed along a one-mile section. An average increase of 1.0 mm (0.039 in) in faulting along a one-mile section will result in an increase of 6.83 in/mi in IRI. Since IRI not exceeding 95 in/mi is considered good by FHWA, anything below this threshold is not as relevant when maintenance is considered. As observable from the table, the per unit increase stabilizes around $0.00038/mi per unit IRI increase. Assuming that approximately half of this additional cost could be reduced by intervention, $0.0002/mi is used as the reduceable additional cost.

The National Highway System (NHS) within Texas is mapped in Figure 8.1 JCP Sections in Texas on the NHS Network, with JCP sections highlighted in red. Totaling in 1243.1 centerline miles and 3245.9 lane-miles, these JCP sections make up 1.4% of total centerline miles and 1.6% of total lane-miles within the entire Texas roadway network.
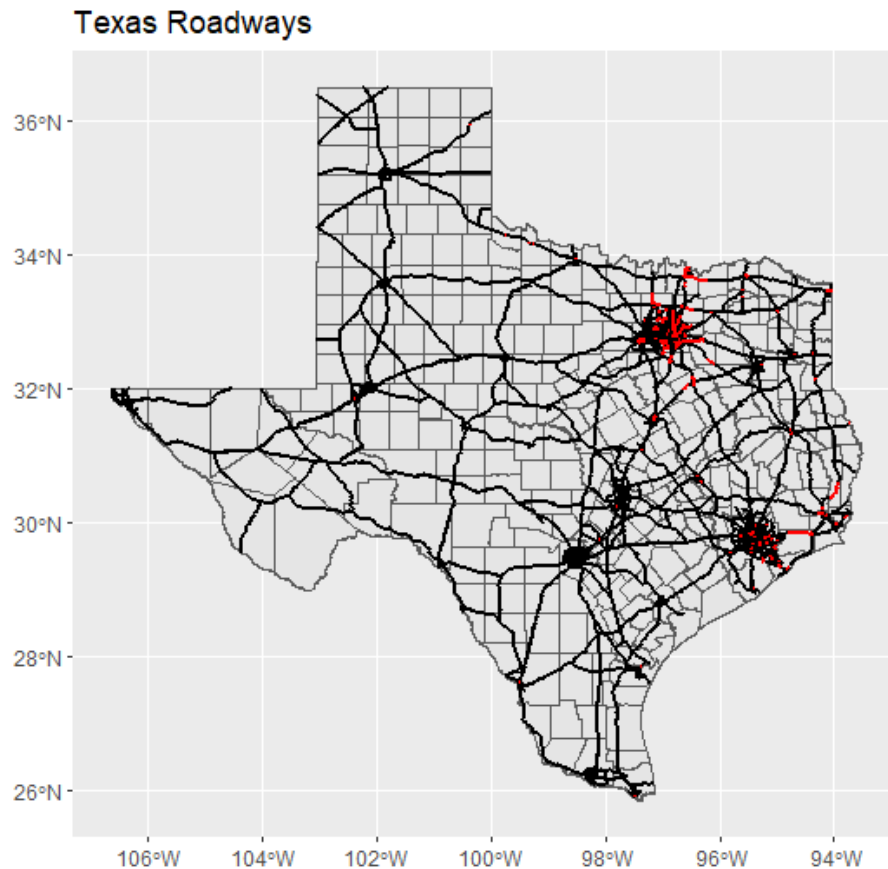

Figure 8.1 JCP Sections in Texas on the NHS Network

Next, a simulation was conducted assuming 5-ft slab length. A total of 437,536 joints are expected to be observed over the length of 1243.1 miles of JCP. At Year 1, each 1-mile section is randomly assigned an average faulting from a normal distribution of 3.0 mm (0.12 in) mean and 1.0 mm (0.039 in) standard deviation. For simplification, traffic volume was assumed to be homogeneous, 5,000 AADT/lane across all sections, and faulting was assumed to increase as a function of pavement age only, with each year elapsed inducing an additional 0.107 mm (0.0042 in) of faulting over time (Saghafi et al., 2009).

Two scenarios were compared. The base case would just treat the network as if the equipment were not available, and maintenance were not triggered by excessive amount of faulting. IRI and user costs just grow naturally as faulting increases over time. While for the project case, with the availability of the equipment, a joint-by-joint level of scanning and monitoring is achievable, and diamond grinding is applied for every joint found with faulting exceeding 3.8 mm (0.15 in), the FAST Act threshold of being classified as fair. A cost of $3.00 per sq. yd was assumed for

diamond grinding based on a 2022 CPAM presentation ($2.75 per sq. yd over five-year average), with the extent to grind assumed from the TxDOT Project 0-1739, shown in Table 8.3 Extent of Diamond Grinding Necessary Based on Faulting (Wilde et al., 1999) and the following equation:

Table 8.3 Extent of Diamond Grinding Necessary Based on Faulting (Wilde et al., 1999)

Faulting Extent, in	Distance from Joint to Grind, ft
F ≤ 0.125	2.5
0.125 < F ≤ 0.25	5.0
0.25 < F ≤ 0.375	7.5
0.375 < F ≤ 0.5	10.0
0.5 < F ≤ 0.675	12.5
0.675 < F ≤ 0.75	15.0
0.125 < F ≤ 0.25	20.0

$$Diamond\ Grinding\ (yd^2)$$
$$= \frac{Mean\ Faulting\,(in)}{2}$$
$$* \frac{Pavement\ Width\,(ft) * Grinding\ Distance\ from\ Joint\,(ft)}{9}$$
$$* \frac{Section\ Length\,(mi) * 5280}{Joint\ Spacing\,(ft)}$$

The comparison is shown in Table 8.4 Comparison of Two Simulated Scenarios. It can be seen that the maintenance cost invested in correcting faulting eventually pays of in the reduction of user cost.

Table 8.4 Comparison of Two Simulated Scenarios

Year	Base Case Cost		Project Case Cost		Benefit from
	User ($)	Maintenance ($)	User ($)	Maintenance ($)	Project ($)
1	6,242,327	0	6,242,327	571,033	-571,033
2	6,639,486	0	5,320,702	72,865	1,245,918
3	7,046,028	0	5,543,540	98,501	1,403,987
4	7,461,173	0	5,710,847	81,397	1,668,930
5	7,884,690	0	5,922,548	87,705	1,874,437
6	8,316,770	0	6,123,543	171,286	2,021,941
7	8,757,007	0	6,124,734	113,476	2,518,797
8	9,205,693	0	6,268,000	111,284	2,826,409
9	9,663,001	0	6,419,485	111,435	3,132,080
10	10,128,999	0	6,573,460	126,514	3,429,024

The full cost-benefit analysis is summarized in Figure 8.2. With a benefit-cost ratio (BCR) of 26 and payback period of 0.4 years, therefore, this project objectively demostarates to have produced significantly more value than invested.

	Project #	0-7060		
	Project Name:			
		Measuring Faulting on Jointed Concrete Pavements		
	Agency: CTR		Project Budget	$499,769
	Project Duration (Yrs)	4	Exp. Value (per Yr) $	1,955,049
	Expected Value Duration (Yrs)	10	Discount Rate	5%
Economic Value				
Total Savings: $	19,050,722		Net Present Value (NPV): $	12,835,215
Payback Period (Yrs):	0.255629914		Cost Benefit Ratio (CBR, $1 : $___): $	26

Years	Expected Value
0	-$499,769
1	-$571,033
2	$1,245,918
3	$1,403,987
4	$1,668,930
5	$1,874,437
6	$2,021,941
7	$2,518,797
8	$2,826,409
9	$3,132,080
10	$3,429,024

Value of Research: NPV
Project Duration (Yrs)
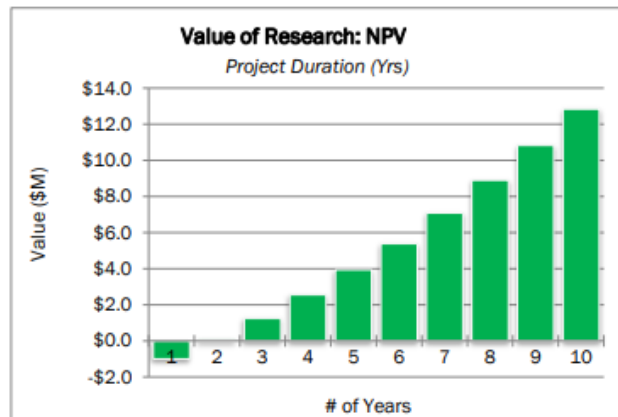
Variable Justification

Figure 8.2 Summary of Value of Research Calculations for Project 0-7060

References

AASHTO M 328-14 (2022), Standard Specification for Inertial Profiler, American Association of State Highway and Transportation Officials, Washington, DC.

AASHTO R 36-21 (2021), Standard Practice for Estimating Faulting of Concrete Pavements, American Association of State Highway and Transportation Officials, Washington, DC.

AASHTO R 56-14 (2014), Standard Practice for Certification of Inertial Profiling Systems, American Association of State Highway and Transportation Officials, Washington, DC.

AASHTO R 57-14 (2014), Standard Practice for Operating Inertial Profiling Systems, American Association of State Highway and Transportation Officials, Washington, DC.

Agurla, M., & Lin, S. (2015, June). Long-term pavement performance automated faulting measurement. In 9th International Conference on Managing Pavement Assets.

American Association of State Highway and Transportation Officials. *Mechanistic-Empirical Pavement Design Guide, Interim Edition: A Manual of Practice.* American Association of State and Highway Transportation Officials, Washington, DC, 2008.

Barman, M., Roy, S., Tiwari, A., & Burnham, T. R. (2022). Joint performance and faulting of ultra-thin and thin structural-fiber reinforced concrete pavements. International Journal of Pavement Engineering, 1-14.

Chang, G. K., Karamihas, S. M., Rasmussen, R. O., Merritt, D., & Swanlund, M. (2008, October). Quantifying the impact of jointed concrete pavement curling and warping on pavement unevenness. In 6th symposium on pavement surface characteristics (SURF), Potoroz, Slovenia.

Chang, G., Nazef, A., Watkins, J., & Karamihas, S. (2010). Automated fault measurement (AFM) in ProVal. Proceedings of Pavement Engineering 2010.

Federal Register. (2015). National Performance Management Measures; Assessing Pavement Condition for the National Highway Performance Program and Bridge Condition for the National Highway Performance Program.

"Fixing America's Surface Transportation Act." Public Law 114-94. 114th Congress, enacted 4 December 2015. United States Statutes at Large, vol. 129, U.S. Government Publishing Office.

Georghiou, L. (2015). Value of research policy paper by the Research, Innovation, and Science Policy Experts (RISE). *European Commission (June 2015)*.

Hao, X., Sha, A., Sun, Z., Li, W., & Hu, Y. (2016). Laser-based measuring method for mean joint faulting value of concrete pavement. Optik, 127(1), 274-278.

Huang, Y., Copenhaver, T., & Hempel, P. (2013). Texas Department of Transportation 3D transverse profiling system for high-speed rut measurement. Journal of Infrastructure Systems, 19(2), 221-230.

Hveem, F. N. (1960). Devices for recording and evaluating pavement roughness. *Highway Research Board Bulletin*, *264*, 1-26.

Islam, S., & Buttlar, W. G. (2012). Effect of pavement roughness on user costs. *Transportation research record*, *2285*(1), 47-55.

Khazanovich, L., Darter, M. I., & Yu, H. T. (2004). Mechanistic-empirical model to predict transverse joint faulting. Transportation Research Record, 1896(1), 34-45.

"Moving Ahead for Progress in the 21st Century Act." Public Law 112-141. 112th Congress, enacted 6 July 2012. United States Statutes at Large, U.S. Government Publishing Office.

Mraz, A., Nazef, A., Lee, H., Holzschuher, C., & Choubane, B. (2012). Precision of Florida Methods for Automated and Manual Faulting Measurements. Transportation Research Record, 2306(1), 131–137. https://doi.org/10.3141/2306-15

Nazef, A., Mraz, A., Iyer, S., & Choubane, B. (2009). Semi-Automated Faulting Measurement for Rigid Pavements: Approach with High-Speed Inertial Profiler Data. Transportation research record, 2094(1), 121-127.

Rao, S., Yu, H. T., Khazanovich, L., Darter, M. I., & Mack, J. W. (1999). Longevity of diamond-ground concrete pavements. Transportation research record, 1684(1), 128-136.

Roberts, J., (2022). Concrete Pavement Preservation & Restoration, *Improved Performance and Customer Satisfaction Through Timely Intervention*.

Saghafi, B., Hassaniz, A., Noori, R., & Bustos, M. G. (2009). Artificial neural networks and regression analysis for predicting faulting in jointed concrete pavements considering base condition. International Journal of Pavement Research and Technology, 2(1), 20-25.

Salter, A. J., & Martin, B. R. (2001). The economic benefits of publicly funded basic research: a critical review. *Research policy*, *30*(3), 509-532.

Selezneva, O., Jiang, J., & Tayabji, S. D. (2000). *Preliminary evaluation and analysis of LTPP faulting data* (No. FHWA-RD-00-076). Turner-Fairbank Highway Research Center.

Spellman, D. L., Woodstrom, J. H., & Neal, B. F. (1972). Faulting of Portland Cement Concrete Pavements. Highway Research Record, (407).

Swanlund, M. (2000). Enhancing Pavement Smoothness. *Public Roads*, *64*(2), 20-22.

Tsai, Y. J., Wu, Y., & Ai, C. (2011, January). Feasibility study of measuring concrete joint faulting using 3d continuous pavement profile data. In Proceedings of the Transportation Research Board 90th Annual Meeting, Washington, DC, USA (pp. 23-27).

Tsai, Y., Wu, Y., Ai, C., & Pitts, E. (2012). Critical assessment of measuring concrete joint faulting using 3D continuous pavement profile data. Journal of transportation engineering, 138(11), 1291-1296.

United States Federal Highway Administration. Highway Performance Monitoring System Field Manual. OMB No. 2125-0028, FHWA, U.S. Department of Transportation, Washington, D.C., 2016.

Vedula, K., Miller, R., Hossain, M., & Cumberledge, G. (2003, August). Adaptability of AASHTO provisional standards for condition surveys for roughness and faulting in Kansas. In Proc., 2003 Mid-Continent Transportation Research Symposium.

Wang, K., Li, L., & Li, J. Q. (2014). Automated joint faulting measurement using 3D pavement texture data at 1 mm resolution. In T&DI Congress 2014: Planes, Trains, and Automobiles (pp. 498-510).

Wang, Q., Zhou, M., Sabri, M. M. S., & Huang, J. (2022). A Comparative Study of AI-Based International Roughness Index (IRI) Prediction Models for Jointed Plain Concrete Pavement (JPCP). *Materials*, *15*(16), 5605.

Wilde, W. J., Waalkes, S., & Harrison, R. (1999). *Life cycle cost analysis of Portland cement concrete pavements* (No. FHWA/TX-00/0-1739-1). University of Texas at Austin. Center for Transportation Research.

Appendix A. Proposed Specification for Measuring and Reporting Faulting (P2)

This appendix describes a test method for evaluating faulting in jointed concrete pavements based on AASHTO Standard Specification R36-21. Faulting is defined as the difference in elevation across a transverse joint or crack and it could be positive of negative as illustrated in Figure A1.
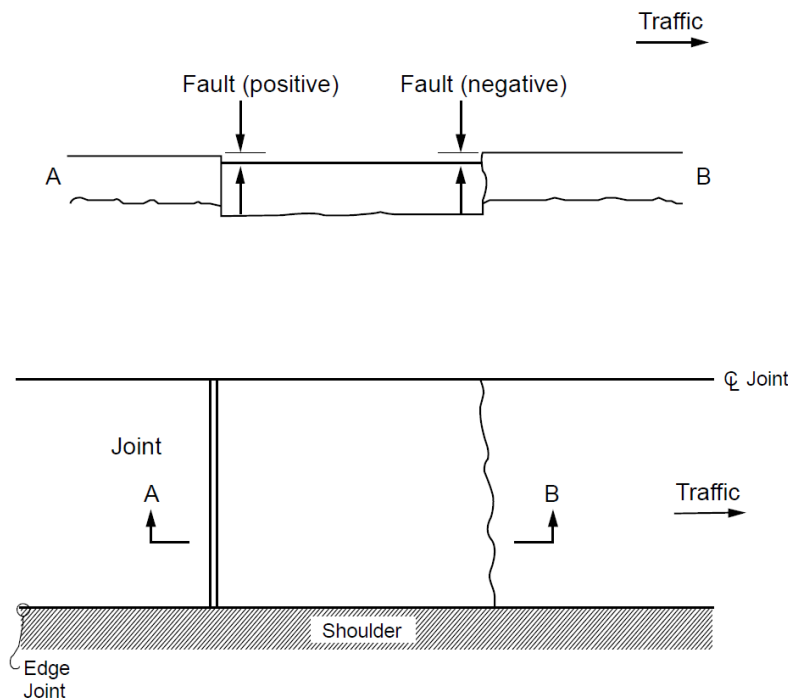
Figure A1 Schematic Representation of Faulting

This specification was specifically established based on the system developed under this research project. However, any piece of equipment that can measure faulting with the required accuracy and that can be adequately calibrated is considered acceptable.

It is TxDOT Maintenance Division's responsibility to designate the lane(s) and direction(s) of travel to be surveyed on the basis of local expertise, sound engineering principles and pavement management needs within the agency. A sampling rate level of at least 50 percent of all transverse joints is recommended at this time. The 50 percent sampling rate should be uniformly spaced (preferably every second joint) throughout the 0.1-mile section. All faulting measurements should be recorded for every 0.1-mile section and the mean, median and standard

deviation should be reported. It is recommended that a precision for faulting be established such that it is calculated to the nearest 0.5 mm (0.02 in.).

Notice that this proposed specification was developed based on AASHTO R36-21 Manual Fault Measurement in order to be compatible with such standards and to be able to compared with other State DOTs' faulting measurements and to meet FHWA requirements. Figure A2 represents the basic principles to measure faulting using a manual hand-held faultmeter.
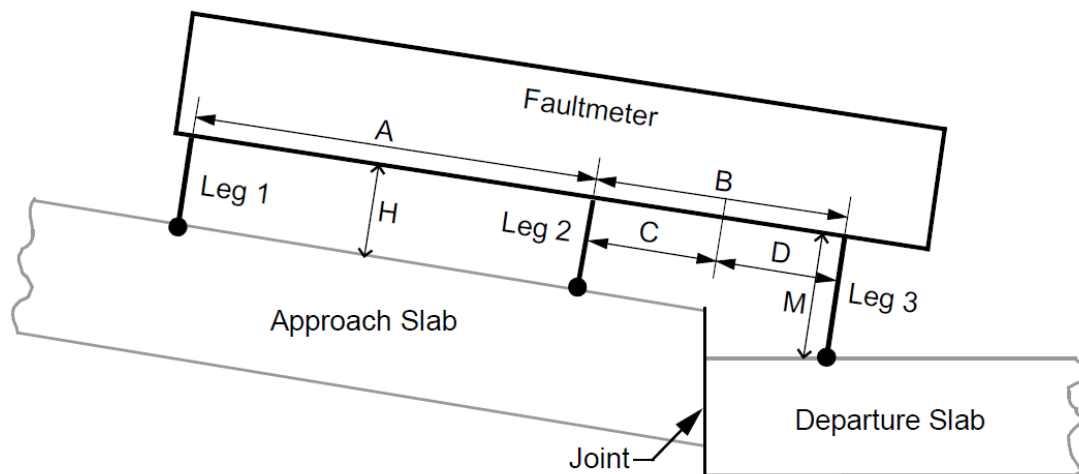
Figure A2 Faulting Measurement using Manual Method

According to AASHTO Standard, faulting (F) can be calculated using the using the following formula:

$$F = M - H \qquad \textbf{(Equation A1)}$$

where:

F : faulting, mm (in.);

M : height for measurement Leg 3, mm (in.);

H : height for Leg 1 and Leg 2, mm (in.);

A : distance between Leg 1 and Leg 2, mm (in.);

B : C + D; B is recommended to be 300 mm (11.8 in.);

C : distance between Leg 2 and the joint location with a value between 76 mm and 226 mm (3 in. and 8.9 in.); and

D : distance between the joint location and Leg 3 with a value between 76 mm and 226 mm (3 in. and 8.9 in.).

The proposed specification was developed with the principle of simulating a hand-help faultmeter for compatibility reasons. However, there are some significant differences between the current AASHTO Standard and this proposed specification that are the result of the much higher-definition system developed in this project. For example, with the faultmeter one reference point is available on the approach slab and one point on the departure slab. When using inertial profilers points could be spaced 19 mm apart which allows to obtain up to seven faulting calculations. With the system developed in this project for each joint, it is possible to obtain between 2,500 and 3,500 faulting readings per joint while traveling at 50 mph.

With the current system, the laser beam passes through a series of custiom-made lenses that project three parallel lines onto the pavement surface that the camera can capture. Driving at 50 mph, each joint can be captured by the three laser lines between four and six times. With this level of measurements density some issues were encountered. Many features around the joint significantly affect the faulting calculations. These features include, but are not limited to: aggressive surface textures, transverse and longitudinal tining, relative slope/grade between slabs, spalling, curl/warp, skewed joints, and sealant-filled joints or the presence of debris. Therefore, as part of the specification, it is important that any significant feature should be recorded.

The first step is the identification of the joint using the joint detection algorithm that was developed using artificial intelligence techniques. This algorithm processes the data and outputs the join probability that all three lasers have detected a joint. When the probability that a joint has been detected is higher than 90 percent for three consecutive profiles, that profile is identified and marked as a joint containing profile.

After that, each profile with joint detected is detrended by the 5.0 m (16.4 ft) rolling average. This step accounts for the potential slanting of the laser line relative to the pavement due to the position and motion of the vehicle on which the equipment is mounted. With a sampling interval between consecutive profiles of 40 mm (1.5 in) along the longitudinal direction, 125 profiles are averaged to form the baseline for detrending. Including the current profile itself, 62 profiles before it and 62 after are used for averaging. A line is fitted through the averaged profile, as shown in Figure A3. Using profile 514 from the Hillsboro data as the example, the averaged line takes data from profile 452 to 576 to calculate their mean. Detrending is conducted by subtracting the profile by the line fitted from the 5.0 m (16.4 ft) rolling average profile.
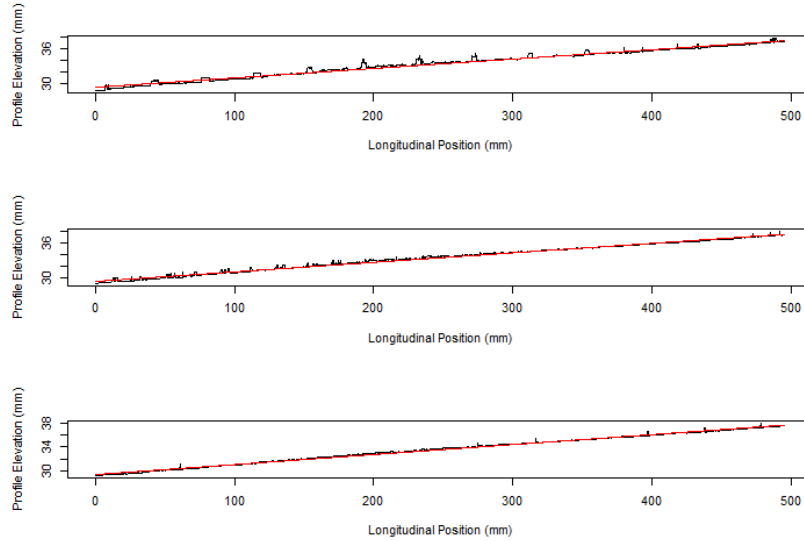
Figure A3 Averaged Profile and Fitted Line for Detrending Profile 514

After removing the linear trend, extreme values, outliers and signal noise are removed by identifying and eliminating points with elevation differences exceeding 2.0 mm from the median across the adjacent 3.0 mm of profile. Figure A4 shows the profile with filtered and unfiltered data plotted, overlapping with each other, where the red line indicates the unfiltered profile and the black line is filtered.
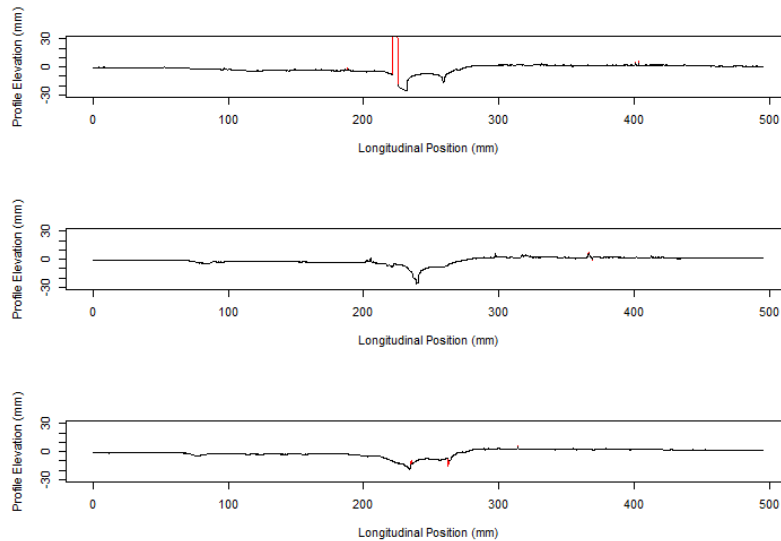

Figure A4 Profile #514 from High-Speed Run 1 before and after Extreme Value Removal

For faulting calculation using the 3-Line laser equipment, the longitudinal position of the measurement is chosen based on the specification detailed in the AASHTO R36-21. As shown in

Figure A5, an offset of 60 mm (2.3 in) adjacent to the joint on either side is marked, while a 50 mm (2.0 in) long segment starting from the offset is used on each slab to calculate the elevation difference.
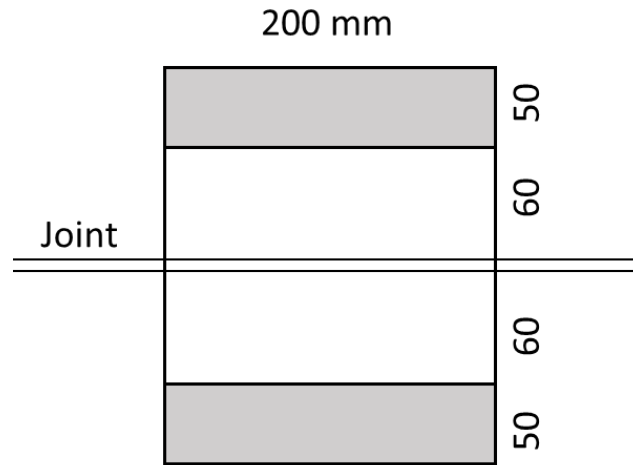
200 mm

Joint

50

60

60

50

Figure A5 Areas Used for 3-Line Laser Faulting Calculation

One of the major reasons that motivated a narrower clearing margin from the joint, as compared to the original 3.0 in (76.2 mm) defined in the AASHTO Specification for the high-speed inertial profiler, is the realistic consideration for the contact area of the tire with the pavement. The area consider in the specification did not take into account that contact area between the pavement and the tire of a commercial vehicle is smaller than the area consider in the specification.

Figure A6 shows the faulting calculation with the adjusted margins along the example profile for all three laser lines. The red line marks the identified joint, the green vertical line indicates the center of the joint, while the two blue boxes mark the segments on the approach and departure slabs used for faulting calculation. Consistent with the convention, the elevation of the departure slab is subtracted from the elebvation of the approach, with a higher approach slab indicating positive faulting, and higher departure resulting on negative faulting.
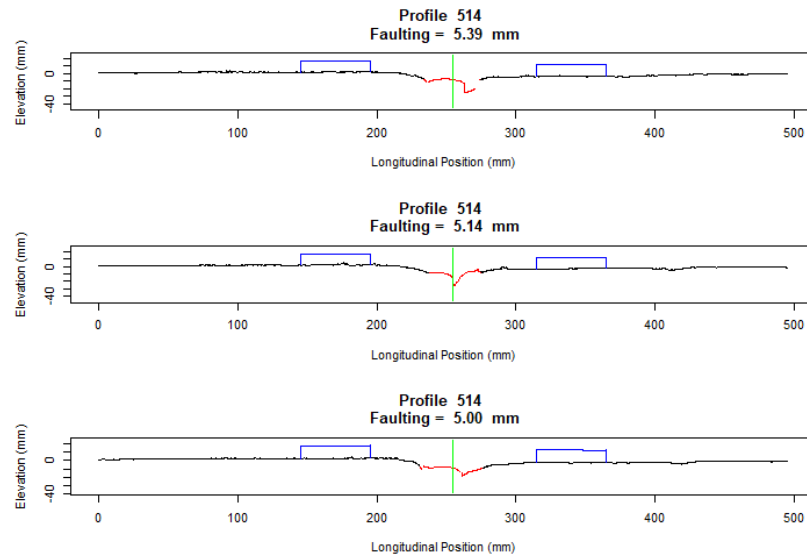
Figure A6 Faulting Calculation for 3-Line Laser Data Using Profile #514 with Longitudinal Position Based on AASHTO R36-21

75

Appendix B. Verification of Faulting Measuring Equipment (P3)

Verification Tools

As part of this research project, the research team developed and tested equipment that measures faulting along an entire joint by placing a line laser scanner on a four-meter-long stage driven by a belt that is moved very precisely at any speed ranging from 1.0 to 300 mm/s (0.04 in/s to 11.8 in/s) at the user's requests. This novel piece of equipment is referred to as the Joint Laser Scanner (JLS). The particular benefit of the equipment, in comparison to other joint measurement devices, is that it measures four meters (13 feet) in a straight line atop a joint. In comparison, other equipment types used for measuring faulting have several issues that the long stage avoids. With the long stage, the laser does not wander about the joint, nor does it have height variations as it moves along the joint. Figure B1 shows the JLS during operation.
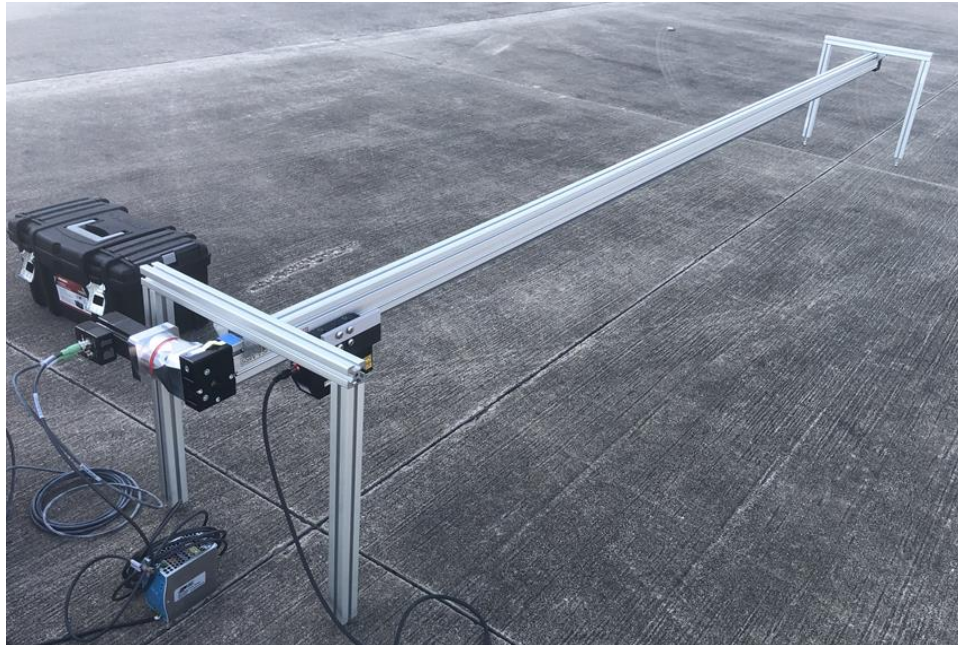

Figure B1 Joint Laser Scanner during Field Operation

In August 2020, the research team took the JLS to the TxDOT Flight Services facility at the Austin-Bergstrom International Airport and measured several joints to calibrate the equipment against micrometer readings. When the equipment is positioned to be in the center of the joint, the joint is seen to be in the middle of the data, as seen in Figure B2.
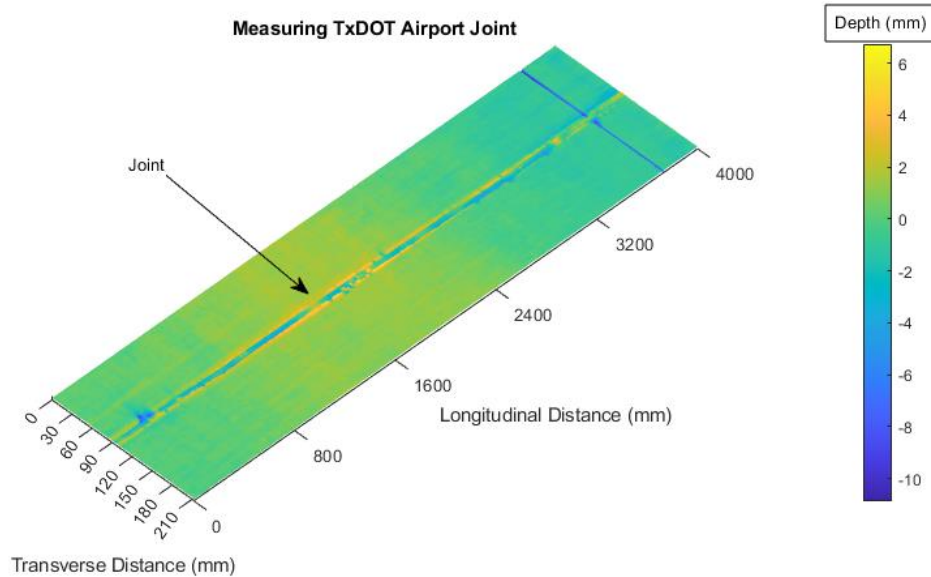
Figure B2 Joint Measured with the Joint Laser Scanner

After calculating faulting from the profiles collected, the results were stable and repeatable to a precision of better than 0.1 mm (0.004 in). For this particular exercise, several joints were measured with each joint having 4,000 samples over a length of 4.0 meters (13 ft). Faulting was calculated along the transverse distance for each of the samples. The joints measured at the airport did not have significant faulting. The results of a particular joint can be seen in Figure B3, with most of the faulting measurements between −1.0 mm (-0.039 in) and 0.7 mm (0.028 in). The corresponding quartiles were Q1 = −0.22 mm (-0.0087 in), Q2 = −0.02 (-0.0008 in), and Q3 = 0.14 mm (0.0055 in).
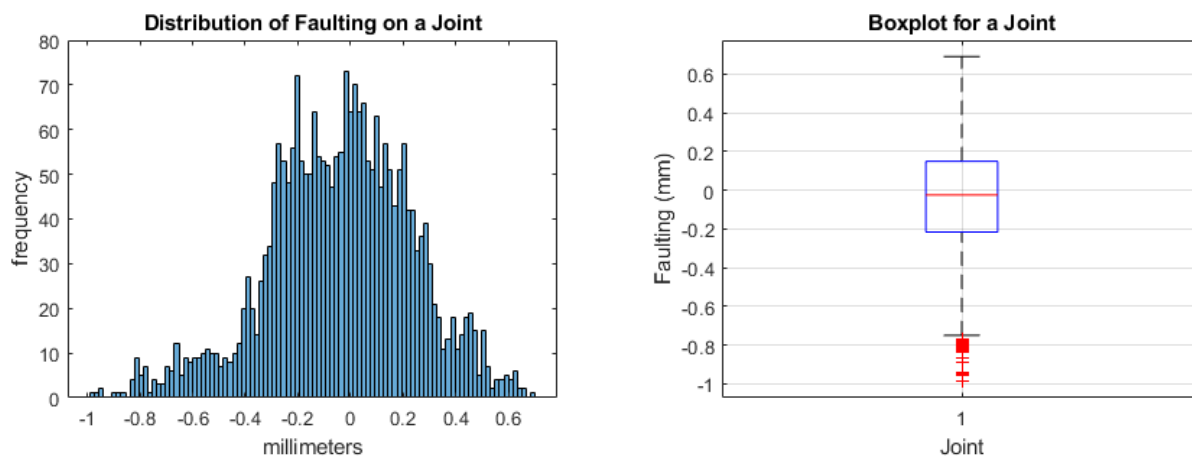

Figure B3 Faulting Calculation Results

In addition to the JLS, the research team developed other tools such as the Pushcart and the HM Robot, which were previously tested and used for joint evaluation in Rockdale (Texas) and other sites with JCP. Both the HM Robot and the Pushcart can be seen in Figure B4.

Figure B4 Pushcart (left) and HM Robot (right) Collecting Data

The Pushcart applies a similar method of measuring joints to that of the 3-Line Laser developed during this project. The single laser line projected by the Pushcart is oriented parallel to the direction of travel (longitudinal direction), capturing a single joint repeatedly throughout the length of the laser line. As the user pushes the four-wheel cart, a fifth wheel on the Pushcart measures the distance traveled and serves to trigger the equipment to capture profiles every 10 mm of travel. The installed laser line captures 2,048 points per profile for a total length of 330 mm (13 in), meaning that a unique joint can be captured up to 33 times.

The HM Robot is another tool that has been used for evaluating joints, specially used for collecting profile data on the transverse axis of a joint, similar to the measurement of the 4-meter-long stage. The user maneuvers the HM Robot through a handheld controller, where direction and speed are adjusted in real-time. When the user moves the robot, a trigger is used to capture profiles every 1.0 mm (0.039 in) of travel. The installed laser line captures 2,048 points per profile for a total length of 330 mm (13 in), collecting discrete profiles along the joint.

Ultimately, all three types of equipment could be used by TxDOT for the purpose of faulting equipment verification to control the quality of the data collected by service providers. However, the four-meter-long JLS is strongly recommended above the other two pieces due to its higher accuracy and lower variability when measuring joints in the field. All of the three equipment

types do require traffic control as they are stationary or low-speed, however, the JLS is more efficient than the other two pieces.

Statistical Considerations

There are approximately 1,150 lane-miles of JCP in Texas, with six districts accounting for more than 92 percent of the total mileage. These districts are Dallas, Beaumont, Houston, Paris, Waco, and Atlanta. For this reason, these districts were selected for locating the verification and control sections that will be used for benchmarking and verifying the faulting measurements collected by the service providers. Figure B5 shows the distribution of the mileage of JCP in Texas, while Figure B6 shows the geographical distribution of the in-service JCP sections.
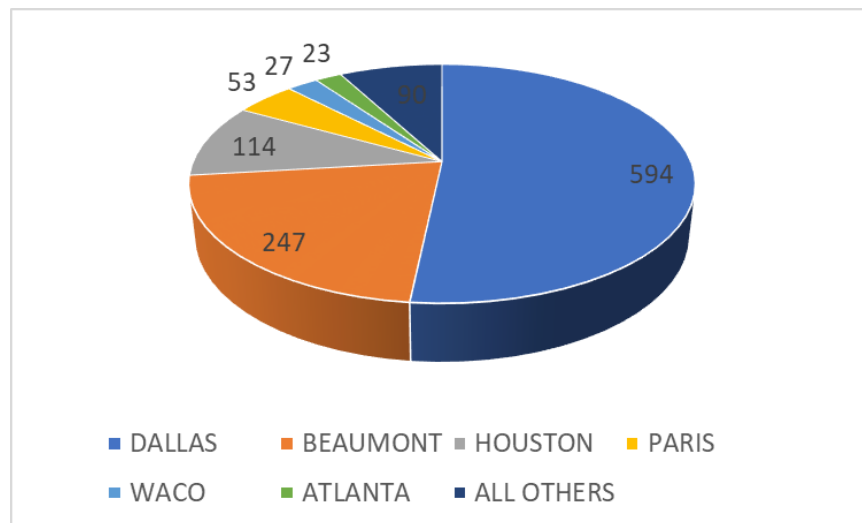

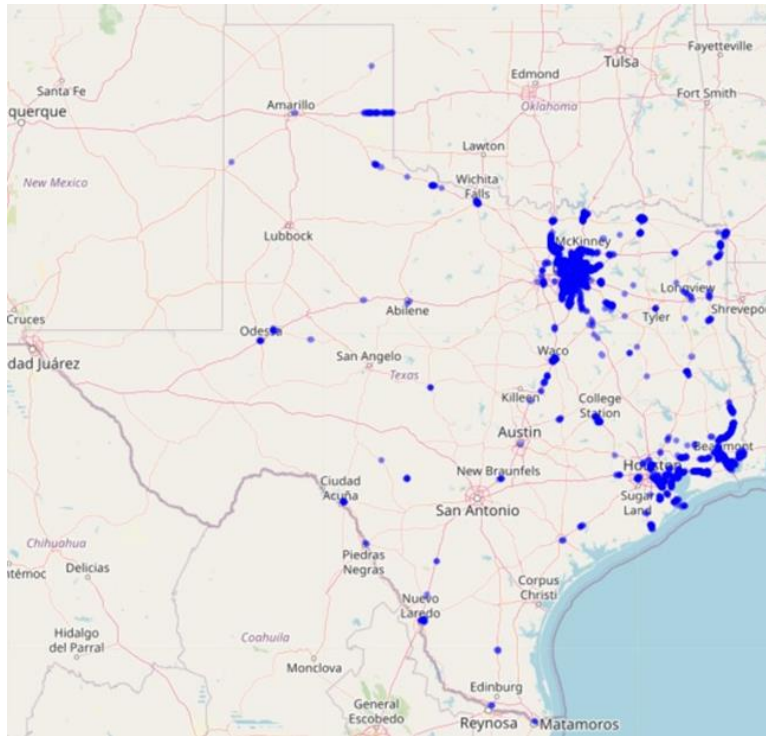*Figure B5 Mileage of Jointed Concrete Pavements in Texas*

Figure B6 Location of Jointed Concrete Pavements in Texas

Historically, popular joint spacings encountered in Texas are 15, 30, and 60 feet, which means that 35, 17, or 8 joints are typically present in a 0.1-mile section of highway. Based on the analysis of the preliminary results of the field testing conducted in this research project, the research team established that an acceptable standard deviation for faulting measures should be in the order of 1.0 mm. Based on the concept of statistical confidence intervals, the potentially achievable precision can be calculated as a function of the sample size and the desired level of confidence. Table B1 shows the maximum precision that is achievable at various levels of confidence for some popular joint spacings. In this case, the precision is expressed as the width of the interval that is necessary to achieve the desired level of confidence. As can been seen in Table B1, if the desired level of precision for a 0.1-mile section of highway is 1.0 mm at 90 percent confidence level or higher, this can only be achieved for joint spacings of 15 feet. For joint spacings of 30 feet and 1.0 mm precision, the maximum possible confidence will be 89 percent. Finally, for joint spacing of 60 feet and 1.0 mm precision, the maximum possible confidence will be 61 percent. In summary, for obtaining high precision (1.0 mm/0.039 in) and high confidence (95 percent) at least 23 joints need to be measured. Therefore, a minimum of three control sections need to be used at each district, assuming the "worst-case scenario" of 60-foot joint spacing. Although rare, such joint spacing does exist such as in Hillsboro, where the section chosen for equipment precision and verification tool testing had concrete slabs of 60 ft long.

Table B1 Achievable Precision at Different Levels of Confidence

Confidence Level (%)		50	60	70	80	90	95
Joint Spacing	No. of Joints	Possible Precision mm (in)					
60'	8	0.88 (0.035)	0.99 (0.039)	1.13 (0.044)	1.31 (0.052)	1.63 (0.064)	1.95 (0.077)
30'	17	0.58 (0.023)	0.65 (0.026)	0.73 (0.029)	0.84 (0.033)	1.02 (0.040)	1.19 (0.047)
15'	35	0.40 (0.016)	0.44 (0.017)	0.50 (0.020)	0.57 (0.022)	0.69 (0.027)	0.79 (0.031)

Verification Procedure

The performance of dynamic verification testing on actual in-service highway sections over a range of faulting values of JCP is recommended. Different surface treatment types on which faulting measurement equipment will be expected to collect data should be included in this testing.

Each test section should be at least 0.1 mile in length, with proper lead-in distance and a safe stopping distance available. Test sections should not include significant grade or grade change. Also, significant horizontal curvature or superelevation should be avoided.

Three 0.1-mile verification and control sections will be selected and scanned with the JLS for establishing the ground truth at each of three districts selected among the following six districts: Dallas, Beaumont, Houston, Paris, Waco, and Atlanta. As mentioned previously, these six districts account for more than 92 percent of the mileage on JPCs in Texas.

Reference Equipment

The research team recommends the use of reference faulting measurement equipment that can meet the repeatability and accuracy criteria for measuring faulting to collect the reference faulting data. They recommend a reference device that can collect longitudinal and transverse data from the test section, and that a JLS be used for this purpose, as it has the highest level of precision available in the market and is very efficient for scanning full joints, up to 4.0 m (13 feet).

Since temperature and moisture have a curling or warping effect on JCPs, reference measurement would ideally be obtained immediately before measurements with the evaluated equipment are made. Preferably reference measurement and equipment verification would be conducted within a two-hour period, in the morning hours to minimize the effects of curling and warping.

As Khazanovic et al. (2004) identified when developing the mechanistic-empirical model to predict transverse joint faulting, the change in joint opening due to seasonal differences in the average temperature of the concrete causes seasonal variation in faulting. Barman et al. (2022) further noted that as the moisture content in granular base and subgrade changes across seasons, their support varies along with it, placing an impact on concrete pavement faulting. To ensure consistency, data collection each year should be conducted during the season with lowest temperature and moisture variations. Fall would be the preferable season as it provides a moderate temperature while avoiding the weak foundation during period of high precipitation.

Faulting measurements should be made at 50 mph or the posted speed on the designated control sections. Data collection should be manually or automatically triggered at the starting location of the section and reported so that a longitudinal position of zero occurs at the starting location. An automatically detectable mark at the end of the section may be used to verify the DMI repeatability and accuracy. Each joint in the 0.1-mile section should be uniquely identified.

The first three characters of the file name shall be reserved for identifying the section tested and the joint number. Joints shall be numbered consecutively starting at one at each control section. This identification shall be established by the testing agency and given to the operator of the profiler on or before the day of testing.

The fourth and fifth character should be TT, for runs made on transverse tinning sections; TL, for runs made on longitudinal transverse sections; or NT, for sections with no tinning.

The sixth and seventh character should designate the distance in feet from the right wheel path that the measurements are being sampled from. The character should be a value from zero to 14 in feet.

The file extension should be appropriate for the data type being transmitted and will be specified by the agency.

Test Results

The results of the verification tests shall be documented by the testing agency. The distribution of the results of the certification shall be determined by the testing agency. Results of certification must include the following information:

- Identification of the faulting equipment tested (i.e., make, model, serial number, software version, owner, etc.);

- Date and time of the reference test;

- Date and time of the verification test;

- Operator of the equipment;

- Faulting measured at each joint;

- Average and median faulting for each 0.1-mile section and standard deviation;

- The difference between the fault measurements computed by the service provider and those from the reference equipment.

The provisional criteria is as follows:

- o For each joint, measurements shall be within ± 2.0 mm (0.079 in), and

- o For the average of the 0.1-mile section, the value shall be within ± 1.0 mm (0.039 in).

- Overall determination from the test: Pass or Fail.

The report must also label each test result with a Pass or Fail, possibly denoted by a color coding with green and red representing pass and fail respectively, depending on whether the given test value meets or fails to meet the prescribed criterion.

Appendix C. Joint Detection Code

```matlab
clear medfiltdata1 medfiltdata2 medfiltdata3 hpfiltdata1 hpfiltdata2 hpfiltdata3 min1
min2 min3 detect detect2 minm minm2 minm3 mintest mintest2 mintest3 index1 index2
index3 lpfiltdata1 lpfiltdata2 lpfiltdata3

Data1=readmatrix('ProfilesR_AOI1.csv');
Data2=readmatrix('ProfilesR_AOI2.csv');
Data3=readmatrix('ProfilesR_AOI3.csv');
Target=readmatrix('Location_of_joints.csv');

tic

s=size(Data1);

ntimesteps=s(1);
sclength=s(2);


%median filter for removing spikes

horizon=40000; %time horizon of data processing
beginstep=1; %first step in data processing
hpf=300; %high pass filter window


medfiltdata1=zeros(horizon,sclength-5);
medfiltdata2=zeros(horizon,sclength-5);
medfiltdata3=zeros(horizon,sclength-5);

for i=1:horizon
    for j=3:sclength-3
        medfiltdata1(i,j-2)=Data1(i+beginstep,j);
    end
end

for i=1:horizon
    for j=3:sclength-3
        medfiltdata2(i,j-2)=Data2(i+beginstep,j);
    end
end

for i=1:horizon
    for j=3:sclength-3
        medfiltdata3(i,j-2)=Data3(i+beginstep,j);
    end
end


hpfiltdata1=zeros(horizon,sclength-5-hpf);
hpfiltdata2=zeros(horizon,sclength-5-hpf);
hpfiltdata3=zeros(horizon,sclength-5-hpf);

for i=1:horizon
    avg=mean(medfiltdata1(i,1:1+hpf));
    hpfiltdata1(i,1)=medfiltdata1(i,1+hpf/2)-avg;
```

```matlab
    for j=2:sclength-5-hpf
        avg = avg+ 1/hpf*(medfiltdata1(i,j+hpf)-medfiltdata1(i,j-1));
        hpfiltdata1(i,j)=medfiltdata1(i,j+hpf/2)-avg;
    end
end


for i=1:horizon
    avg=mean(medfiltdata2(i,1:1+hpf));
    hpfiltdata2(i,1)=medfiltdata2(i,1+hpf/2)-avg;
    for j=2:sclength-5-hpf
        avg=avg+1/hpf*(medfiltdata2(i,j+hpf)-medfiltdata2(i,j-1));
        hpfiltdata2(i,j)=medfiltdata2(i,j+hpf/2)-avg;
    end
end

for i=1:horizon
    avg=mean(medfiltdata3(i,1:1+hpf));
    hpfiltdata1(i,1)=medfiltdata3(i,1+hpf/2)-avg;
    for j=2:sclength-5-hpf
        avg=avg+1/hpf*(medfiltdata3(i,j+hpf)-medfiltdata3(i,j-1));
        hpfiltdata3(i,j)=medfiltdata3(i,j+hpf/2)-avg;
    end
end



lpf=30; %low pass filter parameter

lpfiltdata1=zeros(horizon,sclength-5-hpf-lpf);
lpfiltdata2=zeros(horizon,sclength-5-hpf-lpf);
lpfiltdata3=zeros(horizon,sclength-5-hpf-lpf);

for i=1:horizon
        avg=mean(hpfiltdata1(i,1:1+2*lpf));
        lpfiltdata1(i,2+lpf)=avg;
    for j=2+lpf:sclength-5-hpf-lpf
        avg=avg+1/(2*lpf)*(hpfiltdata1(i,j+lpf)-hpfiltdata1(i,j-lpf-1));
        lpfiltdata1(i,j)=avg;
    end
end



for i=1:horizon
        avg=mean(hpfiltdata2(i,1:1+2*lpf));
        lpfiltdata2(i,2+lpf)=avg;
    for j=2+lpf:sclength-5-hpf-lpf
        avg=avg+1/(2*lpf)*(hpfiltdata2(i,j+lpf)-hpfiltdata2(i,j-lpf-1));
        lpfiltdata2(i,j)=avg;
    end
end

for i=1:horizon
        avg=mean(hpfiltdata3(i,1:1+2*lpf));
        lpfiltdata3(i,2+lpf)=avg;
    for j=2+lpf:sclength-5-hpf-lpf
        avg=avg+1/(2*lpf)*(hpfiltdata3(i,j+lpf)-hpfiltdata3(i,j-lpf-1));
        lpfiltdata3(i,j)=avg;
```

```matlab
    end
end



[min1,index1]=min(lpfiltdata1,[],2);
[min2,index2]=min(lpfiltdata2,[],2);
[min3,index3]=min(lpfiltdata3,[],2);



for i=1:horizon
    mintest(i)=median([min1(i),min2(i),min3(i)]);
end

minm=max(max(min1,min2),min3);
maxm=min(min1,min(min2,min3));


for i=1:horizon
    indexdiff(i)=max( max( abs(index1(i)-index2(i)) ,abs(index1(i)-
index3(i))),abs(index2(i)-index3(i)));
end



hpparam=40;

minm2=0;

for i=1+hpparam/2:horizon-hpparam
    minm2(i+hpparam/2)=minm(i+hpparam/2)-median(minm(i:i+hpparam),'omitnan');
end

sz=size(minm2);

medfparam=20; %median filter parameter
mintest2=0;


for i=1:horizon-2*medfparam
    mintest2(i+medfparam)=mintest(i+medfparam)-
median(mintest(i:i+2*medfparam),'omitnan');
end

mintest3=0;

for i=2:horizon-2*medfparam-1
    mintest3(i)=median(mintest2(i-1:i+1));
end



for i=2:horizon-2*medfparam-1
    if mintest3(i)<-100 && indexdiff(i)<150
        detect(i)=0.8;
    else
```

```matlab
            detect(i)=0;
        end

    end


    for i=5:horizon-2*medfparam-4
        detect2(i)=median(detect(i-2:i+2));
    end



    toc


    plot(detect2) % output result
    hold on
    plot(Target(beginstep:beginstep+horizon))
```

Appendix D. Faulting Calculation Code

```
library(readr)
library(dplyr)
library(pracma)
library(shiny)
library(shinythemes)
library(DT)

highspeed1_1 <- read_csv("highspeed1_1.csv",
              col_names = FALSE, skip = 6)
highspeed1_2 <- read_csv("highspeed1_2.csv",
              col_names = FALSE, skip = 6)
highspeed1_3 <- read_csv("highspeed1_3.csv",
              col_names = FALSE, skip = 6)


highspeed2_1 <- read_csv("highspeed2_1.csv",
              col_names = FALSE, skip = 6)
highspeed2_2 <- read_csv("highspeed2_2.csv",
              col_names = FALSE, skip = 6)
highspeed2_3 <- read_csv("highspeed2_3.csv",
              col_names = FALSE, skip = 6)


highspeed3_1 <- read_csv("highspeed3_1.csv",
              col_names = FALSE, skip = 6)
highspeed3_2 <- read_csv("highspeed3_2.csv",
              col_names = FALSE, skip = 6)
highspeed3_3 <- read_csv("highspeed3_3.csv",
              col_names = FALSE, skip = 6)



# clearing <- 60
# box_width <- 50
# pixel_length <- 0.24185

num_nonzero <- function(x){length(which(x != 0))}

cut_off_val <- function(x) {max(which(apply(x,1,num_nonzero) > 100))}

roll_med_diff <- function(x,radius){
  y <- NULL
```

```r
  for (i in 1:length(x)){
    window_start <- max(min((i-radius),(length(x)-(2*radius + 1))),1)
    window_end <- min(max((i+radius),(2*radius + 1)),length(x))
    diff_val <- x[i] - median(x[window_start:window_end],na.rm = T)
    y <- c(y,diff_val)
  }
  return(y)
}

find_extreme <- function(x,multiple,bound = c('up','down','both')){
  up <- quantile(x,.75,na.rm = TRUE)
  down <- quantile(x,.25,na.rm = TRUE)
  iqr <- IQR(x,na.rm = TRUE)
  if (bound == 'up'){
    which(x - multiple * iqr > up) %>% return()
  }
  else if (bound == 'down'){
    which(down - x > multiple * iqr) %>% return()
  }
  else {
    which(x - multiple * iqr > up|down - x > multiple * iqr) %>% return()
  }
}

inv.seq <- function(i,width) {
  li <- length(i <- as.integer(i))
  if(li == 0) return(expression(NULL))
  else if(li == 1) return(as.expression(i))
  ##-- now have: length(i) = 2
  di1 <- abs(diff(i)) <= width    #-- those are just simple sequences  n1:n2 !
  s1 <- i[!c(FALSE,di1)] # beginnings
  s2 <- i[!c(di1,FALSE)] # endings

  ## using text & parse {cheap and dirty} :
  mkseq <- function(i,j) if(i == j) i else paste(i,":",j, sep="")
  mapply(mkseq, s1,s2)
}

length_return <- function(x,width,length_min,length_max){
  return_val <- NULL
  return_text <- NULL
```

```r
  if (length(inv.seq(x,width)) == 1){
    return (eval(inv.seq(x,width)))
  }
  else for ( i in inv.seq(x,width)){
    if (is.numeric(i)){
      return_val <- c(return_val,length(i))
      return_text <- c(return_text,i)
    }
    else{
      return_val <- c(return_val,length(eval(str2expression(i))))
      return_text <- c(return_text,i)
    }
  }

  valid <- return_text[which(return_val >= length_min & return_val <= length_max)]
  invalid <- return_text[which(return_val < length_min | return_val > length_max)]

  return(list('valid' = valid,'invalid' = invalid))

}


quick_rem <- function(x,radius = 5, thres = 2,upper_bound,lower_bound){
  if (is.list(x)){
    x <- unlist(x)
  }
  if (missing(upper_bound)){
    x[which(x - median(x,na.rm = T) > 20)] <- NA
    x[which(x < - 160 )] <- NA
    x[which(abs(roll_med_diff(x,radius = radius)) > thres)] <- NA
    return(x)
  }
  else{
    x[which(x  > upper_bound)] <- NA
    x[which(x < lower_bound )] <- NA
    x[which(abs(roll_med_diff(x,radius = radius)) > thres)] <- NA
    return(x)
  }
}

loc_jt <- function(x,width,length_min,length_max,min_area){
```

```r
low_quart <- quantile(x,.05,na.rm = T)
extreme <- which(x < low_quart)
temp_return <- extreme %>% length_return(width,length_min,length_max)
temp_length <- temp_return %>% length

if (temp_length == 0){
  return(NULL)
}
else if (temp_length == 1){
  if (is.numeric(temp_return)){
    return(NULL)
  }
  else {
    current_list <- temp_return %>% str2expression %>% eval
    profile_current <- x[current_list]
    profile_current[which(profile_current >= quantile(profile_current,(1 -
width/length(current_list)),na.rm = T))] <- quantile(profile_current,.1,na.rm = T)
    area_below <- ((median(x,na.rm = T) - profile_current)) %>% sum(na.rm = T)
/length(current_list)

  }
  if (length(current_list) >= length_min & length(current_list) <= length_max  & area_below >
min_area){
    return(list('jt_loc' = current_list,'area' = area_below))
  }
  else{
    return(NULL)
  }
}
else{
  return_list <- NULL
  area_below <- min_area
  if (length(temp_return$valid) > 0){
    for (i in temp_return$valid){
      if (is.numeric(i)){
        next
      }
      else {
        current_list <- i %>% str2expression %>% eval
        profile_current <- x[current_list]
```

```r
      profile_current[which(profile_current >= quantile(profile_current,(1 -
width/length(current_list)),na.rm = T))] <- quantile(profile_current,.1,na.rm = T)
       area_below_current <- ((median(x,na.rm = T) - profile_current)) %>% sum(na.rm =
T)/length(current_list)
      }
      if (length(current_list) >= length_min & length(current_list) <= length_max & area_below <
area_below_current){
        return_list <- current_list
        area_below <- area_below_current
      }
     }
    }
   if (length(return_list) >0 & length(area_below) > 0){
     return(list('jt_loc' = return_list,'area' = area_below))
   }
   else {
     return(NULL)
   }
  }
}

three_line_process <- function(line1,line2,line3,profile,detrend_by = list(by = 'center
frame',frame_radius = 62,linear = TRUE),thres = 2){
  profile_num <- profile

  if (is.list(detrend_by)){

    frame_radius <- detrend_by$frame_radius

    if (detrend_by$linear){
      ln_fit1 <- apply(line1[max(1,(profile_num -
frame_radius)):min((profile_num+frame_radius),nrow(line1)),],2,mean)
      ln_fit2 <- apply(line2[max(1,(profile_num -
frame_radius)):min((profile_num+frame_radius),nrow(line2)),],2,mean)
      ln_fit3 <- apply(line3[max(1,(profile_num -
frame_radius)):min((profile_num+frame_radius),nrow(line3)),],2,mean)

      length_profile <- 1:length(ln_fit1)

      lm1 <- lm(ln_fit1 ~ length_profile)
      lm2 <- lm(ln_fit2 ~ length_profile)
```

```
    lm3 <- lm(ln_fit3 ~ length_profile)

    profile_1 <- ((line1[profile_num,] %>% as.numeric %>% quick_rem(radius = 6,thres = thres))
- lm1$fitted.values) %>% rev
    profile_2 <- ((line2[profile_num,] %>% as.numeric %>% quick_rem(radius = 6,thres = thres))
- lm2$fitted.values) %>% rev
    profile_3 <- ((line3[profile_num,] %>% as.numeric %>% quick_rem(radius = 6,thres = thres))
- lm3$fitted.values) %>% rev

    lm1$coefficients[2] * length_profile
  }
  else{
    profile_1 <- ((line1[profile_num,] %>% as.numeric %>% quick_rem(radius = 6,thres = thres))
- apply(line1[max(1,profile_num -
frame_radius):min(profile_num+frame_radius,nrow(line1)),],2,mean)) %>% rev
    profile_2 <- ((line2[profile_num,] %>% as.numeric %>% quick_rem(radius = 6,thres = thres))
- apply(line2[max(1,profile_num -
frame_radius):min(profile_num+frame_radius,nrow(line1)),],2,mean)) %>% rev
    profile_3 <- ((line3[profile_num,] %>% as.numeric %>% quick_rem(radius = 6,thres = thres))
- apply(line3[max(1,profile_num -
frame_radius):min(profile_num+frame_radius,nrow(line1)),],2,mean)) %>% rev
  }
 }

 else if (detrend_by == 'frame'){
   profile_1 <- ((line1[profile_num,] %>% as.numeric %>% quick_rem(radius = 6,thres = thres)) -
apply(line1[((profile_num %/% 256*256)+1):((profile_num %/% 256 + 1)*256),],2,mean)) %>%
rev
   profile_2 <- ((line2[profile_num,] %>% as.numeric %>% quick_rem(radius = 6,thres = thres)) -
apply(line2[((profile_num %/% 256*256)+1):((profile_num %/% 256 + 1)*256),],2,mean)) %>%
rev
   profile_3 <- ((line3[profile_num,] %>% as.numeric %>% quick_rem(radius = 6,thres = thres)) -
apply(line3[((profile_num %/% 256*256)+1):((profile_num %/% 256 + 1)*256),],2,mean)) %>%
rev
 }
 else{
   profile_1 <- (line1[profile_num,] %>% as.numeric %>% quick_rem(radius = 6,thres = thres))
%>% rev
   profile_2 <- (line2[profile_num,] %>% as.numeric %>% quick_rem(radius = 6,thres = thres))
%>% rev
```

```r
    profile_3 <- (line3[profile_num,] %>% as.numeric %>% quick_rem(radius = 6,thres = thres))
%>% rev
  }

  return(list(profile_1 = profile_1,profile_2 = profile_2, profile_3 = profile_3))
}



faulting_calc_temp <- function(line1,line2,line3,profile,detrend_by = list(by = "center frame",
frame_radius = 62, linear = TRUE),frame_radius,profile_detrend = FALSE,loc_jt_par = list(width
= 70,length_min = 75,length_max = 350,min_area_total = 5,min_area = 2),clearing =
60,box_width = 50, pixel_length = 0.24185){

  profile_num <- profile

  output <- three_line_process(line1,line2,line3,profile,detrend_by = detrend_by,thres  = 2)

  profile_1 <- output$profile_1
  profile_2 <- output$profile_2
  profile_3 <- output$profile_3


  profile_sum <- apply(cbind(profile_1,profile_2,profile_3),1,sum)

 jt_loc <-
loc_jt(profile_sum,loc_jt_par$width,loc_jt_par$length_min,loc_jt_par$length_max,loc_jt_par$
min_area_total)$jt_loc

 if (length(jt_loc) == 0){
   return(NULL)
 }

 jt_loc_1 <-
loc_jt(profile_1,loc_jt_par$width,loc_jt_par$length_min,loc_jt_par$length_max,loc_jt_par$min
_area)$jt_loc
 jt_loc_2 <-
loc_jt(profile_2,loc_jt_par$width,loc_jt_par$length_min,loc_jt_par$length_max,loc_jt_par$min
_area)$jt_loc
 jt_loc_3 <-
loc_jt(profile_3,loc_jt_par$width,loc_jt_par$length_min,loc_jt_par$length_max,loc_jt_par$min
_area)$jt_loc
```

```r
  if (length(which(c(length(jt_loc_1) == 0,length(jt_loc_2) == 0,length(jt_loc_3) == 0))) > 2){
    return(NULL)
  }

  if (length(which(c(length(jt_loc_1) == 0,length(jt_loc_2) == 0,length(jt_loc_3) == 0))) >= 1 &
length(which(c(length(jt_loc_1) == 0,length(jt_loc_2) == 0,length(jt_loc_3) == 0))) <3){
    if (1 %in% which(c(length(jt_loc_1) == 0,length(jt_loc_2) == 0,length(jt_loc_3) == 0))){
      jt_loc_1 <- jt_loc
    }
    else if (abs(mean(jt_loc_1) - mean(jt_loc)) > 25){
      jt_loc_1 <- jt_loc
    }
    if (2 %in% which(c(length(jt_loc_1) == 0,length(jt_loc_2) == 0,length(jt_loc_3) == 0))){
      jt_loc_2 <- jt_loc
    }
    else if (abs(mean(jt_loc_2) - mean(jt_loc)) > 25){
      jt_loc_2 <- jt_loc
    }
    if (3 %in% which(c(length(jt_loc_1) == 0,length(jt_loc_2) == 0,length(jt_loc_3) == 0))){
      jt_loc_3 <- jt_loc
    }
    else if (abs(mean(jt_loc_3) - mean(jt_loc)) > 25){
      jt_loc_3 <- jt_loc
    }
  }

  if ((mean(jt_loc_1) - mean(jt_loc_2)) %>% abs > 50 & (mean(jt_loc_1) - mean(jt_loc_3)) %>%
abs > 50){
    jt_loc_1 <- jt_loc
  }
  if ((mean(jt_loc_2) - mean(jt_loc_1)) %>% abs > 50 & (mean(jt_loc_2) - mean(jt_loc_3)) %>%
abs > 50){
    jt_loc_2 <- jt_loc
  }
  if ((mean(jt_loc_3) - mean(jt_loc_1)) %>% abs > 50 & (mean(jt_loc_3) - mean(jt_loc_2)) %>%
abs > 50){
    jt_loc_3 <- jt_loc
  }

  start_1 <- min(jt_loc_1) - 1
```

```r
end_1 <- max(jt_loc_1)+1
start_2 <- min(jt_loc_2) - 1
end_2 <- max(jt_loc_2)+1
start_3 <- min(jt_loc_3) - 1
end_3 <- max(jt_loc_3)+1

if (!(end_1 - start_1 >= 21 & end_2 - start_2 >= 21 & end_3 - start_3 >= 21)){
  return(NULL)
}

center_joint <- round(mean(c(start_1,end_1,start_2,end_2,start_3,end_3)))

slope_rem_1 <- profile_1
slope_rem_2 <- profile_2
slope_rem_3 <- profile_3

if (isTRUE(profile_detrend)){
  x_up_1 <- 1:start_1
  x_down_1 <- end_1:length(slope_rem_1)
  x_up_2 <- 1:start_2
  x_down_2 <- end_2:length(slope_rem_2)
  x_up_3 <- 1:start_3
  x_down_3 <- end_3:length(slope_rem_3)

  slope_1 <- lm(slope_rem_1[c(x_up_1,x_down_1)] ~ c(x_up_1,x_down_1))
  slope_2 <- lm(slope_rem_2[c(x_up_2,x_down_2)] ~ c(x_up_2,x_down_2))
  slope_3 <- lm(slope_rem_3[c(x_up_3,x_down_3)] ~ c(x_up_3,x_down_3))

  slope_rem_1 <- slope_rem_1 - (1:length(slope_rem_1)) * slope_1$coefficients[2] -
slope_1$coefficients[1]
  slope_rem_2 <- slope_rem_2 - (1:length(slope_rem_2)) * slope_2$coefficients[2] -
slope_2$coefficients[1]
  slope_rem_3 <- slope_rem_3 - (1:length(slope_rem_3)) * slope_3$coefficients[2] -
slope_3$coefficients[1]}

 ran_1 = c(range(slope_rem_1,na.rm = TRUE)[1]-20,(range(slope_rem_1,na.rm = TRUE)[2])+20)
 ran_2 = c(range(slope_rem_2,na.rm = TRUE)[1]-20,(range(slope_rem_2,na.rm = TRUE)[2])+20)
 ran_3 = c(range(slope_rem_3,na.rm = TRUE)[1]-20,(range(slope_rem_3,na.rm = TRUE)[2])+20)
```

```r
    upper_box_1 <- round(center_joint - (clearing + box_width)/pixel_length):round(center_joint
- clearing/pixel_length)
    lower_box_1 <- round(center_joint + clearing/pixel_length):round(center_joint + (clearing+
box_width)/pixel_length)
    upper_box_2 <- round(center_joint - (clearing + box_width)/pixel_length):round(center_joint
- clearing/pixel_length)
    lower_box_2 <- round(center_joint + clearing/pixel_length):round(center_joint + (clearing+
box_width)/pixel_length)
    upper_box_3 <- round(center_joint - (clearing + box_width)/pixel_length):round(center_joint
- clearing/pixel_length)
    lower_box_3 <- round(center_joint + clearing/pixel_length):round(center_joint + (clearing+
box_width)/pixel_length)

    if(range(lower_box_1,na.rm = T)[2] >= 2048 |range(lower_box_2,na.rm = T)[2] >= 2048 |
range(lower_box_3,na.rm = T)[2] >= 2048 |range(upper_box_1,na.rm = T)[1] <= 0
|range(upper_box_2,na.rm = T)[1] <= 0 |range(upper_box_3,na.rm = T)[1] <= 0){
      return(NULL)}

    faulting_val3_3 <- - mean(slope_rem_3[lower_box_3],na.rm = T) +
mean(slope_rem_3[upper_box_3],na.rm = T)
    faulting_val3_2 <- - mean(slope_rem_2[lower_box_2],na.rm = T) +
mean(slope_rem_2[upper_box_2],na.rm = T)
    faulting_val3_1 <- - mean(slope_rem_1[lower_box_1],na.rm = T) +
mean(slope_rem_1[upper_box_1],na.rm = T)

    return(c(profile,faulting_val3_1,faulting_val3_2,faulting_val3_3))

}


jt_det <- function(Data1,Data2,Data3,param1 = 100,param2 = 165,hpf = 300,lpf = 30,hpparam =
40,medfparam = 20){

  s <- dim(Data1)

  ntimesteps <- s[1]
  sclength <- s[2]

  horizon <- nrow(Data1)-1
  beginstep <- 1
```

```r
medfiltdata1 <- Data1[(1:horizon) + beginstep,3:(sclength-3)]
medfiltdata2 <- Data2[(1:horizon) + beginstep,3:(sclength-3)]
medfiltdata3 <- Data3[(1:horizon) + beginstep,3:(sclength-3)]

hpfiltdata1 <- data.frame(zeros(horizon,sclength-5-hpf))
hpfiltdata2 <- data.frame(zeros(horizon,sclength-5-hpf))
hpfiltdata3 <- data.frame(zeros(horizon,sclength-5-hpf))

avg <- apply(medfiltdata1[,1:(1+hpf)],1,mean)
hpfiltdata1[,1] <- (medfiltdata1[,1+hpf/2] %>% unlist) -avg
for (j in 2:(sclength-5-hpf)){
  avg <- avg+ sapply(medfiltdata1[,j+hpf] - medfiltdata1[,j-1],function(x){x/hpf})
  hpfiltdata1[,j] <- medfiltdata1[,j+hpf/2] -avg
}

avg <- apply(medfiltdata2[,1:(1+hpf)],1,mean)
hpfiltdata2[,1] <- (medfiltdata2[,1+hpf/2] %>% unlist) -avg
for (j in 2:(sclength-5-hpf)){
  avg <- avg+ sapply(medfiltdata2[,j+hpf] - medfiltdata2[,j-1],function(x){x/hpf})
  hpfiltdata2[,j] <- medfiltdata2[,j+hpf/2] -avg
}

avg <- apply(medfiltdata3[,1:(1+hpf)],1,mean)
hpfiltdata3[,1] <- (medfiltdata3[,1+hpf/2] %>% unlist) -avg
for (j in 2:(sclength-5-hpf)){
  avg <- avg+ sapply(medfiltdata3[,j+hpf] - medfiltdata3[,j-1],function(x){x/hpf})
  hpfiltdata3[,j] <- medfiltdata3[,j+hpf/2] -avg
}

lpfiltdata1=data.frame(zeros(horizon,sclength-5-hpf-lpf))
lpfiltdata2=data.frame(zeros(horizon,sclength-5-hpf-lpf))
lpfiltdata3=data.frame(zeros(horizon,sclength-5-hpf-lpf))

avg <- apply(hpfiltdata1[,1:(1+2*lpf)],1,mean)
lpfiltdata1[,1:(1+2*lpf)] <- avg
for (j in (2+lpf):(sclength-5-hpf-lpf)){
  avg <- avg+(hpfiltdata1[,j+lpf]-hpfiltdata1[,j-lpf-1])/(2*lpf)
  lpfiltdata1[,j] <- avg
}

avg <- apply(hpfiltdata2[,1:(1+2*lpf)],1,mean)
```

```
lpfiltdata2[,1:(1+2*lpf)] <- avg
for (j in (2+lpf):(sclength-5-hpf-lpf)){
  avg <- avg+(hpfiltdata2[,j+lpf]-hpfiltdata2[,j-lpf-1])/(2*lpf)
  lpfiltdata2[,j] <- avg
}

avg <- apply(hpfiltdata3[,1:(1+2*lpf)],1,mean)
lpfiltdata3[,1:(1+2*lpf)] <- avg
for (j in (2+lpf):(sclength-5-hpf-lpf)){
  avg <- avg+(hpfiltdata3[,j+lpf]-hpfiltdata3[,j-lpf-1])/(2*lpf)
  lpfiltdata3[,j] <- avg
}

min1 <- apply(lpfiltdata1,1,min)
index1 <- apply(lpfiltdata1,1,which.min)

min2 <- apply(lpfiltdata2,1,min)
index2 <- apply(lpfiltdata2,1,which.min)

min3 <- apply(lpfiltdata3,1,min)
index3 <- apply(lpfiltdata3,1,which.min)

mintest <- apply(cbind(min1,min2,min3),1,median)

minm <- apply(cbind(apply(cbind(min1,min2),1,max),min3),1,max)
maxm <- apply(cbind(apply(cbind(min1,min2),1,min),min3),1,min)

indexdiff <- apply(cbind(apply(cbind(abs(index1-index2) ,abs(index1-
index3)),1,max),abs(index2-index3)),1,max)

minm2 <- 0

for (i in (1+hpparam/2):(horizon-hpparam)){
  minm2[i+hpparam/2] <- minm[i+hpparam/2] - sapply(minm[i:i+hpparam],median,na.rm = T)
}

sz <- dim(minm2)

mintest2 <- 0

for (i in 1:(horizon-2*medfparam)){
```

```r
    mintest2[i+medfparam] <- mintest[i+medfparam]-median(mintest[i:(i+2*medfparam)],na.rm
= T)
  }


  mintest3 <- 0

  for (i in 2:(horizon-2*medfparam-1)){
    mintest3[i] <- median(mintest2[(i-1):(i+1)],na.rm = T)
  }


  detected <- 0

  for (i in 2:(horizon-2*medfparam-1)){

    if (mintest3[i] < (-param1) & indexdiff[i] < param2){
      detected[i] <- 1}
    else{
      detected[i] <- 0}

  }

  detect2 <- 0

  for (i in 5:(horizon-2*medfparam-4)){
    detect2[i] <- median(detected[(i-2):(i+2)])
  }

  return(detect2)
}


for (run in 1:3){
  last_row <- get(paste0('highspeed',run,'_1')) %>% cut_off_val
  for (aoi in 1:3){
    assign(paste0('highspeed',run,'_',aoi),get(paste0('highspeed',run,'_',aoi))[1:last_row,])
  }
}
```

```r
ui <- navbarPage("3Line Laser Data Processing",
        selected = "Joint Detection",
        collapsible = TRUE,
        inverse = TRUE,
        theme = shinytheme("spacelab"),
        tabPanel("Joint Detection",
            fluidPage(
              sidebarLayout(
                sidebarPanel(
                  selectizeInput(inputId = "id_sel1", label = "Select Run: ", selected = 1,
                            choices = 1:((length(list.files(pattern="*.csv")))/3) ),
                    br(),
                    numericInput(inputId = "id_num", label = "Depth Parameter (Range: 50-
150)",value = 100),
                    numericInput(inputId = "id_num2", label = "Width Tolerance across AOIs
(Range: 150-180)",value = 165),
                    br(),
                    actionButton("detect",
                            "Detect Joint"),
                    downloadButton("download",
                            "Download the data")
                ),
                mainPanel(fluidRow(
                  plotOutput("upperbound")
                )

                )
              )
            )
        ),
        tabPanel("Faulting Calculation",
        fluidPage(

          # Sidebar with a slider input for number of bins
          sidebarLayout(
            sidebarPanel(
              selectizeInput(inputId = "id_sel2", label = "Select Run: ", selected = 1,
                        choices = 1:((length(list.files(pattern="*.csv")))/3)),
              actionButton("go_run",
                        "Go to Run"),
              br(),
```

```
        uiOutput("adjSelection"),
        actionButton("go_jt",
                "Go to Joint"),
        br(),
        uiOutput("adjSelection2"),
        actionButton("go_prf",
                "Go to Profile"),
        numericInput(inputId = "id_num12", label = "Offset (mm)",value = 60),
        numericInput(inputId = "id_num13", label = "Box Width (mm)",value = 50),

        numericInput(inputId = "id_num14", label = "Pixel Length = (mm)",value =
0.24185),

        numericInput(inputId = "id_num7", label = "Tolerable Width Intermission",value =
70),
        numericInput(inputId = "id_num8", label = "Minimum Length",value = 75),
        numericInput(inputId = "id_num9", label = "Maximum Length",value = 350),
        numericInput(inputId = "id_num10", label = "Minimum Total Area below Median
Line",value = 5),
        numericInput(inputId = "id_num11", label = "Minimum Single Area below Median
Line",value = 2),
        br(),
        actionButton("calculate",
                "Calculate!"),
        downloadButton("download2","Download the data")
      ),

      # Show a plot of the generated distribution
      mainPanel(fluidRow(
       splitLayout(cellWidths = c("50%", "50%"),
              plotOutput("distPlot"),
              DT::dataTableOutput("mytable")),
       tags$style(type="text/css",
              ".shiny-output-error { visibility: hidden; }",
              ".shiny-output-error:before { visibility: hidden; }")
      )

      )
     )
    )
   )
```

```
)


# Define server logic required to draw a histogram
server <- shinyServer(function(input,output){

  thedata <- eventReactive(input$detect,{
    run <- input$id_sel1

    hpf <- 300
    lpf <- 30

    hpparam <- 40
    medfparam <- 20

    Data1 <- get(paste0('highspeed',run,'_1'))
    Data2 <- get(paste0('highspeed',run,'_2'))
    Data3 <- get(paste0('highspeed',run,'_3'))

    param1 <- input$id_num
    param2 <- input$id_num2

    detect2 <- jt_det(Data1 = Data1,Data2 = Data2,Data3 = Data3, hpf = hpf,lpf = lpf,hpparam =
hpparam,medfparam = medfparam,param1 = input$id_num,param2 = input$id_num2)

    detect2
  })

  plot_new <- eventReactive(input$detect,
                {
                  run <- input$id_sel1

                  Data1 <- get(paste0('highspeed',run,'_1'))

                  jt_loc <- which(diff(thedata()) == 1)

                  jt_loc <- jt_loc[(which(diff(jt_loc) > 50) + 1)]

                  jt_det_cnt <- length(jt_loc) + 1
```

```r
                plot(thedata(),type = 'l',main = paste0(jt_det_cnt,' Joints Detected in
',nrow(Data1),' Profiles'),xlab = 'Profile Number',ylab = 'Joint Detected')})

  output$upperbound <- renderPlot({plot_new()})

  output$download <- downloadHandler(
    filename = function()
    {paste0("Location_of_joints_run_",input$id_sel1,".csv")},
    content = function(fname){
      write.csv(thedata(), fname)
    }
  )

  output$adjSelection = renderUI({

    run <- eventReactive(input$go_run,input$id_sel2)

    input$go_run
    isolate({
      loc_of_jt <- read_csv(paste0("FaultCalc/Location_of_joints_run_",run(),".csv"))
      jt_run <- which(loc_of_jt$x != 0 & !is.na(loc_of_jt$x))
      run_start <- c(1,which(diff(jt_run) > 50) + 1)
      run_end <- c(which(diff(jt_run) > 50),length(jt_run))
      Run <- cbind(jt_run[run_start],
              jt_run[run_end])

      selectizeInput(inputId = "joint",
              label = "Select Joint: ",
              selected = 1,
              choices = 1:nrow(Run)

    )
  })

})

  output$adjSelection2 = renderUI({

    run <- eventReactive(input$go_run,input$id_sel2)

    jt <- eventReactive(input$go_jt,input$joint)
```

```r
input$go_jt
isolate(
 {loc_of_jt <- read_csv(paste0("FaultCalc/Location_of_joints_run_",run(),".csv"))
 jt_run <- which(loc_of_jt$x != 0 & !is.na(loc_of_jt$x))
 run_start <- c(1,which(diff(jt_run) > 50) + 1)
 run_end <- c(which(diff(jt_run) > 50),length(jt_run))
 data <- cbind(jt_run[run_start],
        jt_run[run_end])

 joint_num <- as.numeric(jt())
 selectizeInput(inputId = "profile",
         label = "Select Profile: ",
         selected = data[joint_num,1],
         choices = data[joint_num,1]:data[joint_num,2]
 ) })
})




jt_plot <- eventReactive(input$go_prf,{
 highspeed1_1 <- highspeed1_1[,4:2051] * .01
 highspeed1_2 <- highspeed1_2[,4:2051] * .01
 highspeed1_3 <- highspeed1_3[,4:2051] * .01

 highspeed2_1 <- highspeed2_1[,4:2051] * .01
 highspeed2_2 <- highspeed2_2[,4:2051] * .01
 highspeed2_3 <- highspeed2_3[,4:2051] * .01

 highspeed3_1 <- highspeed3_1[,4:2051] * .01
 highspeed3_2 <- highspeed3_2[,4:2051] * .01
 highspeed3_3 <- highspeed3_3[,4:2051] * .01

 clearing <- input$id_num12
 box_width <- input$id_num13
 pixel_length <- input$id_num14

 run <- eventReactive(input$go_run,input$id_sel2)

 jt <- eventReactive(input$go_jt,input$joint)
 prf <- eventReactive(input$go_prf,input$profile)
```

```r
   profile_num <- as.numeric(prf())

   output <-
three_line_process(get(paste0('highspeed',run(),'_1')),get(paste0('highspeed',run(),'_2')),get(pa
ste0('highspeed',run(),'_3')),profile_num,detrend_by = list(by = 'center frame',frame_radius =
62,linear = TRUE),thres  = 2)

  profile_1 <- output$profile_1
  profile_2 <- output$profile_2
  profile_3 <- output$profile_3


  profile_sum <- apply(cbind(profile_1,profile_2,profile_3),1,sum)

   jt_loc <-
loc_jt(profile_sum,input$id_num7,input$id_num8,input$id_num9,input$id_num10)$jt_loc

   jt_loc_1 <-
loc_jt(profile_1,input$id_num7,input$id_num8,input$id_num9,input$id_num11)$jt_loc
  jt_loc_2 <-
loc_jt(profile_2,input$id_num7,input$id_num8,input$id_num9,input$id_num11)$jt_loc
  jt_loc_3 <-
loc_jt(profile_3,input$id_num7,input$id_num8,input$id_num9,input$id_num11)$jt_loc


   if (length(which(c(length(jt_loc_1) == 0,length(jt_loc_2) == 0,length(jt_loc_3) == 0))) >= 1 &
length(which(c(length(jt_loc_1) == 0,length(jt_loc_2) == 0,length(jt_loc_3) == 0))) <3){
    if (1 %in% which(c(length(jt_loc_1) == 0,length(jt_loc_2) == 0,length(jt_loc_3) == 0))){
     jt_loc_1 <- jt_loc
    }
    else if (abs(mean(jt_loc_1) - mean(jt_loc)) > 25){
     jt_loc_1 <- jt_loc
    }
    if (2 %in% which(c(length(jt_loc_1) == 0,length(jt_loc_2) == 0,length(jt_loc_3) == 0))){
     jt_loc_2 <- jt_loc
    }
    else if (abs(mean(jt_loc_2) - mean(jt_loc)) > 25){
     jt_loc_2 <- jt_loc
    }
    if (3 %in% which(c(length(jt_loc_1) == 0,length(jt_loc_2) == 0,length(jt_loc_3) == 0))){
     jt_loc_3 <- jt_loc
```

```r
    }
    else if (abs(mean(jt_loc_3) - mean(jt_loc)) > 25){
      jt_loc_3 <- jt_loc
    }
  }

  if ((mean(jt_loc_1) - mean(jt_loc_2)) %>% abs > 50 & (mean(jt_loc_1) - mean(jt_loc_3)) %>%
abs > 50){
    jt_loc_1 <- jt_loc
  }
  if ((mean(jt_loc_2) - mean(jt_loc_1)) %>% abs > 50 & (mean(jt_loc_2) - mean(jt_loc_3)) %>%
abs > 50){
    jt_loc_2 <- jt_loc
  }
  if ((mean(jt_loc_3) - mean(jt_loc_1)) %>% abs > 50 & (mean(jt_loc_3) - mean(jt_loc_2)) %>%
abs > 50){
    jt_loc_3 <- jt_loc
  }

  start_1 <- min(jt_loc_1) - 1
  end_1 <- max(jt_loc_1)+1
  start_2 <- min(jt_loc_2) - 1
  end_2 <- max(jt_loc_2)+1
  start_3 <- min(jt_loc_3) - 1
  end_3 <- max(jt_loc_3)+1

  center_joint <- round(mean(c(start_1,end_1,start_2,end_2,start_3,end_3)))

  slope_rem_1 <- profile_1
  slope_rem_2 <- profile_2
  slope_rem_3 <- profile_3

  ran_1 = c(range(slope_rem_1,na.rm = TRUE)[1]-20,(range(slope_rem_1,na.rm =
TRUE)[2])+20)
  ran_2 = c(range(slope_rem_2,na.rm = TRUE)[1]-20,(range(slope_rem_2,na.rm =
TRUE)[2])+20)
  ran_3 = c(range(slope_rem_3,na.rm = TRUE)[1]-20,(range(slope_rem_3,na.rm =
TRUE)[2])+20)

  upper_box_1 <- round(center_joint - (clearing + box_width)/pixel_length):round(center_joint
- clearing/pixel_length)
```

```
    lower_box_1 <- round(center_joint + clearing/pixel_length):round(center_joint + (clearing+
box_width)/pixel_length)
    upper_box_2 <- round(center_joint - (clearing + box_width)/pixel_length):round(center_joint
- clearing/pixel_length)
    lower_box_2 <- round(center_joint + clearing/pixel_length):round(center_joint + (clearing+
box_width)/pixel_length)
    upper_box_3 <- round(center_joint - (clearing + box_width)/pixel_length):round(center_joint
- clearing/pixel_length)
    lower_box_3 <- round(center_joint + clearing/pixel_length):round(center_joint + (clearing+
box_width)/pixel_length)


    faulting_val3_3 <- - mean(slope_rem_3[lower_box_3],na.rm = T) +
mean(slope_rem_3[upper_box_3],na.rm = T)
    faulting_val3_2 <- - mean(slope_rem_2[lower_box_2],na.rm = T) +
mean(slope_rem_2[upper_box_2],na.rm = T)
    faulting_val3_1 <- - mean(slope_rem_1[lower_box_1],na.rm = T) +
mean(slope_rem_1[upper_box_1],na.rm = T)

    upper_box_1 <- upper_box_1[which(!is.na(slope_rem_1[upper_box_1]))]
    upper_box_2 <- upper_box_2[which(!is.na(slope_rem_2[upper_box_2]))]
    upper_box_3 <- upper_box_3[which(!is.na(slope_rem_3[upper_box_3]))]

    lower_box_1 <- lower_box_1[which(!is.na(slope_rem_1[lower_box_1]))]
    lower_box_2 <- lower_box_2[which(!is.na(slope_rem_2[lower_box_2]))]
    lower_box_3 <- lower_box_3[which(!is.na(slope_rem_3[lower_box_3]))]

    lm_meth2_up_3 <- lm(slope_rem_3[upper_box_3] ~ upper_box_3,na.action = 'na.exclude')
    lm_meth2_down_3 <- lm(slope_rem_3[lower_box_3] ~ lower_box_3,na.action =
'na.exclude')
    lm_meth2_up_2 <- lm(slope_rem_2[upper_box_2] ~ upper_box_2,na.action = 'na.exclude')
    lm_meth2_down_2 <- lm(slope_rem_2[lower_box_2] ~ lower_box_2,na.action =
'na.exclude')
    lm_meth2_up_1 <- lm(slope_rem_1[upper_box_1] ~ upper_box_1,na.action = 'na.exclude')
    lm_meth2_down_1 <- lm(slope_rem_1[lower_box_1] ~ lower_box_1,na.action =
'na.exclude')

    par(mfrow = c(3,1))

    p <- recordPlot()
```

```r
  if (length(jt_loc) == 0|(length(which(c(length(jt_loc_1) == 0,length(jt_loc_2) ==
0,length(jt_loc_3) == 0))) > 2)|(!(end_1 - start_1 >= 21 & end_2 - start_2 >= 21 & end_3 -
start_3 >= 21))| (range(lower_box_1,na.rm = T)[2] >= 2048 |range(lower_box_2,na.rm = T)[2]
>= 2048 | range(lower_box_3,na.rm = T)[2] >= 2048 |range(upper_box_1,na.rm = T)[1] <= 0
|range(upper_box_2,na.rm = T)[1] <= 0 |range(upper_box_3,na.rm = T)[1] <= 0) ){
    plot(1:2048*pixel_length,profile_1,type = 'l',ylim = ran_1,main = paste('Profile
',num2str(profile_num,0)))
    plot(1:2048*pixel_length,profile_2,type = 'l',ylim = ran_2)
    plot(1:2048*pixel_length,profile_3,type = 'l',ylim = ran_3)
  }

  else
  {plot(1:start_1*pixel_length,slope_rem_1[1:start_1],type = 'l',xlim =
c(0,2048*pixel_length),ylim = ran_1,main = paste('Profile ',num2str(profile_num,0),'\n Faulting
= ',num2str(faulting_val3_1,2),' mm'),xlab = 'Longitudinal Position (mm)',ylab = "Elevation
(mm)")
    lines((start_1:end_1)*pixel_length,slope_rem_1[start_1:end_1],col = 'red')
    lines(end_1:length(slope_rem_1)*pixel_length,slope_rem_1[end_1:length(slope_rem_1)])
    lines(rep(center_joint,2)*pixel_length,ran_1,col = 'green')
    lines((upper_box_1[1]*pixel_length) %>%
rep(2),c(slope_rem_1[upper_box_1[1]],(slope_rem_1[upper_box_1[1]] + 15)),col = 'blue')
    lines(upper_box_1*pixel_length,lm_meth2_up_1$fitted.values+15,col = 'blue')
    lines((upper_box_1[length(upper_box_1)]*pixel_length) %>%
rep(2),c(slope_rem_1[upper_box_1[length(upper_box_1)]],(slope_rem_1[upper_box_1[length(
upper_box_1)]] + 15)),col = 'blue')
    lines((lower_box_1[1]*pixel_length) %>%
rep(2),c(slope_rem_1[lower_box_1[1]],(slope_rem_1[lower_box_1[1]] + 15)),col = 'blue')
    lines(lower_box_1*pixel_length,lm_meth2_down_1$fitted.values+15,col = 'blue')
    lines((lower_box_1[length(lower_box_1)]*pixel_length) %>%
rep(2),c(slope_rem_1[lower_box_1[length(lower_box_1)]],(slope_rem_1[lower_box_1[length(l
ower_box_1)]] + 15)),col = 'blue')

    plot(1:start_2*pixel_length,slope_rem_2[1:start_2],type = 'l',xlim =
c(0,2048*pixel_length),ylim = ran_2,main = paste('Profile ',num2str(profile_num,0),'\n Faulting
= ',num2str(faulting_val3_2,2),' mm'),xlab = 'Longitudinal Position (mm)',ylab = "Elevation
(mm)")
    lines((start_2:end_2)*pixel_length,slope_rem_2[start_2:end_2],col = 'red')
    lines(end_2:length(slope_rem_2)*pixel_length,slope_rem_2[end_2:length(slope_rem_2)])
    lines(rep(center_joint,2)*pixel_length,ran_2,col = 'green')
    lines((upper_box_2[1]*pixel_length) %>%
rep(2),c(slope_rem_2[upper_box_2[1]],(slope_rem_2[upper_box_2[1]] + 15)),col = 'blue')
```

```r
    lines(upper_box_2*pixel_length,lm_meth2_up_2$fitted.values+15,col = 'blue')
    lines((upper_box_2[length(upper_box_2)]*pixel_length) %>%
rep(2),c(slope_rem_2[upper_box_2[length(upper_box_2)]],(slope_rem_2[upper_box_2[length(
upper_box_2)]] + 15)),col = 'blue')
    lines((lower_box_2[1]*pixel_length) %>%
rep(2),c(slope_rem_2[lower_box_2[1]],(slope_rem_2[lower_box_2[1]] + 15)),col = 'blue')
    lines(lower_box_2*pixel_length,lm_meth2_down_2$fitted.values+15,col = 'blue')
    lines((lower_box_2[length(lower_box_2)]*pixel_length) %>%
rep(2),c(slope_rem_2[lower_box_2[length(lower_box_2)]],(slope_rem_2[lower_box_2[length(l
ower_box_2)]] + 15)),col = 'blue')


    plot(1:start_3*pixel_length,slope_rem_3[1:start_3],type = 'l',xlim =
c(0,2048*pixel_length),ylim = ran_3,main = paste('Profile ',num2str(profile_num,0),'\n Faulting
= ',num2str(faulting_val3_3,2),' mm'),xlab = 'Longitudinal Position (mm)',ylab = "Elevation
(mm)")
    lines((start_3:end_3)*pixel_length,slope_rem_3[start_3:end_3],col = 'red')
    lines(end_3:length(slope_rem_3)*pixel_length,slope_rem_3[end_3:length(slope_rem_3)])
    lines(rep(center_joint,2)*pixel_length,ran_3,col = 'green')
    lines((upper_box_3[1]*pixel_length) %>%
rep(2),c(slope_rem_3[upper_box_3[1]],(slope_rem_3[upper_box_3[1]] + 15)),col = 'blue')
    lines(upper_box_3*pixel_length,lm_meth2_up_3$fitted.values+15,col = 'blue')
    lines((upper_box_3[length(upper_box_3)]*pixel_length) %>%
rep(2),c(slope_rem_3[upper_box_3[length(upper_box_3)]],(slope_rem_3[upper_box_3[length(
upper_box_3)]] + 15)),col = 'blue')
    lines((lower_box_3[1]*pixel_length) %>%
rep(2),c(slope_rem_3[lower_box_3[1]],(slope_rem_3[lower_box_3[1]] + 15)),col = 'blue')
    lines(lower_box_3*pixel_length,lm_meth2_down_3$fitted.values+15,col = 'blue')
    lines((lower_box_3[length(lower_box_3)]*pixel_length) %>%
rep(2),c(slope_rem_3[lower_box_3[length(lower_box_3)]],(slope_rem_3[lower_box_3[length(l
ower_box_3)]] + 15)),col = 'blue')
  }

  p

})

output$distPlot <- renderPlot({jt_plot()})

thedata2 <- eventReactive(input$calculate,{
```

```
highspeed1_1 <- highspeed1_1[,4:2051] * .01
highspeed1_2 <- highspeed1_2[,4:2051] * .01
highspeed1_3 <- highspeed1_3[,4:2051] * .01


highspeed2_1 <- highspeed2_1[,4:2051] * .01
highspeed2_2 <- highspeed2_2[,4:2051] * .01
highspeed2_3 <- highspeed2_3[,4:2051] * .01


highspeed3_1 <- highspeed3_1[,4:2051] * .01
highspeed3_2 <- highspeed3_2[,4:2051] * .01
highspeed3_3 <- highspeed3_3[,4:2051] * .01



clearing <- input$id_num12
box_width <- input$id_num13
pixel_length <- input$id_num14

run <- eventReactive(input$go_run,input$id_sel2)

jt <- eventReactive(input$go_jt,input$joint)
joint_num <- as.numeric(jt())



loc_of_jt <- read_csv(paste0("FaultCalc/Location_of_joints_run_",run(),".csv"))
jt_run <- which(loc_of_jt$x != 0 & !is.na(loc_of_jt$x))
run_start <- c(1,which(diff(jt_run) > 50) + 1)
run_end <- c(which(diff(jt_run) > 50),length(jt_run))
data <- cbind(jt_run[run_start],
        jt_run[run_end])

output_data <- NULL
for (i in data[joint_num,1]:data[joint_num,2]){
  output_data <-rbind(output_data, faulting_calc_temp(line1 =
get(paste0('highspeed',run(),'_1')),
                              line2 = get(paste0('highspeed',run(),'_2')),
                              line3 = get(paste0('highspeed',run(),'_3')),
                              profile = i,
                              loc_jt_par = list(width = input$id_num7,
                                      length_min = input$id_num8,
                                      length_max = input$id_num9,
                                      min_area_total = input$id_num10,
```

```r
                              min_area = input$id_num11),
                  clearing = input$id_num12,
                  box_width = input$id_num13,
                  pixel_length = input$id_num14))}
  colnames(output_data) <- c('Profile Number','AOI 1','AOI 2','AOI 3')

  output_data
})


output$mytable = DT::renderDataTable({
  round(thedata2(),2)
})



output$download2 <- downloadHandler(
  filename = function(){
    run <- eventReactive(input$go_run,input$id_sel2)

    jt <- eventReactive(input$go_jt,input$joint)
    paste0("Faulting_Calculation_Run_",run(),'_Joint_',jt(),".csv")},
  content = function(fname){
    write.csv(thedata2(), fname)
  }
 )
})

# Run the application
shinyApp(ui = ui, server = server)
```